CREEP, FAILURE AND FRACTURE OF ICE

HANY EL-SAYED HAMZA

CANADIAN THESES ON MICROFICHE

I.S.B.N.

THESES CANADIENNES SUR MICROFICHE

National Library of Canada
Collections Development Branch

Canadian Theses on
Microfiche Service

Ottawa, Canada
K1A 0N4

Bibliothèque nationale du Canada
Direction du développement des collections

Service des thèses canadiennes
sur microfiche

NOTICE

The quality of this microfiche is heavily dependent upon the quality of the original thesis submitted for microfilming. Every effort has been made to ensure the highest quality of reproduction possible.

If pages are missing, contact the university which granted the degree.

Some pages may have indistinct print especially if the original pages were typed with a poor typewriter ribbon or if the university sent us a poor photocopy.

Previously copyrighted materials (journal articles, published tests, etc.) are not filmed.

AVIS

La qualité de cette microfiche dépend grandement de la qualité de la thèse soumise au microfilmage. Nous avons tout fait pour assurer une qualité supérieure de reproduction.

S'il manque des pages, veuillez communiquer avec l'université qui a conféré le grade.

La qualité d'impression de certaines pages peut laisser à désirer, surtout si les pages originales ont été dactylographiées à l'aide d'un ruban usé ou si l'université nous a fait parvenir une photocopie de mauvaise qualité.

Les documents qui font déjà l'objet d'un droit d'auteur (articles de revue, examens publiés, etc.) ne sont pas microfilmés.

THIS DISSERTATION
HAS BEEN MICROFILMED
EXACTLY AS RECEIVED

LA THÈSE A ÉTÉ
MICROFILMÉE TELLE QUE
NOUS L'AVONS REÇUE

NL-339 (r. 82/08)

Canada

CREEP, FAILURE AND FRACTURE OF ICE

by

© Hany Hamza, B.Sc., M.Eng.,

A Thesis submitted in partial fulfillment

of the requirements for the degree of

Doctor of Philosophy

Faculty of Engineering and Applied Science

Memorial University of Newfoundland

August, 1981

St. John's Newfoundland

ABSTRACT

A finite element creep bending model has been developed using thick plate theory. The model agrees very well with available numerical creep models and with field data collected during a load bearing capacity test of fresh-water ice. A simple numerical formula is derived which can predict the time of the onset of failure using the critical strain energy as a failure criterion. This formula agrees very well with available field data.

An algorithm has been developed which is able to predict the viscoelastic response of ice under different uniaxial loading conditions. This algorithm has been generalized using the finite element method, to predict the viscoelastic response due to multiaxial loading. The general finite element model is capable of solving the ice cover - offshore structure interaction problem. A similar procedure has been used to predict the viscoelastic response of the cracked three-point bend test specimen due to constant cross-head speed loading.

The linear and non-linear fracture toughness of artificially grown fresh-water ice has been determined during a small-scale experimental program. The effect of rate of loading, test temperature, specimen dimensions, and grain size on fracture toughness has been investigated.

Finally, the strain rate dependent, critical strain energy per unit volume has been proposed as a failure criterion for ice under different loading rates. The criterion is applicable to ice failure during a laboratory test and failure of ice covers due to interaction with an offshore structure or due to supporting a load for short or long periods of time.

ACKNOWLEDGEMENTS

Of the entire thesis this part is the most pleasant to write since it provides a place for the author to record his appreciation to every body who helped him in any way along the way.

During all the research program, the author had the pleasure of having Professor D.B. Muggeridge as a chairman of his supervisory committee. Dr. Muggeridge, with his expert guidance and pleasant personality, has made the time I have spent on my Ph.D. program one of the most rewarding and pleasant experiences of my educational life.

A great amount of appreciation should go to Dr. P.Smith and Mr. A. Allan for participating in many stimulating discussions and to Messrs. R. Smith, A. Bursey and T. Laaning who devoted a lot of their time to give technical help during the course of the experimental work. The author would like to acknowledge also, a part of his financial support which came in the form of a Fellowship from Memorial University of Newfoundland. Special thanks are due to Ms. Janet Coffen for typing this manuscript.

The last acknowledgement is usually reserved for one's wife, and since the author dosen't yet have one, the author would like to extend his thanks and appreciation to his parents for their moral support and all his good friends who were there to share all the happy moments and to support and cheer up the author in all the difficult moments.

TABLE OF CONTENTS

LIST OF FIGURES

LIST OF TABLES

1. INTRODUCTION

Late in the nineteenth century, the Russian investigators were first to realize the need for more knowledge about ice mechanical properties due to early problems with the design of dams and ice breakers. Recently, due to increased activities in the Arctic and Antarctic regions, there is more demand for the solution of a wide variety of difficult ice related problems. Some of these problems are: The formation of crevasses, the adhesion of ice to surfaces, the bearing capacity of floating ice covers and snow surfaces and crusts, the initiation of snow and ice avalanches, the formation of open leads and pressure ridges in sea and lake ice covers, the forces exerted on structures by moving ice floes and jams, the design of a new generation of ice breakers, and the utilization of ice as an indigenous construction material.

1.1 Crystal Structure of Ice

Ice is the solid state of water. Depending on the freezing temperature and pressure ice can exist as one of nine different types. The stable phase of ice at ordinary low pressures is usually known as ice I. Two different crystal structures of ice I exist, one has a hexagonal structure and is known as Ih, the other has a cubic structure and is known as ice Ic. A complete phase diagram of ice is shown in Figure 1. Ice Ih is the stable type of ice with which most people are familiar. Glen, 1974, reviewed in full detail the actual arrangement of the water molecule in ice Ih which is shown in Figures 2, 3 and 4. In nature, ice is a polycrystalline material, that is, it is composed of a large number of single crystals in different orientations. The main kinds of polycrystalline ice are (Michel and Ramseier, 1971):

1. Randomly oriented polycrystalline tertiary ice. This type can be obtained by freezing water of randomly oriented ice nuclei.
2. Columnar ice with C - axes parallel to the column lengths (secondary ice, S1). This kind of ice is normally obtained when water freezes due to the fact that ice crystals form with their C - axis perpendicular to the surface.
3. Columnar ice with C - axes perpendicular to the column lengths (secondary ice, S2). This can be obtained by seeding the water at 0°C with fine ice grains which will lead to this type of ice due to the fact that ice grows more rapidly perpendicular to the axis of summetry of the ice crystal which is C- axis.

1.2 Mechanical Properties of Ice

In the last few decades, researchers have been studying extensively the different mechanical properties of fresh-water and sea-water ice by doing small-scale or full scale tests. The state-of-art of this subject have been presented by different investigators at different times like Weeks and Assur (1967, 1969), Glen (1975), Gold (1977), Schwarz and Weeks (1977) and Mellor (1979). The available literature about ice mechanical properties can be classified into the following categories:

1.2.1 Tensile Strength

Two main types of tests have been used to determine the tensile strength of ice. These are the direct tensile test and the ring tensile test. Till now, the uniaxial tensile test is considered the best way to determine un-

ambiguously the tensile strength of ice. Other tests usually induce complicated-stress states within the sample which require some simplifying assumptions before strength values can be calculated from the test results. Many devices have been proposed in order to solve the problems associated with gripping the ends of the specimen. Dykins (1970) has used dumb-bell specimens which were attached to the testing machine by gripping heads. A similar method in which the ice was frozen to metal end cups which are pulled by steel cables, has been used by Hawkes and Mellor (1972).

Results produced by Peyton (1966) and Dykins (1970) have shown that ice tensile strength strongly depends on the direction of loading: Ice can be two to three times stronger when the tension is applied in the vertical direction than in the horizontal.

1.2.2 Compressive Strength

Many investigators have tried to measure the compressive strength of ice using different sample geometries, like cylinders, prisms and cubes. It has been observed that the measured strength depends considerably on end conditions, sample dimensions, stress rate, ice structure and orientation, and specimen temperature.

The International Association for Hydraulic Research (IAHR) Standardization Task Group has suggested a new method for testing ice in compression by using low-modulus urethane which is laterally confined by an aluminum cylinder to prevent radial deformation.

Previous investigations on fresh-water ice have shown that the compressive strength increases if the ratio of crystal size to sample size exceeds a certain value. This effect, so called size effect, has not as yet, been investigated for sea ice.

1.2.3 Fracture Toughness

Very recently a few investigators have tried to determine the fracture toughness of ice. This has opened the door for the application of fracture mechanics techniques to ice problems. The technique approaches the ice strength from a more realistic point of view based on the fact that ice in the field contains a large number of randomly oriented cracks. The work by Liu and Loop (1972), Vaudrey (1977) and Goodman (1977) have shown the need for more work to be done to investigate the effect of the test temperature and loading rate on fracture toughness, and to determine an adequate parameter which controls the nonlinear and viscoelastic fracture toughness of ice. Very recent work by Urabe, Iwasaki and Yoshitake (1981), Urabe (1981), Kolle (1981), and Hoare (1981) should provide more experimental data to help to understand the effect of different parameters on the fracture toughness of ice.

Also, a careful review of the available data about different mechanical properties of ice, shows that the effect of the rate of loading and the test temperature on the viscoelastic response of ice has always the general pattern which is shown in Figure 5. The author thinks that the development of a mathematical model which can explain and predict the observed general behaviour, can be a useful tool in the future.

1.3 Load Bearing Capacity of Ice Covers

In the past years, the load bearing capacity of a floating ice cover under vertical or in-plane loading has presented an interesting challenge to ice mechanics researchers. This had led to numerous papers in which investigators tried to predict the load bearing capacity based on experi-

mental data or theoretical analyses which treated ice as an elastic and/or viscoelastic material. A careful review to the available literature will indicate that the previous work can be divided into the following categories:

Purely Theoretical

Several analytical attempts have been made to determine the elastic and viscoelastic response of ice covers due to different load configurations. Nevel (1976) has developed a complete theory to predict the long-term response of floating ice cover under a static load. The theory is based on a multi-element viscoelastic model which can predict the deflection and stresses as a function of time for a given load configuration. The reader is referred to the same reference for a complete review of the state-of-art.

Combined Theoretical and Experimental

Assuming ice is an elastic material, the maximum stress criterion has been used in predicting the failure load for ice covers. This has led to the familiar formula (Meyerhof, 1962; Nevel, 1968; Gold, 1971):

$$P_{all} = Ch^2 \qquad (1)$$

An early formula by Zubov (1942) takes into account the effects of temperature, the dimensions of the load and the salinity.

$$P_{all} = KMACh^2 \qquad (2)$$

where K, M, A, and C are constants, h is the ice cover thickness,

and P_{all} is the allowable load.

Another investigator has considered the strain criterion as a suitable failure criterion for ice as a viscoelastic material (Kerr, 1975). This has led to the following equation for the allowable deflection:

$$w_{all} = a\, h^{1/2} \tag{3}$$

where a is a constant with dimensions of $(\text{length})^{1/2}$. Recently Beltaos (1977) has pointed out that the maximum stress and maximum strain criteria are not suitable to predict the failure of ice. He has proposed that the strain energy criterion may be more useful to predict the onset of failure and the complete failure of ice covers. This criterion leads to the following equation

$$(W_p)_{oF} = Ch^{5/2} \tag{4}$$

where $(W_p)_{oF}$ is the potential energy at the onset of failure, C is a constant and h is the ice cover thickness. The criterion has shown a good agreement with available field data on fresh-water and salt-water ice covers.

Empirical

Formulae based on field data have been used to predict the subsequent deflection history of ice covers. Beltaos and Lipsett (1978) have proposed a simple equation which can evaluate the complete deflection history after knowing the initial part of the deflection history.

The reader can notice that all the available numerical models in the literature can predict the elastic response and/or the long-term response of

floating ice covers under very simple load configurations. The author thinks that there is a serious need for a creep bending model which can predict the viscoelastic response of a floating ice cover under a general loading configuration and for general boundary conditions.

1.4 Ice Forces on Offshore Structures

One of the most important forces in the design of structures in ice infested water are the horizontal and vertical thrusts applied to the structures by ice. Neill (1976), in his review paper, has classified the ice action on structures into four principal modes as described in Table 1.

The problem of ice forces on structures has received considerable attention in the recent past, but the amount of experimental data is still very small, and the available data has various deficiencies which make them difficult to use directly for design or for verification of analytical methods. Designers have generally relied on empirical formulae, design codes and their own individual judgement (Neill, 1976).

The mechanical properties of ice are so complex and variable that the analytical approach of estimating ice forces on a structure will only be acceptable when it is supported by full-scale measurements and evaluation of structure performance. The number of variables influencing ice forces is so great that field data alone cannot be expected to give enough information for design unless they can be fitted into a logical analytical framework. The gap between theoretical analysis and full-scale data may be bridged by small-scale experiments (Neill, 1976).

The mode of failure of an ice sheet is due to crushing (see Figure 6) when the aspect ratio (structure width/ice thickness) is small. It has

been observed by many investigators (Schwarz, et al., 1974, Hirayama, et al, 1972, Zabilansky, et al, 1975 and Afanas'ev, et al, 1972) during small-scale tests that the ice sheet fails in the buckling mode when the aspect ratio is greater than 6.

1.4.1 Failure of Ice Sheets: Crushing Mode

The failure of ice sheets in a crushing mode is a complex phenomenon because of the fact that many parameters affect the ice forces generated on the marine structures. Much research work has been done in estimating the ice forces due to crushing, but considerable work still remains to be done in this field to treat the various deficiencies in the available experimental data to get enough information, especially from full-scale measurements, to be used by designers and for verification of analytical results. Small-scale tests in the laboratory are providing some insight into this complex problem.

Korzhavin (1971) presented the following empirical formula to estimate the maximum effective ice pressure ($P_e = P/2bh$, see Figure 6) in a steady crushing mode.

$$\text{Effective pressure } p_e = \frac{C_i m K \sigma_c}{(V/V_o)^{1/3}} \qquad (5)$$

where C_i is the indentation coefficient, m the coefficient for plan shape of the nose, K the contact coefficient, V the velocity of ice sheet in meters per second, V_o the reference velocity equal to 1 meter per second and σ_c the compressive (cube) strength of ice. A discussion on the values of various parameters in Korzhavin's formula is given in Neill (1976).

Schwarz, et al (1974), Hirayama, et al (1972) and Zabilansky, et al (1976) have conducted small-scale experiments to determine the factors which affect the ice forces exerted by ice sheets on vertical marine struct-

ures. There seems to be general consensus that ice forces depend upon the aspect ratio, strain rate and the compressive strength of ice. Neill (1976) has given the following simplified relation between four dimensionless groups for an isotropic, infinite, uniform ice sheet against a rigid vertical pile or pier.

$$\frac{P}{2bh\sigma_c} = f\left[\frac{b}{h}, \frac{V}{2b\dot{\varepsilon}}, \frac{E}{\sigma_c}\right] \qquad (5)$$

where P is the force developed, h the ice sheet thickness, 2b the pile diameter or pier width, V the velocity of ice sheet, σ_c the compressive strength, $\dot{\varepsilon}$ the corresponding test strain rate, and E the modulus of elasticity. Schwarz, et al (1974) have suggested some more parameters in their dimensional analysis, e.g. temperature, ratio of structure width to grain size, etc.

Neill (1976) has briefly discussed some of the full-scale tests done in North America and Europe. Some correlation with empirical formulae has been indicated by the full-scale measurements, but the complete verification of analytical results is not possible due to the complexities inherent in full-scale tests and the variability of the ice properties.

1.4.2 Failure of Ice Sheets: Buckling Mode

As mentioned earlier, the ice sheet fails in a buckling mode when the aspect ratio (2b/h) is larger than six.

Recently, some attention is being paid to the buckling problem of a plate on an elastic foundation in order to determine the ice forces generated on marine structures. Kivisild (1969) has presented a few formulae to calculate the buckling load without giving any derivation. Kerr (1977)

has solved the buckling problem of a tapered beam floating on water. The justification of considering a tapered beam is due to the fact that radial vertical cracks have been observed to originate from the loading region and radiate outward in the ice sheet. Takagi (1976) developed a theoretical solution to the buckling problem of a floating plate stressed uniformly along the periphery of an internal hole.

1.5 Scope of the Present Work

This thesis can be divided into two main parts. Part I presents numerical models to predict the time dependent response of a floating ice cover and the safe time of any field operation on an ice cover together with results of a load bearing capacity test. Part II presents the results of a small-scale experimental program to determine the linear and non-linear fracture toughness of fresh-water ice and a numerical model which can predict the viscoelastic response of a viscoelastic material due to the interaction with another domain.

In Part I, a finite element numerical model is presented to solve the non-linear problem of creep bending of a plate with or without an elastic foundation. The initial strain approach has been adopted to solve the resulting non-linear simultaneous equations. The algorithm uses a thick plate finite element which takes into account the effect of the shearing deformation. The model has shown good agreement with available creep models and with the collected field data during a load bearing capacity test on fresh-water ice. A simple relation is proposed which could predict the subsequent deflection history of an ice cover to the onset of failure. This relation was then used together with the critical strain energy as a failure criterion,

to derive a formula which could predict the time required to reach the onset of failure. The formula has shown good agreement with available field data.

Part II presents the formulation of the time dependent response of homogeneous, isotropic and linearly viscoelastic materials under a uni-axial constant cross-head speed loading condition. The procedure can be used after minor changes to calculate the viscoelastic response due to constant stress rate or constant strain rate loading conditions. The finite element model can predict the general viscoelastic response of ice due to the interaction with another domain, e.g. testing machine or off-shore structure. The model proves theoretically that the apparent yield stress of the ice, due to constant strain rate or constant cross-head speed loading, happens when the generated strain rate in the specimen reaches the strain rate applied by the testing machine. The procedure is then used to provide a deeper insight into the viscoelastic response of a cracked three-point bend test specimen due to constant cross-head speed loading. Also, the results of a small-scale experimental program to determine the linear and non-linear fracture toughness of artificially grown fresh-water ice are reported. The effect of the rate of loading, specimen thickness, span length, test temperature and the grain size on fracture toughness has been investigated.

1.6 References

Afanas'ev, V.P., Dolgopolov, Yu. V. and Shreishtein, Z.J., 1972, "Ice Pressure on Isolated Structures in the Sea", in Russian, Trudy Leningrad, Arkt, i Antarkt. Inst., V300, pp. 61-80, English Translation by CRREL, DT 346.

Beltaos, S., 1977, "A Strain Energy Criterion for Failure of Floating Ice Sheets", Can. J. Civil Eng., V5, N3, pp. 352-361.

Beltaos, S. and Lipsett, A.W., 1978, "An Empirical Analysis of the Creep of Floating Ice Sheets", Workshop on the Bearing Capacity of Ice Covers, NRC ACGR Tech. Memo. No. 123, pp. 124-158.

Dykins, J.E., 1970, "Ice Engineering-Tensile Properties of Sea Ice Grown in a Confined System", U.S. Naval Civil Eng. Laboratory, Tech. Dept. R689.

Glen, J.W., 1974, "The Physics of Ice", CRREL, Monograph II - X2A, Hanover, New Hampshire.

Glen, J.W., 1975, "The Mechanics of Ice", CRREL, Monograph II - C2b, Hanover, New Hampshire.

Gold, L.W., 1971, "Use of Ice Covers for Transportation", Can Geotechnical J., V8, pp. 170 - 181.

Gold, L.W., 1977, "Engineering Properties of Fresh-Water Ice", J. of Glaciology, V19, pp. 197 - 212.

Goodman, D., 1977, "Creep and Fracture of Ice and Surface Strain Measurements on Glaciers and Sea Ice", Ph.D. Dissertation, Univ. of Cambridge, U.K.

Hawkes, J. and Mellor, M., 1972, "Deformation and Fracture of Ice Under Uniaxial Stress", J. of Glaciology, V11, N61, pp. 103 - 131.

Hirayama, K., Schwarz, J. and Wu, H., 1972, "Model Techniques for the Investigation of Ice Forces on Structures", Proc. POAC - 73, University of Iceland.

Hoare, R.D., 1981, "The Application of Fracture Mechanics to a Full-Scale Ice Structure Interaction", Proc. POAC-81, Quebec City, Canada.

Kerr, A.D., 1975, "The Bearing Capacity of Floating Ice Plates Subjected to Static or Quasi-Static Loads - A Critical Survey", CRREL, Research Report, 333, Hanover, New Hampshire.

Kerr, A.D., 1977, "The Determination of Horizontal Forces That a Floating Ice Plate Exerts on a Structure", Personal Communications.

Kivisild, M.R., 1969, "Ice Impact on Marine Structures", Ice Seminar Sponsored by the Petroleum Society of the Canadian Institute of Mining and Metallurgy and the American Petroleum Institute, Calgary, Alberta, 6 pp.

Kolle, J.J., 1981, "Fracture Toughness of Ice, Crystallographic Anisotropy", POAC-81, Québec City, Canada.

Korzhavin, K.N., 1971, "Action of Ice on Engineering Stuructures", Tech. Translation T.L. No. 260, U.S. Army, CRREL, Hanover, New Hampshire.

Liu, H.W. and Loop, Sp.W., 1972, "Fracture Toughness of Fresh-Water Ice", Draft Report, CRREL, Hanover, New Hampshire.

Mellor, M., 1979, "Mechanical Properties of Polycrystalline Ice", Proc. of Symp. on Physics and Mechanics of Ice, Copenhagen, pp. 217 - 245.

Meyerhof, G.G., 1962, "Bearing Capacity of Floating Ice Sheets", Trans. ASCE, V 127, Part 1, pp. 524 - 567.

Michel, B., and Ramseier, R.O., 1971, "Classification of River and Lake Ice", Can. Geotech. J., V 8, pp. 36 - 45.

Neill, C.R., 1976, "Dynamic Ice Forces on Piers and Piles - An Assessment of Design Guidelines in the Light of Recent Research", Can. J. Civil Eng., V3, pp. 305 - 341

Nevel, D.E., 1968, "Bearing Capacity of Floating Ice Sheets", CRREL, Hanover, New Hampshire.

Nevel, D.E., 1976, "Creep Theory for a Floating Ice Sheet", CRREL, Special Report 76-4, Hanover, New Hampshire.

Peyton, H.R., 1966, "Sea Ice in Cook Inlet", Univ. of Alaska, Arctic Envir. Eng. Lab. Rept.

Schwarz, J., Hirayama, K. and Wu, H., 1974, "Effect of Ice Thickness on Ice Forces", Proceedings of the Offshore Technology Conference, Houston, Texas, Paper No. OTC 2048.

Schwarz, J. and Weeks, W.F., 1977, "Engineering Properties of Sea Ice", J. of Glaciology, V1, N81, pp. 499 - 531.

Takagi, S., "The Buckling Pressure of an Elastic Plate Floating on Water and Stressed Uniformly Along the Periphery of an Internal Hole", The Trans. of the 22nd. Conf. of Army Mathematicians, 1976.

Urabe, N., 1981, "Fracture Toughness of Sea Ice, In-situ Measurements and their Applications", POAC 81, Quebec City, Canada.

Urabe, N., Iwasaki, T., and Yoshitake, A., 1981, "Strain Rate Dependent Fracture Toughness of Sea Ice", IAHR, Quebec City, Canada.

Vaudrey, K.D., 1977, "Ice Engineering -- Study of Related Properties of Floating Sea Ice Sheets and Summary of Viscoelastic Analysis", Tech. Rept. R860, Civil Eng. Lab., Naval Construction Battalion Center, Port Hueneme, California, U.S.A.

Weeks, W. and Assur, A., 1967, "The Mechanical Properties of Sea Ice", CRREL, Monograph II - C3, Hanover, New Hampshire.

Weeks, W. and Assur, A., 1969, "Fracture of Lake and Sea Ice", CRREL Research Dept. 269, Hanover, New Hampshire.

Zabilansky, L.J., Nevel, D.E. and Haynes, F.D., 1975, "Ice Forces on Model Structures", Second Canadian Hydrotechnical Conference, Burlington, Ontario, Canada.

Zubov, N.N., 1942, "The Basis of Road Construction on the Ice Cover", Text in Russian, Gidrometeoizdat, Moscow.

No.	DESCRIPTION	TYPICAL ENVIRONMENT	ILLUSTRATION
1	Impact of moving sheets and floes	Rivers at break - up coastal water with appreciable currents	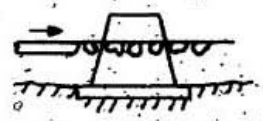
2	Static pressure from expanding or contracting sheets	Lakes, sheltered coastal water temp changes and jacking by refreezing of cracks.	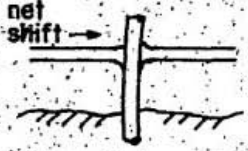
3	Slow pressure from ice pack or jam	Exposed coastal waters, rivers.	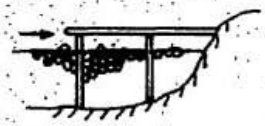
4	Vertical movement	Tidal locations with heavy ice build - up.	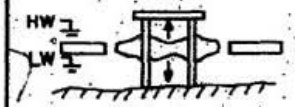

Table 1 Principal modes of ice action.
(From Neil, 1976)

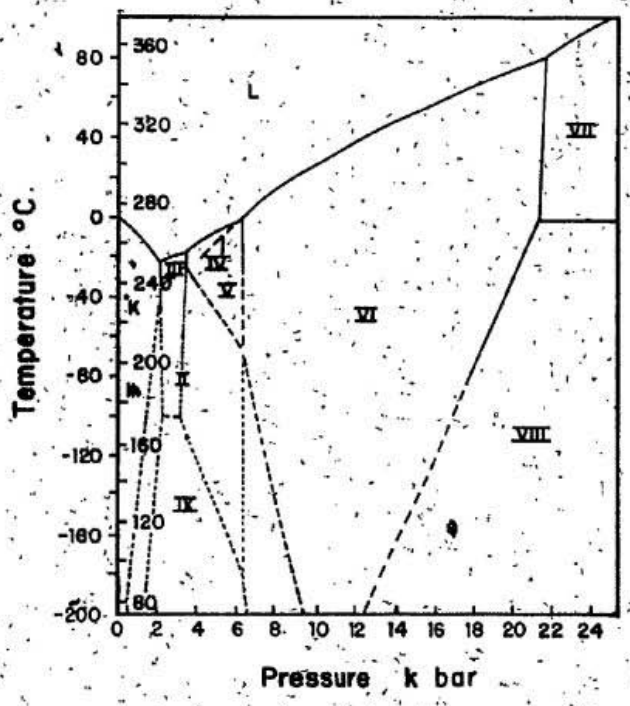

Fig. 1 Phase diagram of ice. Dashed lines are extrapolated or calculated boundaries. Metastable phases (apart from ice IV and Ic) are shown by light lines. (From Glen, 1974)

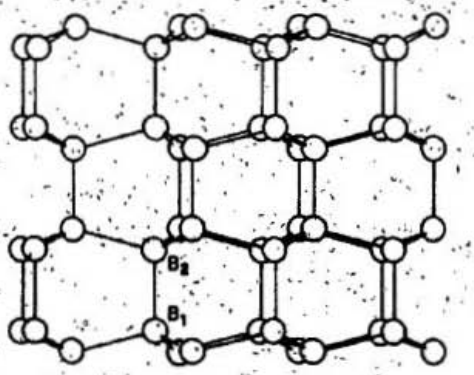

Fig. 2 The arrangement of water molecules in ice Ih. Note that the three water molecules bonded to B_2 are vertically above those bonded to B_1 (From Glen, 1974)

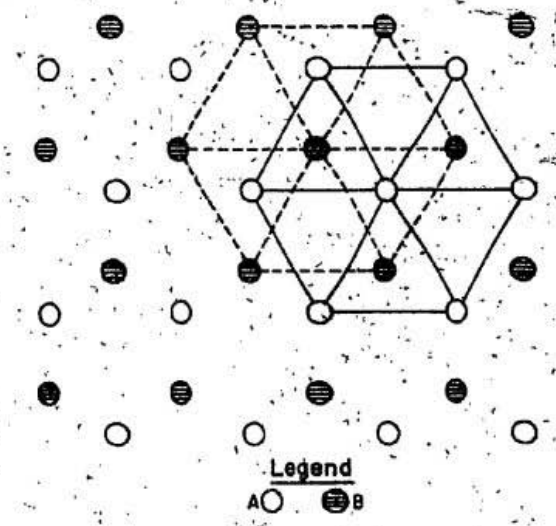

Fig. 3 Projection of the structure of ice Ih onto the basal plane. Molecules are arranged in the stacking sequence ABBAABBAABBAA···. Large straight hexagonal holes penetrate the structure. (From Glen, 1974)

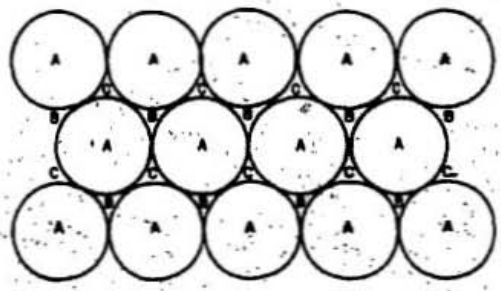

Fig. 4 A close - packed layer of spheres. Another similar layer can be placed on top either in position B or position C. If the layers are stacked in the sequence ABABABA... we have the hexagonal close - packed structure. If they are packed ABCABCABC... we have the cubic close - packed structure or face - centered cubic structure. (From Glen, 1974)

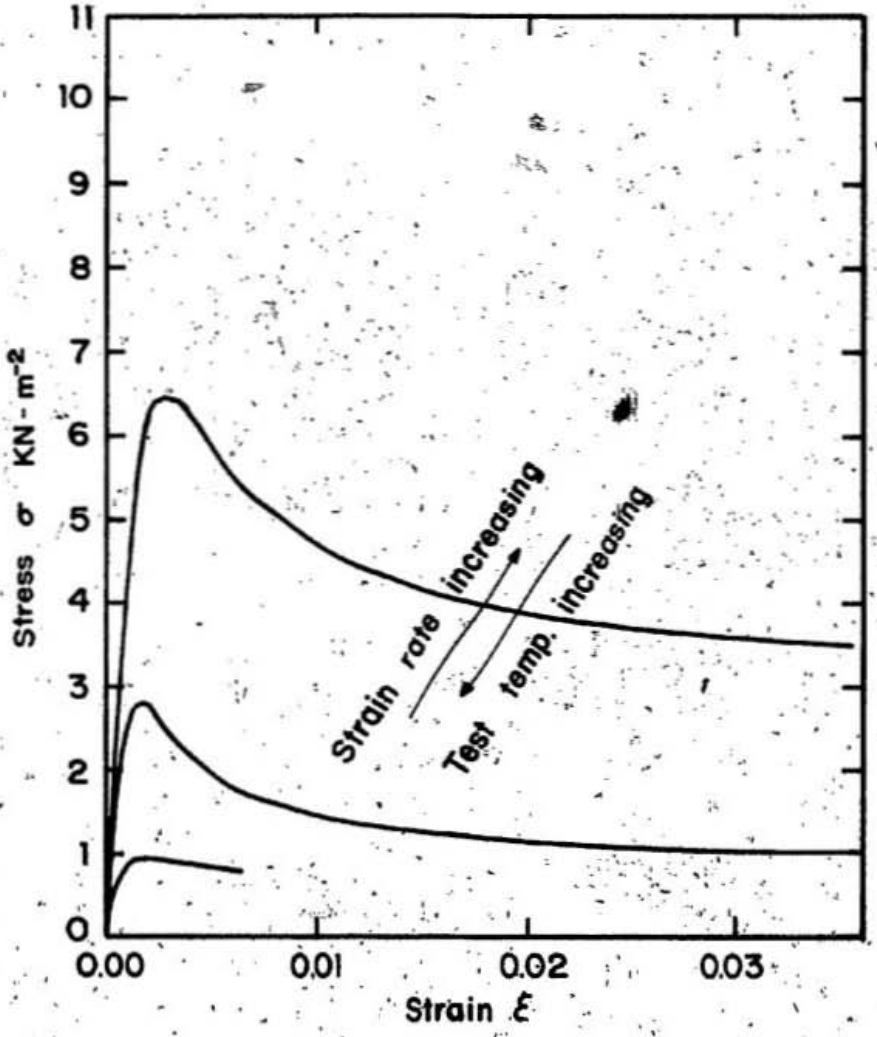

Fig. 5 Dependence of stress on strain.

*The above behaviour can be observed under both tensile and compression loading

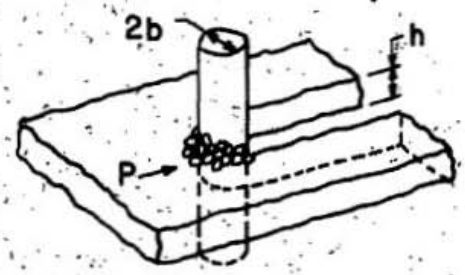

Effective pressure, $P_e = P/2bh$

Fig. 6 Definition of effective pressure.
(From Neil, 1976)

2. ELASTIC CREEP BENDING ANALYSIS OF PLATES USING THE FINITE ELEMENT METHOD

2.1 Scope

The finite element method is used to solve the nonlinear problem of creep bending of a plate. The initial strain approach has been adapted to solve the resulting nonlinear simultaneous equations. The algorithm leads to a time incremental set of equations.

An isoparametric thick plate bending element was used and good agreement was obtained between the present work and some of the available literature for plates with and without elastic foundations.

2.2 Introduction

Two mathematical models are available to describe the time dependent behaviour of engineering materials. One is a viscoelastic model which uses one or more dashpot and spring elements connected in parallel or/and in series. The second model is a creep model based on an experimentally determined relation which describes the apparent time dependent behaviour of a material. The present paper deals with the time dependent response of engineering materials using the creep model.

Venkatraman and Hodge (1958, 1964) have studied the steady state creep behaviour of uniformly loaded simply supported and clamped circular plates using the Tresca criterion and associated flow rule. Patel and Venkatraman (1962, 1963) have used the complementary energy approach to study the creep bending response of compressible circular plates. Using energy theorems of elasticity, Bentson et al (1966) have obtained solutions to the problem of simply supported circular plates.

Hrudey (1973) has used the finite element method to solve the creep problem of circular and square plates. He has used the Newton-Raphson method to solve the resulting nonlinear simultaneous equations. Murat (1976) has also used the finite element method together with an initial strain approach to solve an axisymmetrically loaded infinite plate on an elastic foundation.

The previous work was limited either to thin plate theory or axisymmetric plate problems. The present model utilizes thick plate theory and is capable of handling any load configuration. The algorithm is useful for both classical applied mechanics problems and practical engineering problems such as the bearing capacity of floating ice covers (Hamza, Muggeridge, and Laidley, 1981).

2.3 Finite Element Formulation for a Plate on an Elastic Foundation

The stress-strain relationship for a plate bending isoparametric element based on Mindlin's theory (Hinton et al, 1975) may be expressed as follows:

$$\{M\} = [D_f]\ \{X\} \tag{7}$$

and

$$\{Q\} = [D_s]\ \{\phi\} \tag{8}$$

where $\{M\}^t = \{M_{xx}\ M_{yy}\ M_{xy}\}$

is the bending moments vector

$\{Q\}^t = \{Q_{xz}\ Q_{yz}\}$

is the transverse shearing forces vector

$[D_f]$ is the flexural rigidity matrix

$[D_s]$ is the shear rigidity matrix

$\{X\}^t = \{X_x \; X_y \; X_{xy}\}$

is the bending deformation vector

and $\{\phi\}^t = \{\phi_x \; \phi_y\}$

is the shear deformation vector.

More details about this element and its application to different plate bending problems may be found in Hinton (1975).

The total potential energy of a plate resting on an elastic foundation may be written as

$$\pi_p = \frac{1}{2}\int_A (\{M\}^t\{X\} + \{Q\}^t\{\phi\})dA \qquad (9)$$

$$+ \frac{1}{2}\int w^t f\, w \, dA - \int q\, w \, dA$$

where f is the modulus of the elastic foundation

w is the transverse deflection of the plate

q is the density of the lateral loading

2.4 Creep Constitutive Equations in Bending

The following development will be confined to the secondary steady state creep which may be described by the following equation for a uniaxial state of stress (Murat, 1976):

$$\frac{\dot{\varepsilon}_c}{\dot{\varepsilon}_n} = \left(\frac{\sigma}{\sigma_n}\right)^n \qquad (10)$$

where $\dot{\varepsilon}_n$ is a constant with dimensions of strain rate, σ_n is a constant with dimensions of stress, $\dot{\varepsilon}_c$ is the creep strain rate, and σ is the uniaxial applied stress.

Consider a rod with rectangular cross section which has two axes of symmetry x and y, a height 2h and width b, under a bending moment in the plane YOZ. The bending moment will have the following form:

$$M = 2 \int_0^h b \sigma \, y \, dy \tag{11}$$

substituting equation (10) in equation (11), we get

$$M = 2b \int_0^h y \, \sigma_n \left(\frac{\dot{\varepsilon}_c}{\dot{\varepsilon}_n}\right)^{1/n} dy \tag{12}$$

Assuming the rod sections will remain plane after deformation, the deformation rate at any height y will have the form

$$\dot{\varepsilon} = \dot{K} \, y \tag{13}$$

where $\dot{K}$ is the rate of change of curvature of the centre line of the rod. Substituting equation (13) in equation (12) and after simple integration we get

$$M = \frac{2n}{2n+1} b \, h^2 \, \sigma_n \left(\frac{h}{\dot{\varepsilon}_n}\right)^{1/n} \dot{K}^{1/n} \tag{14}$$

let

$$\dot{K}_n = \frac{\dot{\varepsilon}_n}{h} \quad \text{and} \quad M_n = \frac{2n}{2n+1} b \, h^2 \, \sigma_n \tag{15}$$

it follows that

$$\dot{K} = \dot{K}_n \left(\frac{M}{M_n}\right)^n \tag{16}$$

Under a multi-axial state of stress, equation (10) can be extended using the following flow rule (Murat, 1976):

$$\frac{\dot{\varepsilon}_{c_{ij}}}{\dot{\varepsilon}_n} = \frac{3}{2} \frac{1}{\sigma_n} \sigma_e^{n-1} S_{ij} \tag{17}$$

where σ_e is the effective stress

S_{ij} is the stress deviator

Following the same principles, the creep power law under uniaxial pure bending may be extended to a multiaxial state of bending as follows:

$$\frac{\dot{K}_{c_{ij}}}{\dot{K}_n} = \frac{3}{2} \frac{1}{M_n^n} M_e^{n-1} M_{ij}^* \tag{18}$$

where $M_e^2 = M_{xx}^2 + M_{yy}^2 - M_{xx} M_{yy} + 3 M_{xy}^2$

is called the effective bending moment (considering the plate will be under a state of plane stress)

$$M_{ij}^* = M_{ij} - \frac{1}{3} \delta_{ij} M_{kk} \tag{19}$$

is called the bending moment deviator.

The above analysis would be enough if thin plate theory is being used where the transverse shearing forces are neglected. However, since Mindlin's theory is being used in the present work, further analysis is required to take into account the effect of transverse shear deformation.

From thick plate theory, the transverse shearing force has the following form

$$Q = \int_{-h}^{h} \tau \, dy \tag{20}$$

integration yields

$$Q = \tau \cdot \left(\frac{2h}{\alpha}\right) \tag{21}$$

where $\alpha = 1.2$ (22)

The constant α is used to allow for warping of the cross-section (Hinton, Razzaque and Zienkiewicz, 1975).

Substituting equation (21) in equation (10) with $\dot{\varepsilon}_c$ replaced by $\dot{\gamma}_c$ and σ replaced by τ, we get

$$\dot{\gamma}_c = \frac{\dot{\varepsilon}_n}{\sigma_n^n} \cdot \frac{1}{(2h_s)^n} \cdot Q^n \tag{23}$$

One can notice that the creep constants in equation (14) do not equal the creep constants in equation (23). Also, the reader should be aware of the fact that the dimensions of the bending moment in equation (14) and equation (18) are FLL^{-1}, while the dimensions of the transverse shearing force in equation (23) are FL^{-1}.

In order to be able to use both equations (18) and (23) together, a multiplication by a length is required for equation (23). This length is the plate thickness (2h). We suggest to write equation (23) in the following form:

$$\dot{\gamma}_{c_{ij}} = \frac{\dot{\varepsilon}_n}{\sigma_n^n} \frac{2h}{(2h_s)^{2n-1}} M_e^{n-1} Q_{ij} \tag{24}$$

The reader may notice again that the final creep constants in equations (18) and (24) are not equal and are functions of the plate thickness. This will lead to the fact that the thick plate will creep at a different rate than a thin plate.

2.5 Plate Bending Creep - Initial Strain Approach

The incremental initial strain method (Zienkiewicz, 1971) has been adapted in order to predict the creep response of plate bending problems. In this approach the total time of analysis is divided into small time

intervals within which the state of stress is assumed to remain constant. At time $t = 0$ the elastic stresses and strains are calculated by an elastic analysis. The increment of creep strain $\{\Delta\varepsilon_c\}$ which occurs during the first time interval Δt is then calculated from this stress level.

Treating $\{\Delta\varepsilon_c\}$ as an initial strain, a new state of stress and strain at the end of the time increment can be calculated. The later state of stress is then used to calculate the creep strain increment in the next time interval. The process is then repeated.

Solution Procedure

Assume $\{\sigma\}$ is the generalized stress vector, and $\{\varepsilon\}$ is the generalized strain vector; then at time t_n:

The creep strain rate $\{\dot{\varepsilon}_c\}_n$ is computed from the previous stress level.

The creep strain rate is assumed to remain constant, for small Δt, and the creep strain increment may be calculated from

$$\{\Delta\varepsilon_c\}_n = \{\dot{\varepsilon}_c\}_n \Delta t \tag{25}$$

The effective load, is calculated from

$$\{\Delta R\}_n = \int_A [B]^t [D] \{\Delta\varepsilon_c\}_n \, dA \tag{26}$$

where $[B]^t$ is the strain matrix and

$$[D] = \begin{bmatrix} [D_f] & 0 \\ 0 & [D_s] \end{bmatrix}$$

The change in displacement due to the effective load is computed from the relation

$$[K]\ \{\Delta q\}_n = \{\Delta R\}_n \tag{27}$$

The change in the strain and stress is given by

$$\{\Delta\varepsilon\}_n = [B]\ \{\Delta q\}_n \tag{28}$$

$$\{\Delta\sigma\}_n = [D]\ (\{\Delta\varepsilon\}_n - \{\Delta\varepsilon_c\}_n) \tag{29}$$

Where [K] is the general stiffness matrix, and $\{\Delta q_n\}$ is the general displacement vector.

The stress and strain level at the end of the time increment is computed from

$$\{\varepsilon\}_{n+1} = \{\varepsilon\}_n + \{\Delta\varepsilon_c\}_n \tag{30}$$

$$\{\sigma\}_{n+1} = \{\sigma\}_n + \{\Delta\sigma\}_n \tag{31}$$

Finally the whole cycle is repeated.

2.6 Time Steps - Stability Criterion

It has been observed in the previous work on creep and visco-plasticity that the accuracy of the solution depends very much on the time step length. If the time step is above a certain critical value, oscillating results will be obtained showing instability in the solution. The following criterion, which has been suggested by Zienkiewicz and Cormeau (1974), has been used successfully.

$$\bar{\varepsilon}_c \cdot \Delta t = \alpha \cdot \bar{\varepsilon} \tag{32}$$

where $\bar{\varepsilon}_c$ is the effective creep strain rate

α is a constant and has a value in the range 0.1 to 0.15

$\bar{\varepsilon}$ is the effective strain

Another general limit was applied between any two successive steps:

$$\Delta t_{n+1} \leq 1.5\ \Delta t_n \tag{33}$$

In all the numerical examples presented in this work, the above empirical stability criterion has been used. Smaller values for the constant α did not improve the accuracy of the numerical results and larger values have given less accurate and/or unstable results.

2.7 Equilibrium Correction

The present algorithm adapts an explicit integration scheme which was observed to drift numerically from the equilibrium condition. There are several procedures in the literature for correcting this numerical drift. Stricklin, Haisler and Reisemann (1973) have discussed the merits of different options. The following simple correcting approach has been used in the present work. First, the out-of-balance force is calculated at each time step using the following relation:

$$\{f\} = \{\Delta R\}_n - \{\Delta R_o\}_n \tag{34}$$

where $\{f\}$ is the out-of-balance load vector

$\{\Delta R_o\}_n$ is the reference load vector

$$= \int [B]^t [D] \{\Delta\varepsilon\}_n \, dA \tag{35}$$

$\{\Delta R\}_n$ is the effective load vector

This out-of-balance load vector is then added to the effective load vector at the next time increment. This approach avoids any iteration process and thus reduces the computation time.

2.8 Numerical Examples

1. Infinite Plate on an Elastic Foundation

Murat (1976) has solved the creep problem of a floating ice cover. An axisymmetric infinite plate on an elastic foundation was used in order to simulate this practical problem. The plate is loaded with a circular uniformly distributed load over a radius R. The same problem was solved using the present plate bending finite element model, Fig. 7. Fig. 8 shows good agreement between the results of the two finite element models ($c = 0.2737 \times 10^{-10}$, $n = 3.5$).

2. Simply Supported Plate

Hrudey (1973) has used an iterative approach in order to solve the creep bending problem of simply supported square plates. A finite element idealization, shown in Fig. 9, has been used to predict the creep response. Figures 10 to 12 show a comparison between the present work and both Hrudey's (1973) and Ranlet's (1969) work.

The reader will notice in Figs. 11 and 12 that the present model predicts smaller stresses than those predicted by the previous models. In Hrudey's and Ranlet's work, the steady state creep bending response of the plate has been calculated neglecting the primary creep response of the plate. In the primary creep phase, the creep strain rate is relatively higher than in the steady state which will lead to faster stress relaxation, i.e. lower stresses at the steady state. The numerical results of the present work have indicated that, using equations (18) and (24), the creep bending response of plates will have higher strain rates in the primary phase than in the secondary phase. This has been observed before by Murat (1976).

2.9 Conclusions

An algorithm, to solve the creep bending problem of thick plates, has been presented. The uniaxial creep bending constitutive equation has been extended to multiaxial creep bending state by adapting a flow rule which is similar to the one used in three-dimensional creep problems. The algorithm adapts the initial strain approach in order to solve the resulting nonlinear simultaneous equations. Good agreement has been obtained between the proposed model and available numerical creep models as well as long-term load bearing capacity field data. The present approach together with the flow rule (equations 18 and 24), which has never been used before in creep bending, represent a simple accurate way to solve creep bending problems.

2.10 REFERENCES

Bentson, J., Patel, S.A., and Venkatraman, B., 1966, "Creep Analysis of Circular Plates by Energy Methods", Int. J. Non-linear Mechanics, V1, pp. 81-93.

Hamza, H., Muggeridge, D.B. and Laidley, T., 1981, "Elastic Creep Bending Analysis of Floating Ice Covers", Proc. IAHR, University of Laval, Quebec, Canada.

Hinton, E., Razzaque, A., Zienkiewicz, O.C., and Davies, J.D., 1975, "A Simple Finite Element Solution for Plates of Homogeneous Sandwich and Cellular Construction", Proc. Inst. Civil Eng., V59, Part 2, pp. 43-65.

Hrudey, T.M., 1973, "A Creep Bending Analysis of Plates by the Finite Element Method", Int. J. Solids and Structures, V9, pp. 291-303.

Murat, J.R., 1976, "Axi-symmetric Finite Element Formulation of Non-homogeneous Floating Ice Sheets, Part II: Creep Analysis", Ecole Polytechnique de Montréal, EP 76-R37.

Patel, S.A. and Venkatraman, B., 1962, "Creep Bending of Compressible Plates", Int. J. Mech. Sci., V4, pp. 137 - 146.

Patel, S.A. and Venkatraman, B., 1963, "Creep of Compressible Circular Plates", Int. J. Mech. Sci., V5, pp. 77 - 85.

Ranlet, D., 1969, "Creep Analysis of Square Plates", Polytechnic Institute of Brooklyn, PIBAL Rept. No. 69 - 48.

Stricklin, J.A., Haisler, W. and Reiseman, W., 1973, "Evaluation of Solution Procedures of Material and/or Geometrically Non-linear Structural Analysis", AIAA J., V11, pp. 292-299.

Venkatraman, B., and Hodge, P.G., 1958, "Creep Behavior of Circular Plates", J. Mech. Phys.Solids, V6, pp. 163-176.

Venkatraman, B. and Hodge, P.G., 1964, "A Further Note on the Creep Behavior of Circular Plates", J. Mech. Phys. Solids, V12, pp. 191-197.

Zienkiewicz, O.C., 1971, "The Finite Element Method in Engineering Science", McGraw-Hill, London, Second Edition.

Zienkiewicz, O.C., and Cormeau, I.C., 1974, "Visco-Plasticity - Plasticity and Creep in Elastic Solids - A Unified Numerical Solution Approach", Int. J. Num. Meth. Eng., V8, pp. 821 - 845.

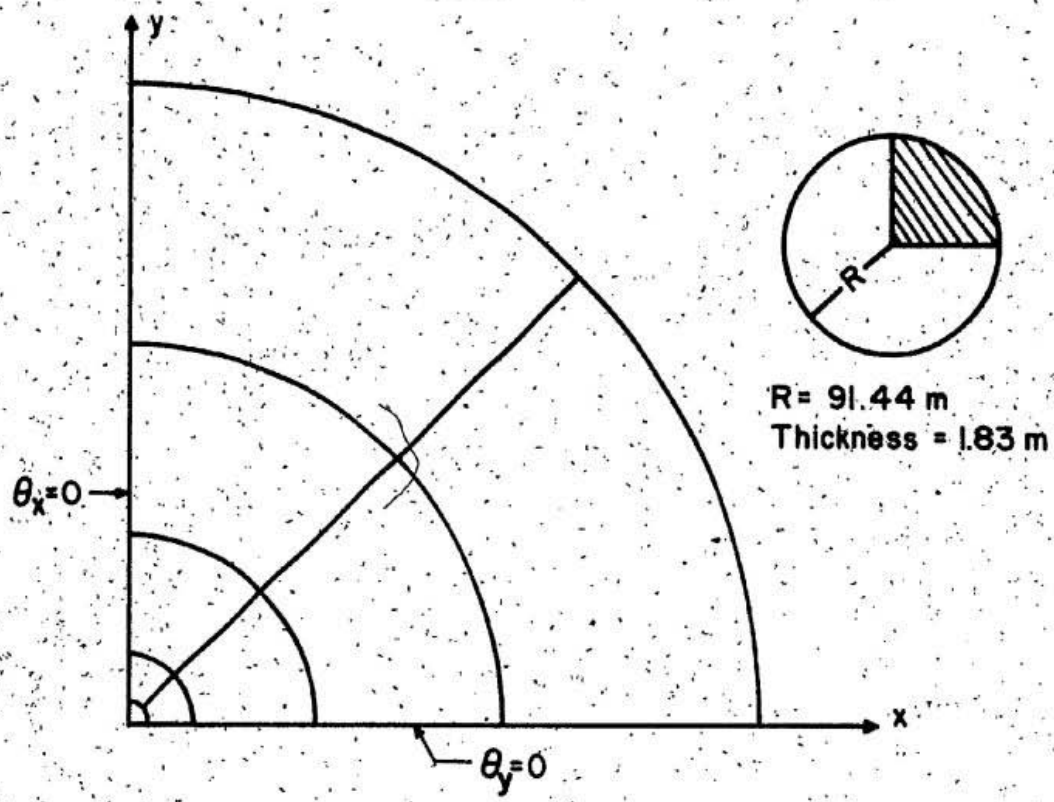

Fig. 7 Finite Element Model for an Infinite Plate on an Elastic Foundation.

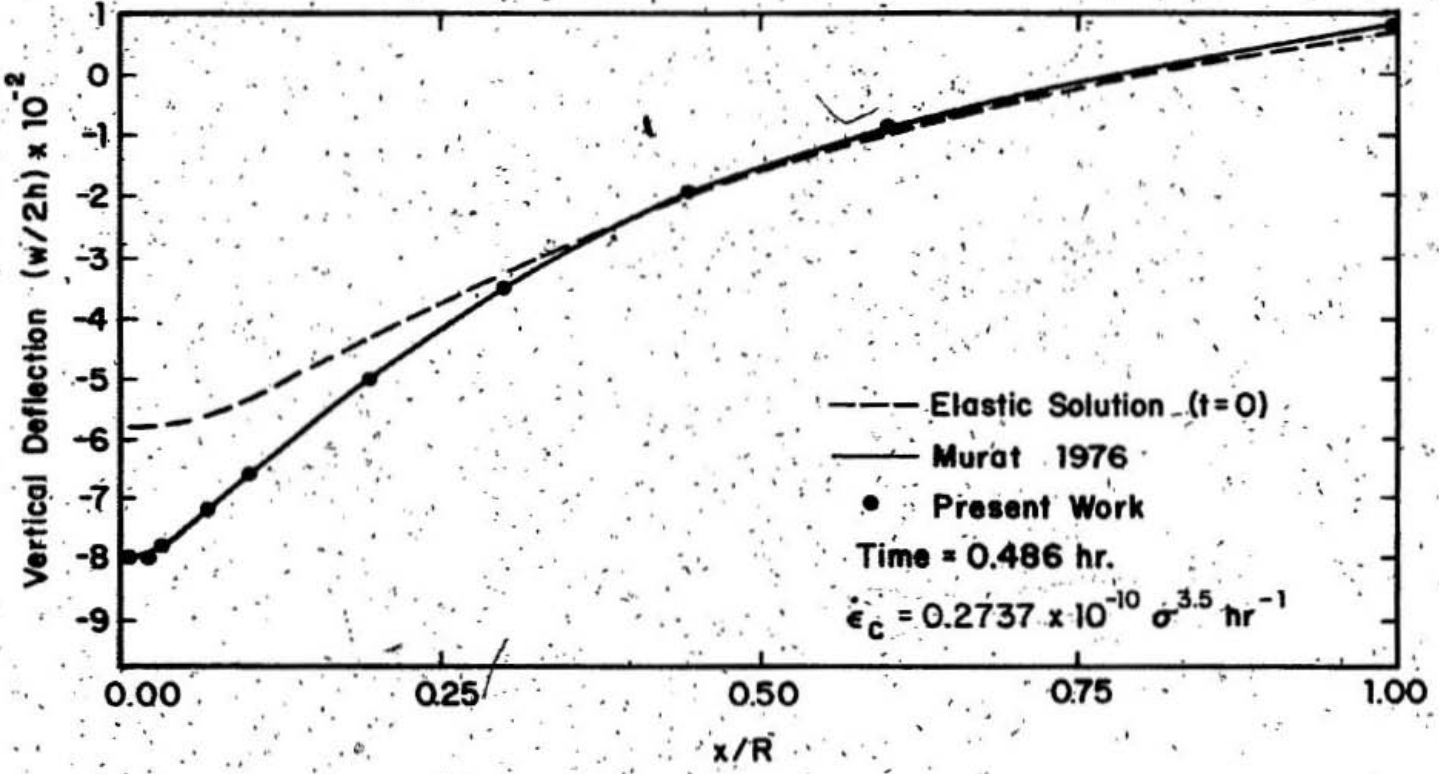

Fig. 8 Elastic and Creep Deflection of an Axi-symmetrically Loaded Infinite Plate on an Elastic Foundation

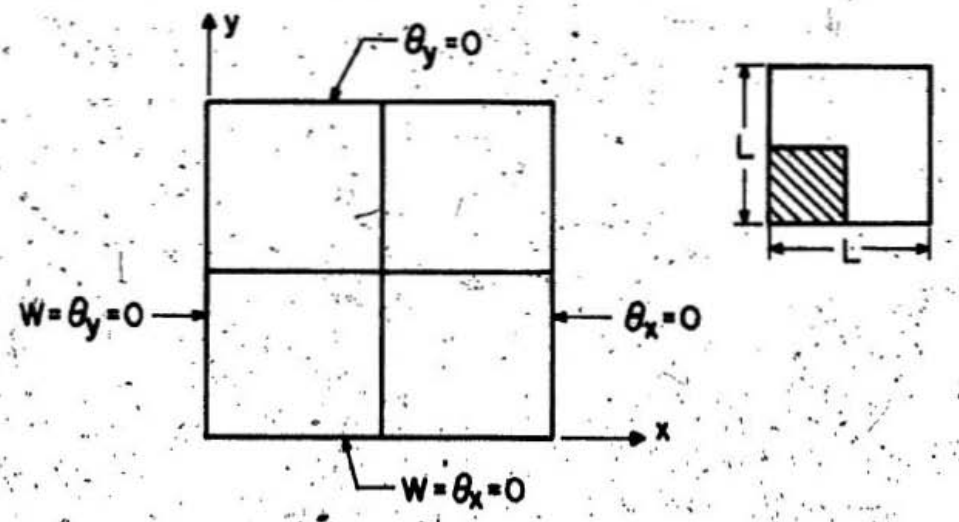

Fig. 9 Finite Element Model of a Simply Supported Square Plate.

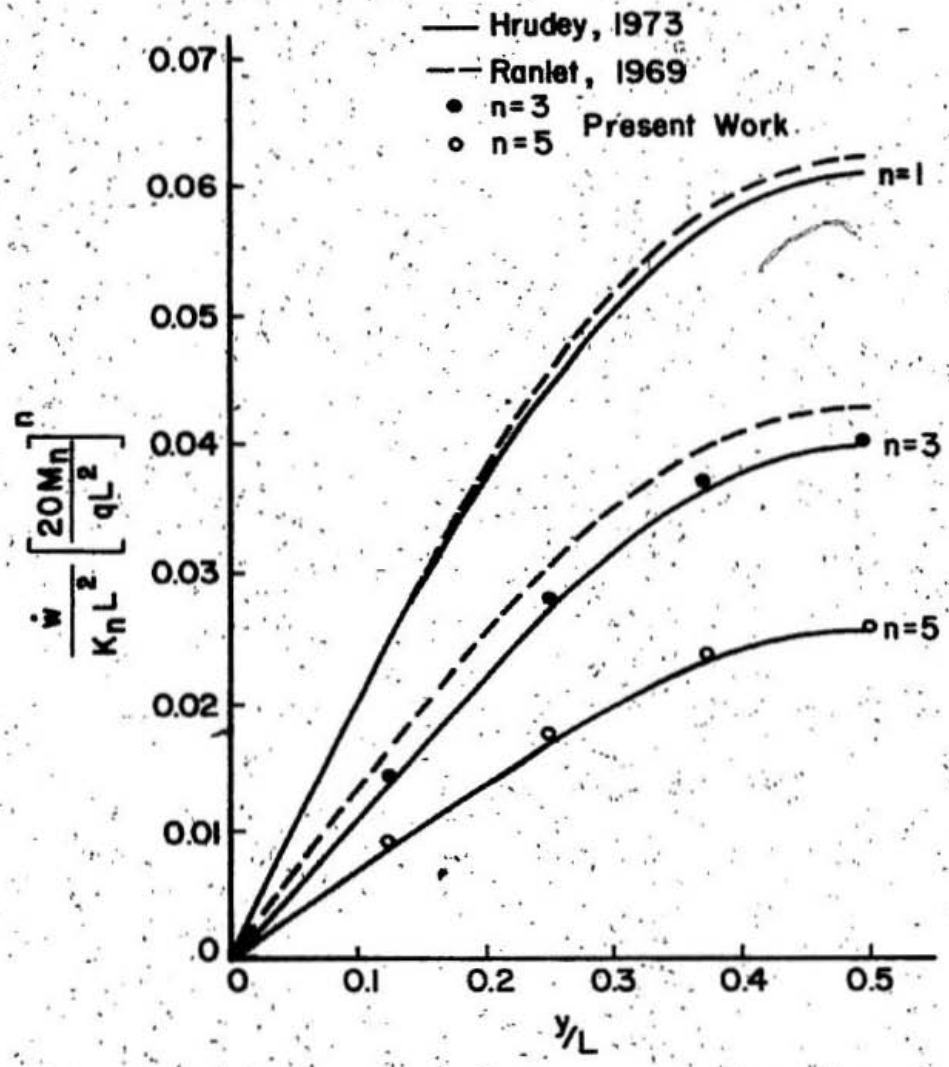

Fig. 10 Rate of Vertical Deflection Along x/L = 0.5, Simply Supported Square Plate Under Uniform Load

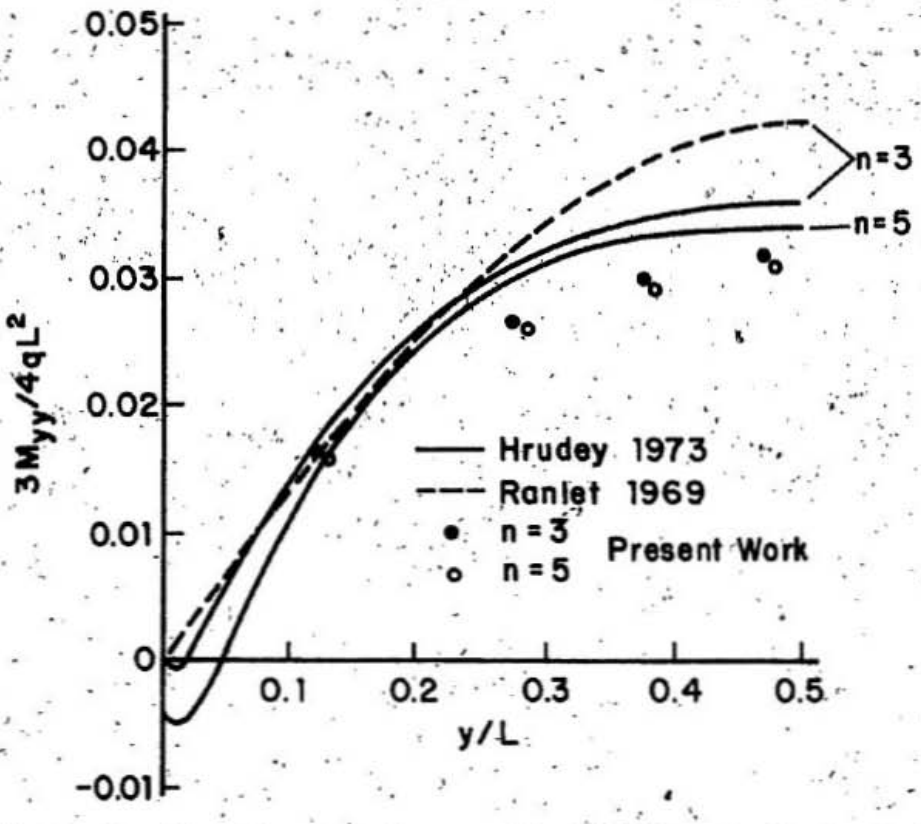

Fig. 11 Bending Moment Along x/L=0.5, Simply Supported Square Plate Under Uniform Load.

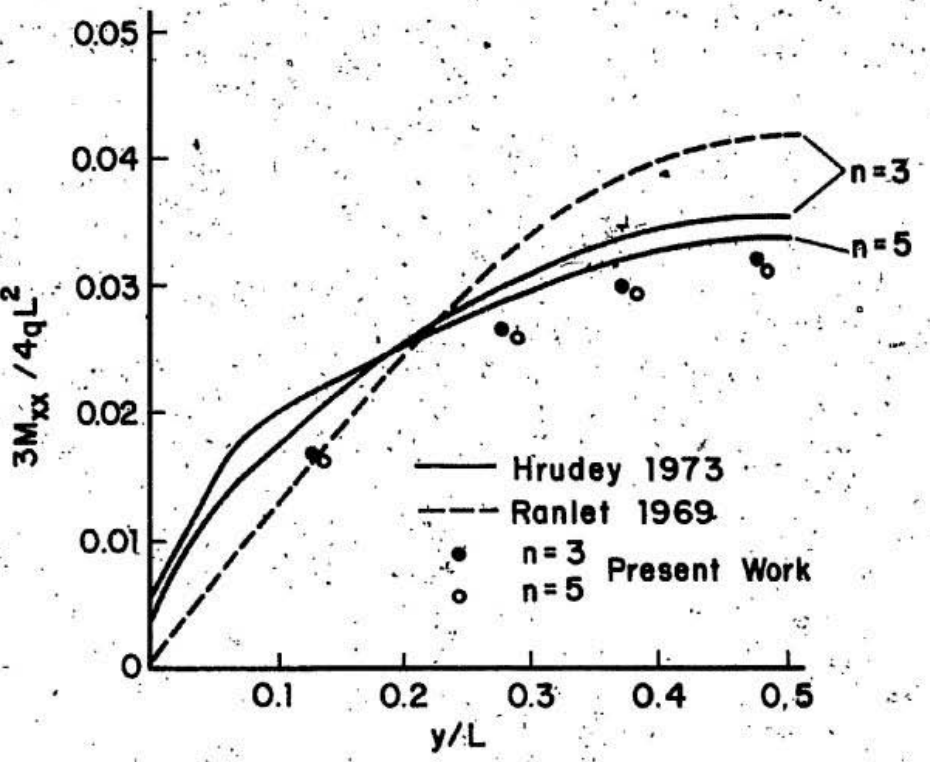

Fig.12 Bending Moment Distribution Along x/L=0.5, Simply Supported Square Plate Under Uniform Load.

3. ELASTIC CREEP BENDING ANALYSIS OF FLOATING ICE COVERS

3.1 Scope

This work will present the experimental results obtained during a prototype long term load bearing capacity test. The numerical results obtained from the creep bending model developed before, have shown good agreement with the experimental data. A simple relation is proposed to predict the subsequent deflection history of an ice cover till the onset of failure. Finally, an equation is presented which is able to predict the time required to reach the onset of failure. The formula has shown good agreement with available field data.

3.2 Introduction

Over the years, ice covers have been used for winter transportation and as landing fields for aircraft. This has created an increasing interest in the mechanical properties of ice and the failure phenomena of ice, under different types of loading.

A careful review to the available literature will indicate that the previous work can be divided into the following categories:

Purely Theoretical

Nevel (1976) has presented a complete theory to predict the long-term response of floating ice covers under a static load. The theory is based on a multi-element viscoelastic model which can predict deflection and stresses as a function of time for a given load. A complete review of the state-of-art is given in the same reference.

Combined Theoretical and Experimental

Experimental and theoretical failure formulae have been developed which lead to an expression for the critical value of an observable quantity, e.g. load, deflection, or maximum strain energy. Kerr (1975) has presented a critical review of the available failure criteria which use different analytical approaches. In a more recent work, Beltaos (1978) has proposed that the maximum value of the strain energy be used as a failure criterion for floating ice covers under any load history. The criterion appears to agree with field experiments in predicting the onset of failure and the final failure of fresh water and sea water ice covers.

Empirical

Formulae based on a field data have been used to predict the subsequent deflection history of ice covers. Beltaos and Lipsett (1978) have proposed a simple equation which can evaluate the complete deflection history after knowing the initial part of the deflection history.

The present chapter will include details of a prototype load bearing capacity test, comparison between the experimental results obtained during this test and the results of a numerical creep bending model developed before, and a simple relation to predict the complete deflection history until the on-set-of failure. An analytical formula is also derived which can predict the time of the onset of failure for a given load configuration and type of ice.

3.3 Experiment

The load bearing capacity test was carried out on Long Pond which is

a fresh water pond located on the North side of the Campus of Memorial University (See Laidley, Laurentius and Hamza, 1980). The site location together with the bathymetery of the pond in the immediate vicinity of the experiment are shown in Fig. 13.

The load used for the experiment was a circular swimming pool, 0.91 m high with a mean diameter of 3.52 m. The total applied load was 72,760 N with a calculated loading rate of 97 N/sec. An array of three strainmeter was placed along a radial line from the load, as shown in Fig. 14, in order to monitor the surface strains during loading the ice cover and during the period of ice cover relaxing due to the creep phenomena. The strainmeters were uniformally positioned along a radial line at distances of 1/2, 2/3 and full characteristic length of the ice cover. The locations of the strainmeters were chosen in order to obtain surface strain histories in the area where the initial failure would probably start. This provided us with data which has allowed us to understand the failure phenomena in bending, evaluate the performance of the strainmeters under these conditions and compare the field data with the theoretical results. A rough estimate of the characteristic length was calculated from Gold's (1965) expression for columnar fresh-water ice of $\ell = 16h^{3/4}$. To avoid using screws in fixing the strainmeter to the ice cover which could introduce cracks, the strainmeter were frozen into the ice cover using sand mounts and slush.

A standard engineer's Dumpy level has been used in measuring the deflection profile of the ice cover. The instrument was set up approximately five times the characteristic length away from the load so that deflection in the ice cover would not influence the consistency of the

horizontal reference plane. The locations of the stations were chosen to be relatively close together near the load and to be further apart as they went away from the load. Measurements indicated that the vertical deflection of the ice cover is almost zero at a distance, away from the load, about four times the characteristic length. During the loading of the ice sheet, deflection profiles were measured every three minutes for the first thirty minutes and thereafter every 15 minutes.

The nearness of the Long Pond site has enabled close observations to be maintained on the ice thickness growth rate and meteorological conditions under which ice formation and growth have occured. Ice thickness measurements were initiated on December 25th and continued until February 18th. An ice growth diary is included in Appendix I.

Two ice cores have been taken on March 4th and used to obtain thin sections for microscopic ice core analysis. All three major ice types (p - primary, s - secondary and t - tertiary) have been identified. Photographs and a sketch of the number of the ice layers and ice types identified are shown in Appendix II.

A record of the vertical temperature profile through the ice sheet was obtained by freezing a thermistor array into the ice.

3.4 Numerical Analysis

a. Deflection History

For instantaneous loading, the total deflection at any time will be assumed to be composed of two components

$$w_t = w_e + w_c \tag{36}$$

where

w_t is the total deflection

w_e is the elastic component of deflection

w_c is the creep component of deflection

The following simple relation is suggested by the author to represent the creep deflection rate of a floating ice cover

$$\dot{w}_c \alpha \left(\frac{p}{h^2}\right)^3 t^{m-1} \qquad o<m<1 \qquad (37)$$

which leads after simple integration to the following expression for the creep deflection

$$w_c = c_2 \left(\frac{p}{h^2}\right)^3 t^m \qquad (38)$$

where

$\dot{w}_c$ is the creep rate of deflection

w_c is the creep component of deflection

p is the total applied load

h is the ice cover thickness

t is the time

c_2 is a function of ice cover thickness and temperature

Expressing the elastic deflection component in similar fashion, the total deflection will have the following form:

$$w_t = c_1 \left(\frac{p}{h^2}\right) + c_2 \left(\frac{p}{h^2}\right)^3 t^m \qquad (39)$$

where c_1 is a function of the elastic modulus, temperature and the ice cover thickness.

The reader will notice that the values of both c_1 and c_2 will be determined using a simple procedure for every problem without the need to derive the exact mathematical form of any of c_1 and c_2.

The assumption of instantaneous loading is a pure theoretical one. In actual field operation, loading usually is of a ramp type. The actual deflection during the loading phase will be greater than for instantaneous loading depending on the rate of loading. In order to approximate the actual problem, the load will be assumed to be applied instantaneously and then kept constant over a period of time t_e, where t_e is the loading time. This will lead to the following expression for the total deflection at the end of the loading

$$w_t = c_1\left(\frac{p}{h^2}\right) + c_2\left(\frac{p}{h^2}\right)^3 t_e^{\,m} \qquad (40)$$

The formula of the total deflection for a ramp loading, at any time $t > t_e$, will have the following form:

$$w_t = c_1\left(\frac{p}{h^2}\right) + c_2\left(\frac{p}{h^2}\right)^3 t_e^{\,m} + c_2\left(\frac{p}{h^2}\right)^3 (t-t_e)^m \quad \text{for} \quad t > t_e \qquad (41)$$

The constants c_1 and c_2 will be evaluated from the initial part of the deflection history. This curve fitting process should be done for each field operation.

b. Time of the Onset of Failure

Similar analysis will be carried out in this section in an attempt to predict the time required to reach the onset of failure of an ice cover. Following a similar assumption, the total work done by the external loads on the ice cover will be divided into two separate components as follows:

$$E_t = E_e + E_c \tag{42}$$

$$= kpw_e + pw_c \tag{43}$$

where

E_t is the total work done

E_e is the work done during loading

E_c is the work done after loading.

k is a constant which depends on the rate of loading.

k = 0.5 for instantaneous loading

= 0.55 - 0.75 for ramp loading

The work done during loading can be obtained by substituting equation 40 into the expression for E_e in equation 42.

$$E_e = 0.5\, p\, c_1 \left(\frac{p}{h^2}\right) \left[1 + \frac{2c_2}{c_1} \left(\frac{p}{h^2}\right)^2 t_e^{\,m}\right] \tag{44}$$

This will give the value of k to be

$$k = 0.5 \left[1 + \frac{2c_2}{c_1} \left(\frac{p}{h^2}\right)^2 t_e^{\,m}\right] \tag{45}$$

It should be noted that the second term in the above equation can be thought of as a correction factor to account for the effect of the rate of loading.

The work done by the reaction forces (fluid elastic foundation) has been calculated by Beltaos (1978) to equal

$$E_R = 0.25\, p\, (w_e + w_c) \tag{46}$$

where E_R is the work done by reaction forces. Subtracting equation 46 from equation 43 will give the net stored potential energy in the floating

ice cover as

$$E_n = (k-0.25)\, p\, w_e + 0.75\, p\, w_c \qquad (47)$$

At the onset of failure, the net stored potential energy in the floating ice cover should equal to the critical value proposed by Beltaos (1977)

$$E_n\Big|_{oF} = c_{oF}\, h^{5/2} \quad (c_{oF} = 331\ \text{KN.m.m}^{-2.5}) \qquad (48)$$

Equating equation 48 with equation 47 we will give an estimate to the time required to reach the onset of failure

$$t_{oF} = \left[\frac{c_{oF}\, h^{5/2} - (k-0.25)\, p w_e}{0.75\, c_2 p\, (\frac{p}{h^2})^3}\right]^{1/m} + t_e \qquad (49)$$

If we consider the work done by the external forces instead of the net stored potential energy, equation 49 will have the following form:

$$t_{oF} = \left[\frac{c_{oF}\, h^{5/2} - k\, p w_e}{c_2 p\, (\frac{p}{h^2})^3}\right]^{1/m} + t_e \qquad (50)$$

It is worthwhile to point out that the above formulae can not be used to predict the time required to reach the complete failure. Any attempt to do that using equation 49 or 50 will over estimate the time. This can be explained by the fact that the deflection rate after the onset of failure will be much higher than that predicted by equation 37.

c. Temperature Dependency

It was mentioned earlier that both c_1 and c_2 are temperature dependent which will lead to the fact that t_{oF} will also be temperature dependent.

This dependency may have the following form:

$$c_1 = c_1' \exp(-Q/RT) \quad (51)$$

$$c_2 = c_2' \exp(-Q/RT) \quad (52)$$

where

Q is the activation energy ($Q = 66.9$ kJ.mol^{-1})

R is the gas constant

T is the absolute temperature

c_1', c_2' are functions of ice cover thickness and modulus of elasticity

Finally, it should be mentioned that estimating t_{oF} using the previous analysis will give an upper bound to the actual time. Since it is well known that ice covers may suffer from cracking activity during the primary and secondary creep phases, which will lead to a higher effective creep rate, it is recommended that the theoretically estimated time should be reduced to about 0.8 of its value in order to predict the actual time for a certain field operation.

3.5 Comparison with the Field Data

The last task in this work is to compare the collected field data with the proposed and available numerical models. The collected data includes elastic deflection profiles, deflection profile histories and surface strain histories at three selected locations.

a. Deflection Measurement

Assuming that the total deflection after completion of loading is an elastic deflection, a reasonable agreement (see Fig. 15) between the

finite element elastic results and the field data was obtained using the following values

$$\nu = 0.333$$

$$E = 3.4 \times 10^{6} \text{ kN m}^{-2}$$

Using the results of the elastic analysis as an initial condition for the creep analysis, the creep bending model was used to predict the time response of the ice cover, Figs. 16 and 17 show good agreement between the numerical results and the field data. The best curve fit between the finite element results and field data was obtained using the following relation:

$$\dot{\varepsilon}_c = 5.0 \times 10^{-12} \sigma^3 \quad \text{min}^{-1} \tag{53}$$

where the stress, σ, has the units, kNm^{-2}

The reader will notice that there is one field data point in each of Fig. 15 and Fig. 16 which is deviated from both the finite element solution and other field data points. The author believes that there was an error in measuring the vertical deflection at these two points.

b. Surface Strain History

The strainmeter outputs, recorded on a Rustrak chart recorder, are reproduced in Figure 18 and correlated with the load history. The relative position of the strainmeters can be seen in Figure 14. However, the output of strainmeter J4 is not shown. This is because a misalignment of the LVDT core caused a frictional problem within the instrument and although the output did exhibit the same general strain patterns as instruments of J3 and J5, no meaningful quantitative measurements could be obtained from its record. The strainmeter records have only been re-

produced for the first 3 1/2 hours since no significant change in the strainmeter outputs were recorded after this time. The asymptotic values of strain were reached after approximately 40 minutes for strainmeter J5 and after 160 minutes for J3. The maximum values of the surface strains, recorded at these times, were 65 micro strain for J3 which was positioned 2.51 m from the centre of the load and 30 micro strain for J5, located 7.65 m from the centre point. A theoretical estimate of the magnitude of the surface strain may be obtained by using the geometrical definition of strain:

$$\varepsilon = \frac{h}{2} \frac{1}{R} \tag{54}$$

where

ε is the surface strain

h is the ice sheet thickness,

R is the radius of curvature of the ice surface.

For the elastic portion of the test, this may be evaluated utilizing Wyman's (1950) solution where:

$$\frac{1}{R} = \frac{\partial^2 w}{\partial r^2} \tag{55}$$

This has been done and the results shown in Figure 19 with the position of strainmeters J3 and J5 also indicated.

According to Figure 19, during the loading process the ice surface under J3 should be in compression and the surface under strainmeter J5 in tension. The strainmeter records shown in Figure 6 show that this is what occurs. Strainmeter J5 is undergoing tension from the start and the discontinuities due to cracking of the ice sheet are tensile events. At the commencement of loading, strainmeter J3 starts to undergo compression,

is then affected by the cracking of event 1 and suffers a tensile shift, then continues to experience compression. However, once loading has been completed, both strainmeters record only surface tensile strains.

The theoretical values of the elastic surface strain at the mid-point of the strainmeter's gauge lengths are +12 microstrain for J5 (tensile) and -42 microstrain for J3 (compressional). To compare these values with the experimental data it is necessary to correct the recorded values to compensate for the effects of the ice cracking induced discontinuities. For strainmeter J5 all discontinuities are tensile and therefore must be subtracted from the measured strain values to obtain that portion due to the elastic part alone. The same type of procedure must be used for strainmeter J3. However, the ice beneath this instrument is in compression and thus all tensile crack discontinuities must be added to the measured strain values. The crack discontinuity identified as event #2 on the J3 record is the only compressive discontinuity measured once the test began and therefore its contribution must be subtracted from the J3 value.

Using this procedure, the measured elastic surface strain values were +15 microstrain for J5 and -20 microstrain for J3. The J5 calculated and measured values agree well, but the J3 values do not. This may be due to the large strain gradient that exists within one characteristic length of the load. The use of a guage length of 1 m may be too large to obtain accurate measurements of strain close to the load, due to linear averaging across a highly non-linear strain gradient.

c. Time of Onset of Failure

In order to check the numerical analysis presented in a previous section which predicted the time of the onset of failure, an attempt was made to compare the model with independent field data published by Beltaos (1977). First an attempt was made to get a reasonable curve fit between equation 41 and the field data. Good agreement has been obtained using the following values

$$m = 0.66$$

$$c_2 = 0.3447 \times 10^{-12}$$

for a loading time of approximately 24 minutes, and substituting the above values for m and c_2 in equation 49, we get

$$t_{oF} = 88.8 \text{ min.}$$

This value is in excellent agreement with the actual value which is approximately 90 minutes. If equation (50) is used instead, we get

$$t_{oF} = 89.9 \text{ min.}$$

which is again in excellent agreement with the field data.

3.6 Ice Cracking

The event markers in Figure 18 indicate the times as which significant events occurred along the load bearing test. Other than event #0 at which time the pool loading commenced, all other events relate to cracking of the ice sheet in the vicinity of the load was heard, but not seen, at times noted as events #1, #2, #3 and #5. The strainmeter records support this by indicating discontinuities at the first three of

these events but not for event #5. Event #4 shows a minor discontinuity in both strainmeters, but no ice cracking was recorded at the time of this event.

As discussed in section 3.4, once the test began, all recorded cracking activity except event #2 near J3 showed the tensile release of stress and the creation or further opening of existing cracks. The exception as recorded by J3 indicates that there must have been at least two cracks since the ice under J3 underwent compression while J5 simultaneously recorded a tensile event.

3.7 References

Beltaos, S., (1978), "A Strain Energy Criterion for Failure of Floating Ice Sheets" Can. J. Civ. Eng., V. 5(3), pp. 352-361.

Beltaos, S. and Lipsett, A.W., (1978), "An Empirical Analysis of the Creep of Floating Ice Sheets". Workshop on the Bearing Capacity of Ice Covers. NRC ACGR Tech. Memo. No. 123, pp. 124-158.

Gold, L.W., (1965), "The Initial Creep of Columnar Grained Ice. Pt. I: Observed Behavior. Pt. II: Analysis, Can. J. Phys., V43, pp. 1434.

Kerr, Arnold D., (1975), "The Bearing Capacity of Floating Ice Plates Subjected to Static or Quasi-Static Loads - A Critical Survey." CRREL Research Report No. 333, March, 1975.

Laidley, T.E., Laurentius, T.B. and Hamza, H., (1980), "A Load Bearing Capacity Test on a Freshwater Ice Cover", C-CORE, Memorial University of Newfoundland, Tech. Rept. 80-8.

Nevel, D.E., (1976), "Creep Theory for a Floating Ice Sheet", CRREL, Special Report 76-4.

Wyman, M., (1950), "Deflections of an Infinite Plate". Can. J. Res. A. 28, pp. 293-302.

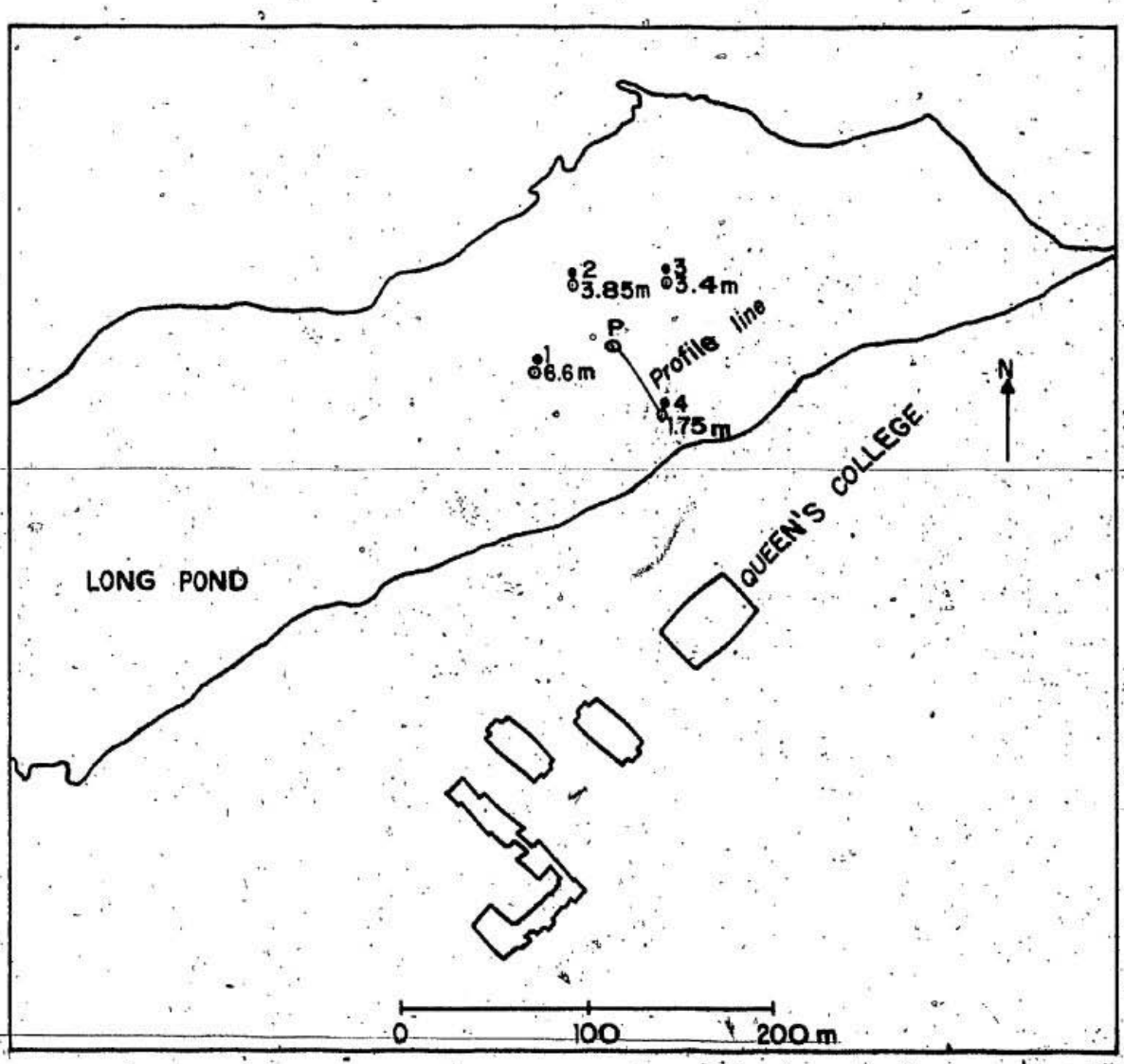

Fig. 13 Experiment location.

LAYOUT OF LOAD SITE

Load Diameter - 3.52m

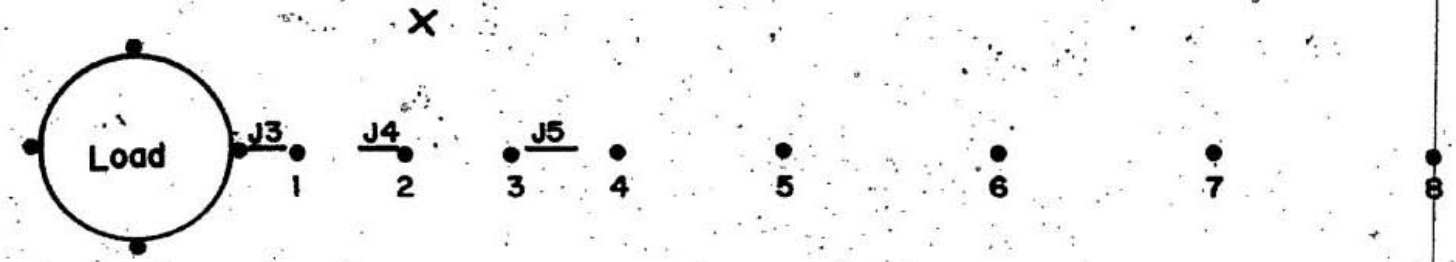

× Position of Thermistor Array

— Position of Strainmeters

• Points at which Deflections were measured

Position	Distance from ℄ load (m)
Thermistor	6
Strainmeter J3	2.51
Strainmeter J4	4.57
Strainmeter J5	7.56
Point 1	3
2	5
3	7
4	9
5	12
6	16
7	20
8	24

Scale 1:125

Fig. 14 Equipment configuration.

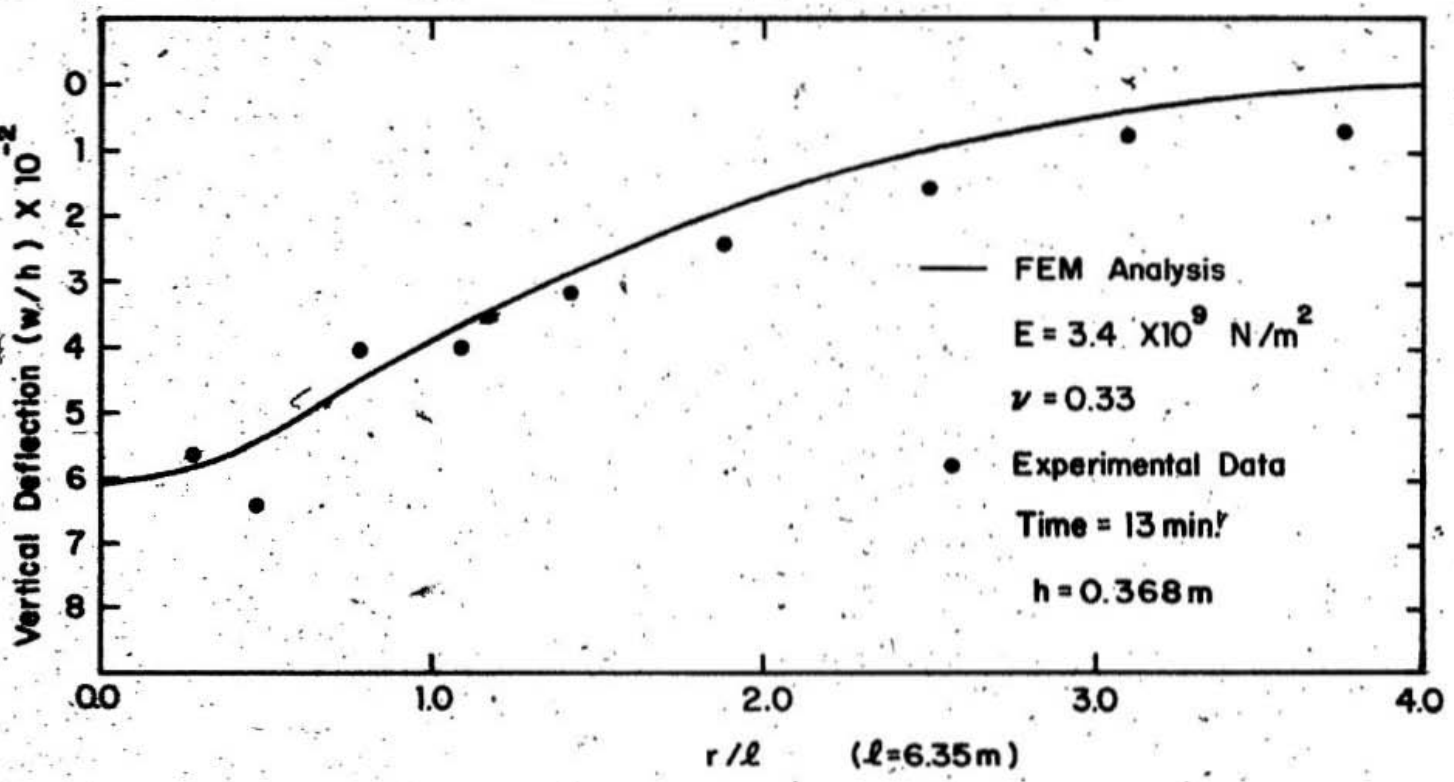

Fig. 15 Elastic deflection profile of ice cover.

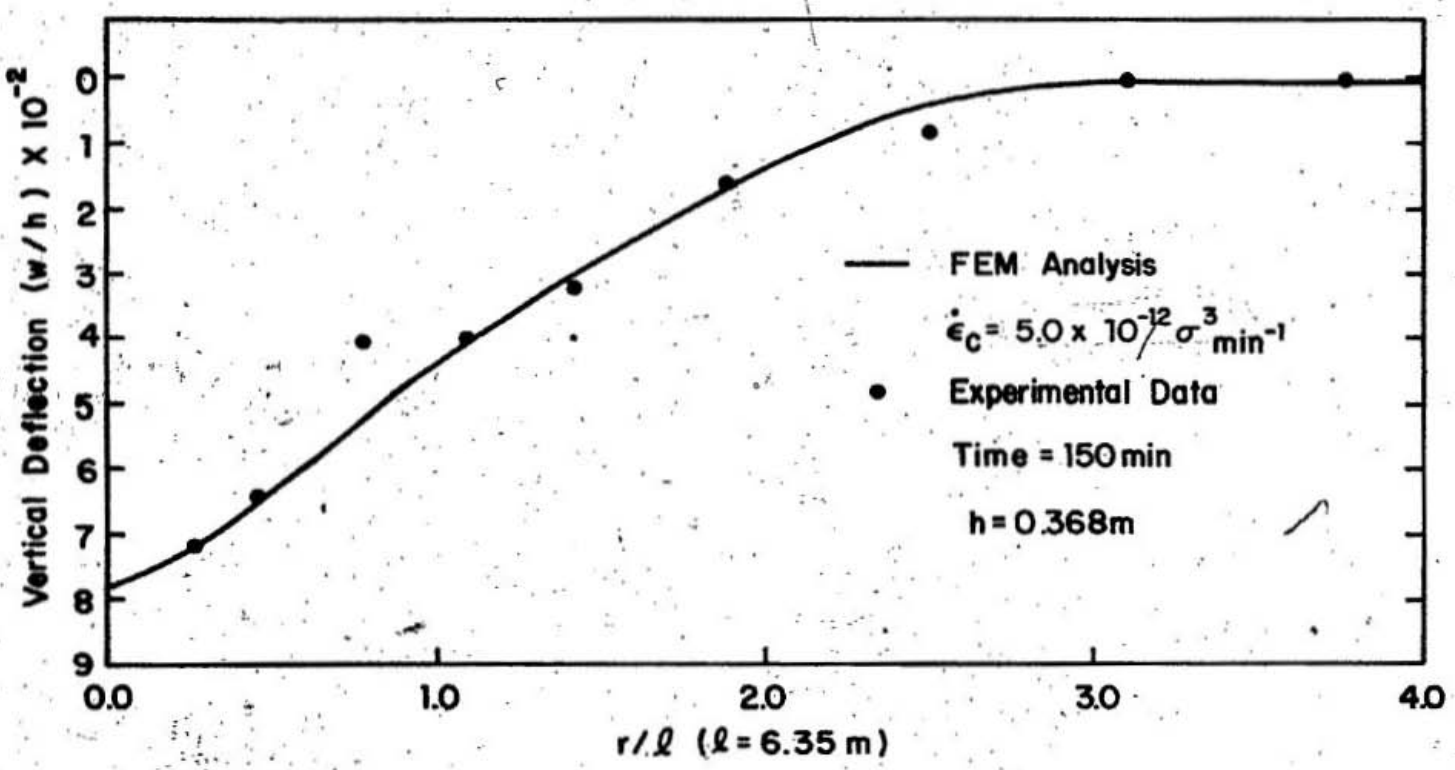

Fig. 16 Creep deflection profile of ice cover.

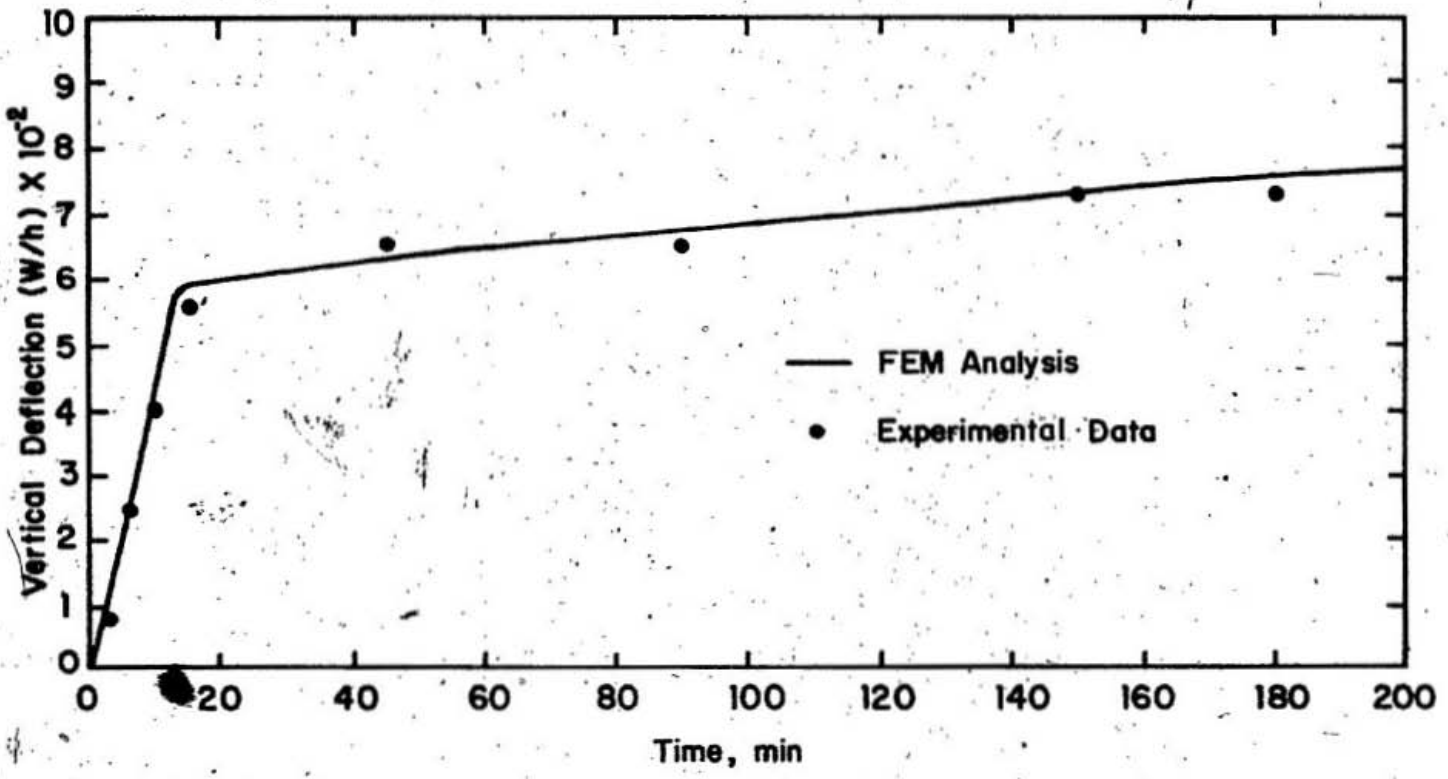

Fig. 17 Deflection history of ice cover at the load.

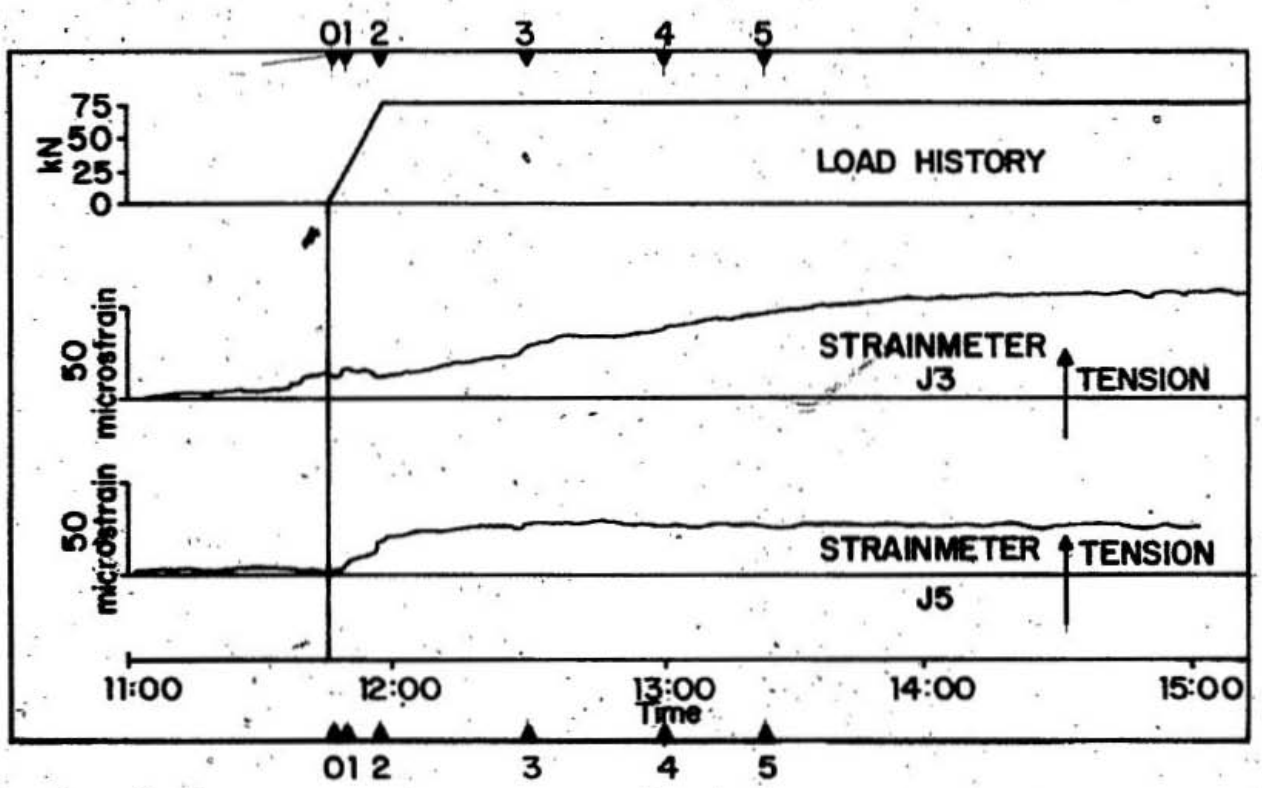

Fig. 18 Surface strain history.

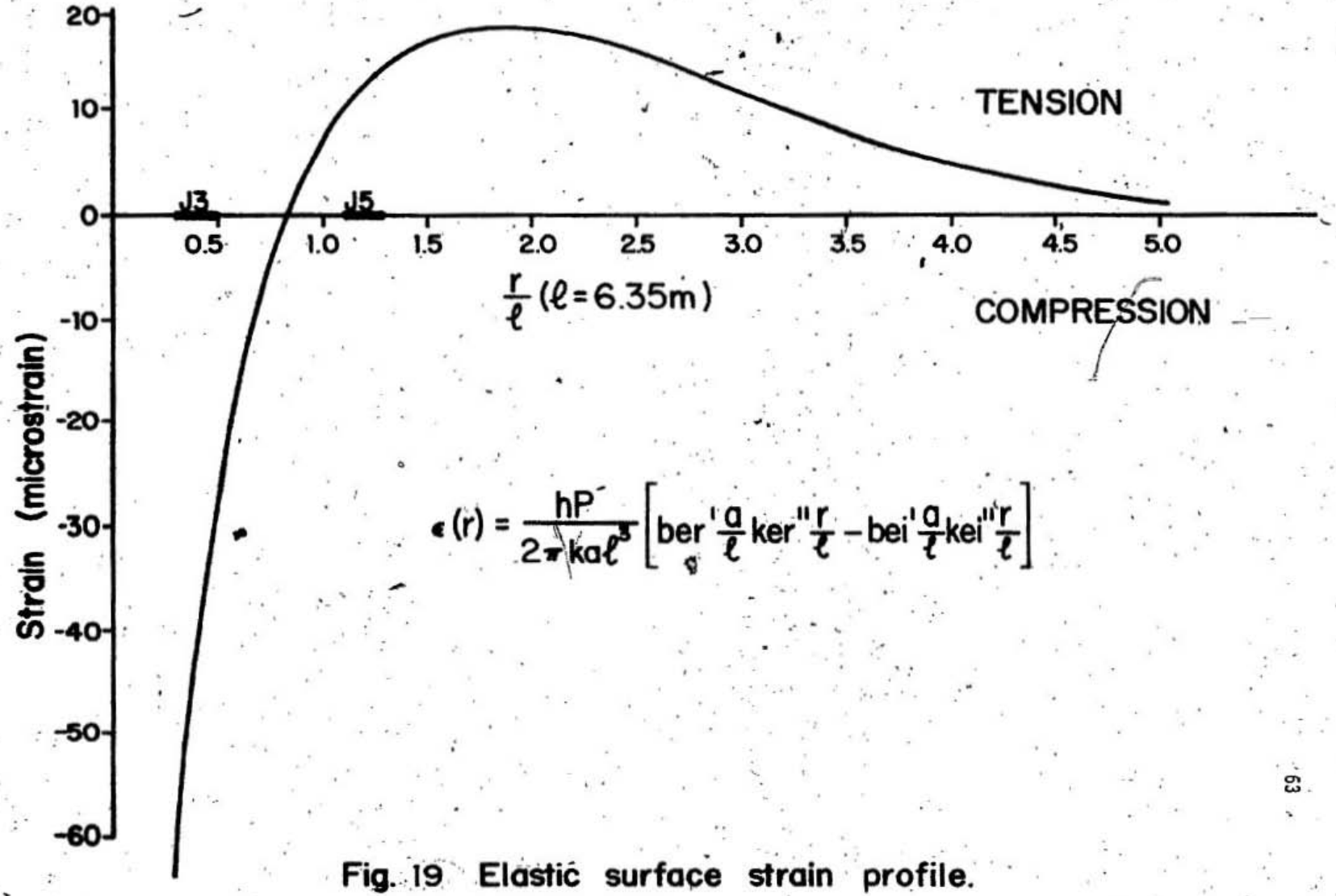

Fig. 19 Elastic surface strain profile.

4. RESPONSE OF VISCOELASTIC MATERIALS UNDER DIFFERENT LOADING CONDITIONS

4.1 Scope

This work is concerned with the formulation of the response of homogeneous, isotropic and linearly viscoelastic materials under uniaxial constant cross-head speed loading conditions. The procedure can be used, after minor changes, to calculate the viscoelastic response due to constant stress rate or constant strain rate loading conditions. The finite element method is then used to extend the present formulation to multiaxial state of stresses. The finite element model can predict the general viscoelastic response of ice due to the interaction with any other domain, e.g. testing machine or offshore structure. The model proves theoretically that the apparent yield stress of the ice due to constant strain rate or constant cross-head speed loading is due to the fact that the generated strain rate in the specimen exceeds the strain rate applied by the testing machine. Finally, the procedure is used to provide a deeper insight into the viscoelastic response of cracked three-point bend test specimens due to constant cross-head loading.

4.2 Introduction

Many engineering materials have shown a behaviour that depends on the type and rate of loading. Ice is a typical material which can respond as an elastic (brittle) or ductile (plastic) material depending on the rate and type of loading. Many investigators have studied the material properties of ice (mode of failure, elastic modulus, yield stress) as a function of temperature and rate of loading. A good review can be found

in Weeks and Assur (1967) and Schwarz and Weeks (1977).

Investigators have found that ice will fail in a brittle mode of failure if the rate of loading is relatively high with higher apparent stress of failure. However the mode of failure will change considerably as the rate of loading decreases till it becomes a ductile mode of failure for relatively very low rates of loading. It was observed, also, that ice will have an apparent lower yield stress at those low rates of loading.

It was demonstrated by Sinha (1979 a,b) that loading a compression test specimen under constant cross-head speed will lead to an increasing effective strain rate which will reach the nominal strain rate at or close to the apparent yield stress. He showed, also, that stiffer testing machines will result in an effective higher stress rate and the failure will tend to be brittle or premature, while less stiff testing machines will result in lower stress rates and apparent ductile yield failures. A comprehensive experimental program is usually necessary to predict the effect of the rate of loading on certain material properties.

In the present chapter, a numerical procedure will be presented (see Hamza and Muggeridge, 1981) which will enable us to predict the dependency of the mode of failure, elastic modulus and yield stress on the rate of loading and test temperature. Using the finite element method together with the incremental initial strain approach, the procedure will be generalized to a multi-axial state of stress. Finally, the procedure will be used to provide a deeper insight into the visco-elastic response of a cracked three point bend specimen due to a constant cross-head speed loading condition.

4.3 Creep Under Varying Stresses

In order to extend the uniaxial creep law to a multi-axial creep model under general loading, two ingredients are required: A flow rule to extend the uniaxial law to multi-axial loading situations, and a hardening rule for varying stresses and temperature.

In the following analysis, a Norton power law will be used which, under uniaxial stress, has the following form

$$\dot{\varepsilon}_c = \dot{\varepsilon}_n \left(\frac{\sigma}{\sigma_n}\right)^n \tag{56}$$

Where n is a scalar constant, $\dot{\varepsilon}_n$ is a constant with the dimensions of rate of deformation, σ_n is a constant with the dimensions of stress, $\dot{\varepsilon}_c$ is the creep strain rate, and σ is the applied stress.

Assuming, the material is isotropic and incompressible, and creep does not occur under hydrostatic stresses, the flow rule will have the following form

$$\dot{\varepsilon}_{c_{ij}} = \frac{3}{2} \left(\frac{\varepsilon_n}{\sigma_n}\right) \sigma_e^{n-1} \, S_{ij} \tag{57}$$

where σ_e is the effective stress and is defined by

$$\sigma_e^2 = \frac{3}{2} S_{ij} \cdot S_{ij} \tag{58}$$

S_{ij} is the stress deviator and is defined by

$$S_{ij} = \sigma_{ij} - \frac{1}{3} S_{ij} \sigma_{kk} \tag{59}$$

There are three existing hardening rules in the literature: A time hardening rule; a strain hardening rule and a modified superposition principle, of these the strain hardening and modified superposition have been found to better represent the experimental results.

In the present work, the strain hardening rule will be used. It may be expressed, for the uniaxial case, in the following form

$$\dot{\varepsilon}_c = \varepsilon_n \left(\frac{\sigma}{\sigma_n}\right)^n \varepsilon_t^p \qquad (60)$$

where σ is the current stress, ε_t is the current total strain, $\dot{\varepsilon}_c$ is the current creep strain rate and n, p are constants.

4.4 Constant Cross-head Speed Loading

4.4.1 Formulation

Let us assume that the increment in the total strain at any moment can be divided into two separate components as follows

$$\Delta\varepsilon_t = \Delta\varepsilon_e + \Delta\varepsilon_c \qquad (61)$$

where

$\Delta\varepsilon_t$ is the total strain increment

$\Delta\varepsilon_e$ is the elastic strain increment

$\Delta\varepsilon_c$ is the creep strain increment

In the present analysis we will distinguish between two types of elastic modulus. The first one is the material elastic modulus, E, which is a material property and is constant. The second one is the effective or apparent modulus E_e which decreases as the test progresses and has a maximum value equal to E at the beginning of the test and a minimum value at or close to the ultimate stress. It will be assumed, also, that the elastic strain increment is persistently related to the stress increment through the material elastic modulus E.

Since the present problem is a nonlinear one, an incremental approach

will be adapted in solving the controlling equations. The test time period will be divided into time increments during which the stress will increase by $\Delta\sigma$ and the creep strain rate will be assumed to remain constant.

At time t_m and during the time interval Δt_{m+1}, the stress rate will have the value

$$\dot{\sigma}_{m+1} = E_{e_m} (V/L) C_{F_m} \qquad (62)$$

where

$\dot{\sigma}_{m+1}$ is the stress rate during Δt_{m+1}

E_{e_m} is the effective elastic modulus at t_m

$C_{F_m} = K_e / (K_{s_m} + K_e)$

K_e is the stiffness of the testing machine and supporting accessories

K_{s_m} is the stiffness of the specimen at t_m

$= E_{e_m} A/L$ (for compression or tensile test)

V is the cross-head speed

L is the specimen initial length

The total strain rate during Δt_{m+1} may be calculated from

$$\dot{\varepsilon}_{t_{m+1}} = \frac{\dot{\sigma}_{m+1}}{E} + \frac{\dot{\varepsilon}_n}{\sigma_n^n} (\sigma_{m+1})^n \varepsilon^p_{t_m} \qquad (63)$$

The effective modulus of elasticity may be calculated from

$$E_{e_{m+1}} = \frac{\dot{\sigma}_{m+1}}{\Delta\varepsilon_{t_{m+1}}} \Delta t \tag{64}$$

The total strain at the end of the time increment Δt_{m+1} will be

$$\varepsilon_{t_{m+1}} = \varepsilon_{t_m} + \dot{\varepsilon}_{t_{m+1}} \Delta t \tag{65}$$

The same steps will be repeated for t_{m+1}.

The reader will notice that the above procedure can be used for constant stress rate or constant strain rate loading if $\dot{\sigma}_{m+1}$ or $\dot{\varepsilon}_{t_{m+1}}$, respectively, have been kept constant during the test. This will lead to a decreasing cross-head speed in the case of constant strain loading and to an increasing cross-head speed in the case of constant stress rate loading.

The reader should recognize the fact that the maximum value for $\dot{\varepsilon}_{t_{m+1}}$ which the test machine can apply to the test specimen due to constant cross-head speed loading will have the following value:

$$\dot{\varepsilon}_{t_{m+1}}\Big|_{max} = V/L \tag{67}$$

Upon reaching this maximum value, the loading condition will change to a constant strain rate loading condition.

4.4.2 Temperature Effect

The temperature effect on the viscoelastic response will be incorporated into the creep component of the strain. Sinha (1978 a, b) has suggested the following dependency.

$$\left(\frac{\dot{\varepsilon}_n}{\sigma_n^n}\right) = C_1 \exp - (Q/RT)$$

Where

C_1 is a constant

Q is the activation energy

R is the gas constant

T is the absolute test temperature

4.4.3 Finite Element Procedure

In this section, in order to generalize the previous procedure, a finite element formulation is presented. The initial strain approach has been adapted to solve the nonlinear problem of creep under varying stresses, (Zienkiewicz, 1971). The algorithm leads to incremental equations of deformation. Assuming that at time t_m, the state of stress and strain is $\{\sigma\}_m$ and $\{\varepsilon\}_m$, the algorithm is as follows (symbols have the same meaning as in Chapter 2):

1 - For the time increment Δt_{m+1}, calculate the corresponding change in the applied load $\{\Delta p\}_{m+1}$, then solve the following problem.

$$[K]\{\Delta q\}_{m+1} = \{\Delta p\}_{m+1} \tag{68}$$

2 - Calculate the corresponding changes in the strain and stress vectors.

$$\{\Delta\varepsilon\}^1_{m+1} = [B]\{\Delta q\}_{m+1} \tag{69}$$

$$\{\Delta\sigma\}^1_{m+1} = [E]\{\Delta\varepsilon\}_{m+1} \tag{70}$$

3 - Update the strain and stress vectors

$$\{\sigma\}^1_{m+1} = \{\sigma\}_m + \{\Delta\sigma\}^1_{m+1} \tag{71}$$

$$\{\varepsilon\}^1_{m+1} = \{\varepsilon\}_m + \{\Delta\varepsilon\}^1_{m+1} \tag{72}$$

4 - Compute the creep strain from

$$\Delta\varepsilon_{c_{m+1}} = c(\sigma^1)^n_{m+1}\ \varepsilon^p_m\ \Delta t_{m+1} \tag{73}$$

5 - Calculate the effective load from

$$\{\Delta R\}_{m+1} = \int_A [B]\ [E]\ \{\Delta\varepsilon_c\}_{m+1}\ dA \tag{74}$$

6 - Compute the change in the displacement vector due to the effective load.

$$\{\Delta q\}_{c_{m+1}} = [K]^{-1}\ \{\Delta R\}_{m+1} \tag{75}$$

7 - Compute the change in the strain and stress vectors.

$$\{\Delta\varepsilon\}_{m+1} = [B]\ \{\Delta q\}_{c_{m+1}} \tag{76}$$

$$\{\Delta\sigma\}_{m+1} = [E]\ \{\Delta\varepsilon\}_{m+1} - \{\Delta\varepsilon\}_{c_{m+1}} \tag{77}$$

8 - Update the strain and stress vectors.

$$\{\varepsilon\}_{m+1} = \{\varepsilon\}^1_{m+1} + \{\Delta\varepsilon_c\}_{m+1} \tag{78}$$

$$\{\sigma\}_{m+1} = \{\sigma\}^1_{m+1} + \{\Delta\sigma\}_{m+1} \tag{79}$$

9 - Go to (1) for the next time increment

The reader will notice that the finite element procedure is quite general and it can be used for any type of loading condition with minor changes and for two and three dimensional and plate bending problems.

4.5 Analysis of a Three-point Bend Test Specimen

In this section an analysis using the previous procedure will be developed for the cracked three-point bend test specimen. The purpose of this analysis is to provide a deeper insight into the effect of different parameters on the viscoelastic response and apparent strength of the test specimen in order to be able to predict in advance whether the specimen will respond in a brittle or ductile manner and select an adequate failure criterion and fracture toughness parameter. The following relations will be used in the analysis (Tada et al, 1973):

$$K_1 = \sigma\sqrt{\pi a}\, F_1\left(\frac{a}{w}\right) \tag{80}$$

$$\delta = \frac{4\sigma a}{E} F_2\left(\frac{a}{w}\right) \tag{81}$$

$$x_{total} = x_{no\ crack} + x_{crack} \tag{82}$$

$$x_{crack} = \frac{\sigma S}{E} F_3\left(\frac{a}{w}\right) \tag{83}$$

where

$$\sigma = \frac{3PS}{2wh}$$

P is the applied load

S is the span of the specimen

w is the specimen width

h is the specimen thickness

a is the crack length

K_1 is the stress intensity factor in the opening mode (mode I) (Tada et al, 1973)

δ is the crack opening displacement (COD)

$x_{no\ crack}$ is the deflection of the specimen if there is no crack

x_{crack} is the increase in the deflection due to the crack

x_{total} is the resulting deflection

$$F_1\left(\frac{a}{w}\right) = 1.090 - 1.735\left(\frac{a}{w}\right) + 8.20\left(\frac{a}{w}\right)^2 - 14.18\left(\frac{a}{w}\right)^3 + 14.57\left(\frac{a}{w}\right)^4 \quad \text{for } S/w = 4 \ \&\ 0.45 < \frac{a}{w} < 0.55 \tag{84}$$

$$= 1.107 - 1.552\left(\frac{a}{w}\right) + 7.71\left(\frac{a}{w}\right)^2 - 13.55\left(\frac{a}{w}\right)^3 + 14.25\left(\frac{a}{w}\right)^4 \quad \text{for } S/w = 8 \ \&\ 0.45 < \frac{a}{w} < 0.55$$

$$F_2\left(\frac{a}{w}\right) = 0.76 - 2.28\left(\frac{a}{w}\right) + 3.87\left(\frac{a}{w}\right)^2 - 2.04\left(\frac{a}{w}\right)^3 + \frac{0.66}{\left(1-\frac{a}{w}\right)^2} \quad \text{for } 0.45 < \frac{a}{w} < 0.55 \tag{85}$$

$$F_3\left(\frac{a}{w}\right) = \left[\frac{a/w}{1-\frac{a}{w}}\right]^2 \{5.58 - 19.57\left(\frac{a}{w}\right) + 36.82\left(\frac{a}{w}\right)^2 - 34.94\left(\frac{a}{w}\right)^3 + 12.77\left(\frac{a}{w}\right)^4\} \quad \text{for } 0.45 < \frac{a}{w} < 0.55 \tag{86}$$

Following the previous procedure we may assume that

$$\Delta\delta_t = \Delta\delta_e + \Delta\delta_c \tag{87}$$

$$\Delta x_t = \Delta x_e + \Delta x_c \tag{88}$$

where

$\Delta\delta_e$ is the elastic COD Component

$\Delta\delta_c$ is the creep COD component

$\Delta\delta_t$ is the total COD

Δx_e is the elastic deflection component

Δx_c is the creep deflection component

Δx_t is the total deflection

The creep components of the COD and deflection may be calculated from the following relations:

$$\Delta\delta_c = c_2\sigma^n\delta_t^p.4a.\ F_2(\tfrac{a}{w}).\ \Delta t \qquad (89)$$

$$\Delta x_c = c_3\sigma^n x_t^p.S.F_3(\tfrac{a}{w}).\Delta t \qquad (90)$$

where c_2 and c_3 are constants.

The temperature effect on the viscoelastic response of the test specimen may be incorporated in the creep component of the COD and deflection as in equation 67.

4.6 Results and Discussions

A computer program has been developed to predict the viscoelastic response of ice under uniaxial loading. The program has been used to study the effect of the cross-head speed, the test temperature, the stiffness of the test machine, and the specimen dimensions, on the apparent viscoelastic response of the ice test specimen. The numerical data is plotted in Figs. 20-23.

In Fig 20, the stress-strain curve has been plotted for different cross-head speeds (XHS). The model proves that the ice test specimen will show an apparent strength when the applied deformation rate equals the induced deformation rate in the specimen. The curves indicate that the apparent strength of ice increases as the cross-head speed increases. This situation will continue to be true until the cross-head speed is high enough so the ice test specimen will reach the actual strength and then break before it reaches an equilibrium condition between the applied deformation and the generated deformation rates. Good agreement can be noticed, also, between the numerical result: and the experimental data obtained by Sinha (1979a) for the same specimen dimensions and rate of loading.

Fig. 21 shows the test temperature effect on the measured stress-strain diagram. The curves show that the apparent strength increases as the test termperature decreases. In Fig. 22, the effect of the testing machine stiffness is demonstrated. The reader will notice that as the stiffness of the testing machine decreases, the ice specimen will have a ductile-like response. This agrees with the experimental data reported recently by Sinha (1979b). Fig. 23 demonstrates the effect of test specimen cross-section (A) on the apparent viscoelastic response. As the cross-sectional area increases, the internal deformation rate decreases which will lead to a ductile-like response and a lower apparent strength.

Further study about the effect of the previous parameters on the viscoelastic response of a cracked three-point bend specimen and load-crack opening displacement curve, has indicated exactly similar effects to those indicated in Figs. 20-23.

Previous results indicate the following:

1 - Loading rate, specimen dimensions, stiffness of the testing machine, and test temperature have a considerable effect on the apparent viscoelastic response and measured strength of ice.

2 - For relatively slow rates of loading the apparent strength increases and can be interpreted as an equilibrium condition between the rate of loading applied by the testing machine, and the deformation rate in the test specimen. As the rate of loading reaches a certain critical value, the ice sample will break before reaching this equilibrium condition giving a real value to the ice strength. For rates of loading higher than this critical value, ice strength should have a constant

value or show a little decrease, due to the impact effect, as the rate of loading increases. This agrees with the available experimental data (Schwarz and Weeks, 1977) which indicate that ice strength has a maximum value at a strain rate of about 10^{-3} sec $^{-1}$. This critical loading rate would be a function of the other parameters.

3 - The coupled scale effect due to ice-structure interaction, has a considerable influence on the apparent behaviour of ice. For a larger domain, ice will respond in a ductile - like manner with lower apparent strength. This agrees with the reported field data which show that ice covers will have lower crushing strength for higher values of aspect ratio.

Hamza, H., and Muggeridge, D.B., (1981), "A Numerical Model to Predict the Apparent Strength and Fracture Toughness of Visco-elastic Materials Under Different Loading Conditions", accepted for presentation in the 5th Canadian Fracture Conf.

Schwarz, J. and Weeks, W.F., (1977), "Engineering Properties of Sea Ice", J. of Glaciology, V19, N81, pp. 499-531.

Sinha, N.K., (1978a), "Short-Term Rheology of Polycrystalline Ice", J. of Glaciology, V21, N85, pp. 457-473.

Sinha, N.K., (1978b), "Rheology of Columnar-Grained Ice", Experimental Mechanics, V18, N12, pp. 464-470.

Sinha, N.K., (1979a), "Rate Sensitivity of Compressive Strength of Columnar-Grained Ice", SESA Spring Meeting, San Francisco, California, May 20-25.

Sinha, N.K., (1979b), "Effect of Test System Stiffness on Ice Strength", POAC-79, The Norwegian Institute of Technology, Trondheim, Norway, August 13-17.

Tada, H., Paris, P. and Irwin, G., (1973), "The Stress Analysis of Cracks Handbook", Del. Research Corporation, Hellertown, Pennsylvania.

Weeks, W. and Assur, A., (1967), "The Mechanical Properties of Sea Ice", CRREL, Monograph II-C3, Hanover, New Hampshire, U.S.A.

Zienkiewicz, O.C., (1971), "The Finite Element Method in Engineering Science", McGraw-Hill, London, Second Edition.

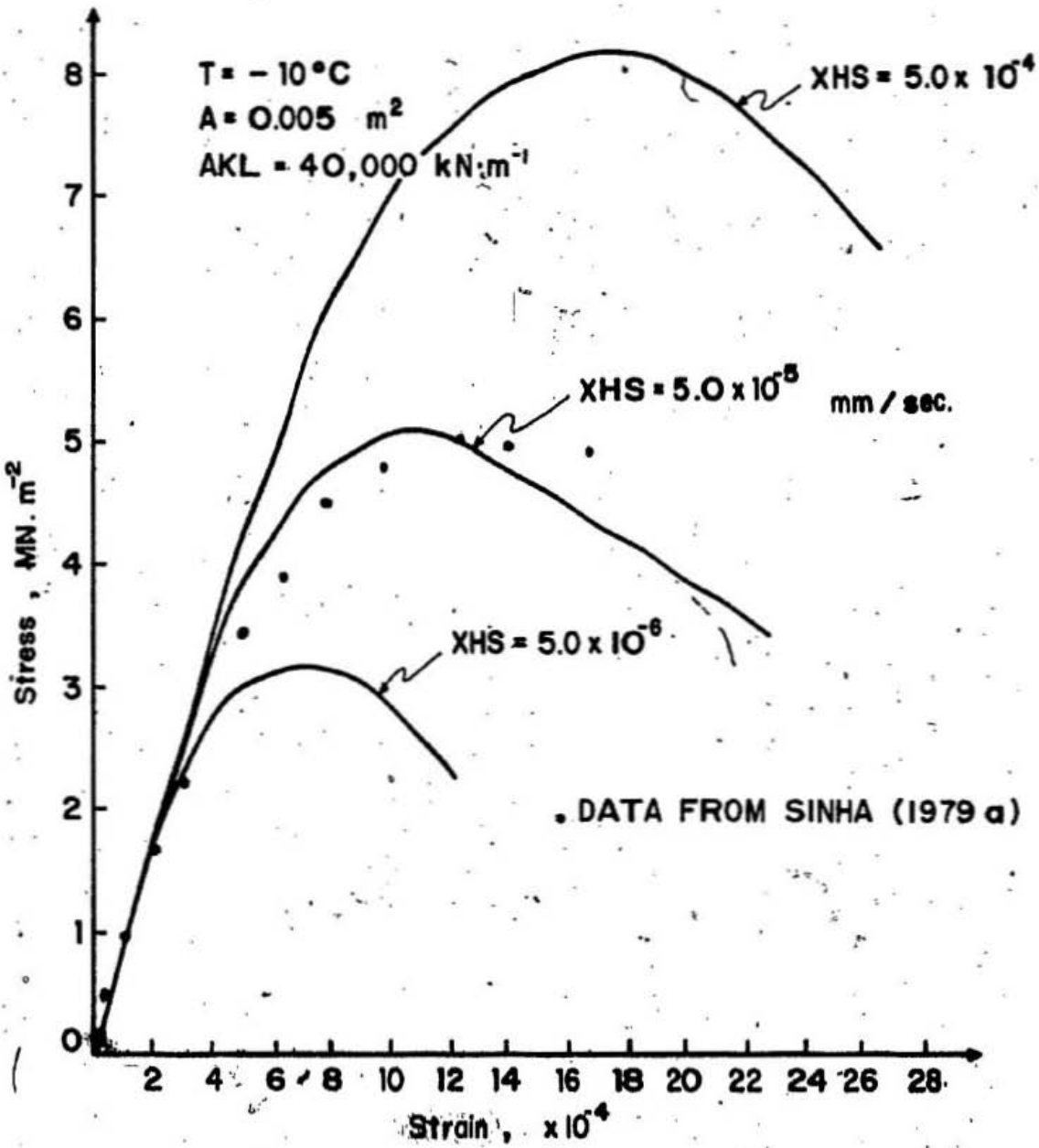

Fig. 20: Stress - Strain diagram for different cross - head speed (XHS).

* $E = 9 \times 10^6$ kpa, $C = 5 \times 10^{-12}$, $n = 3$, $p = 0.5$, $L' = 0.25$ m

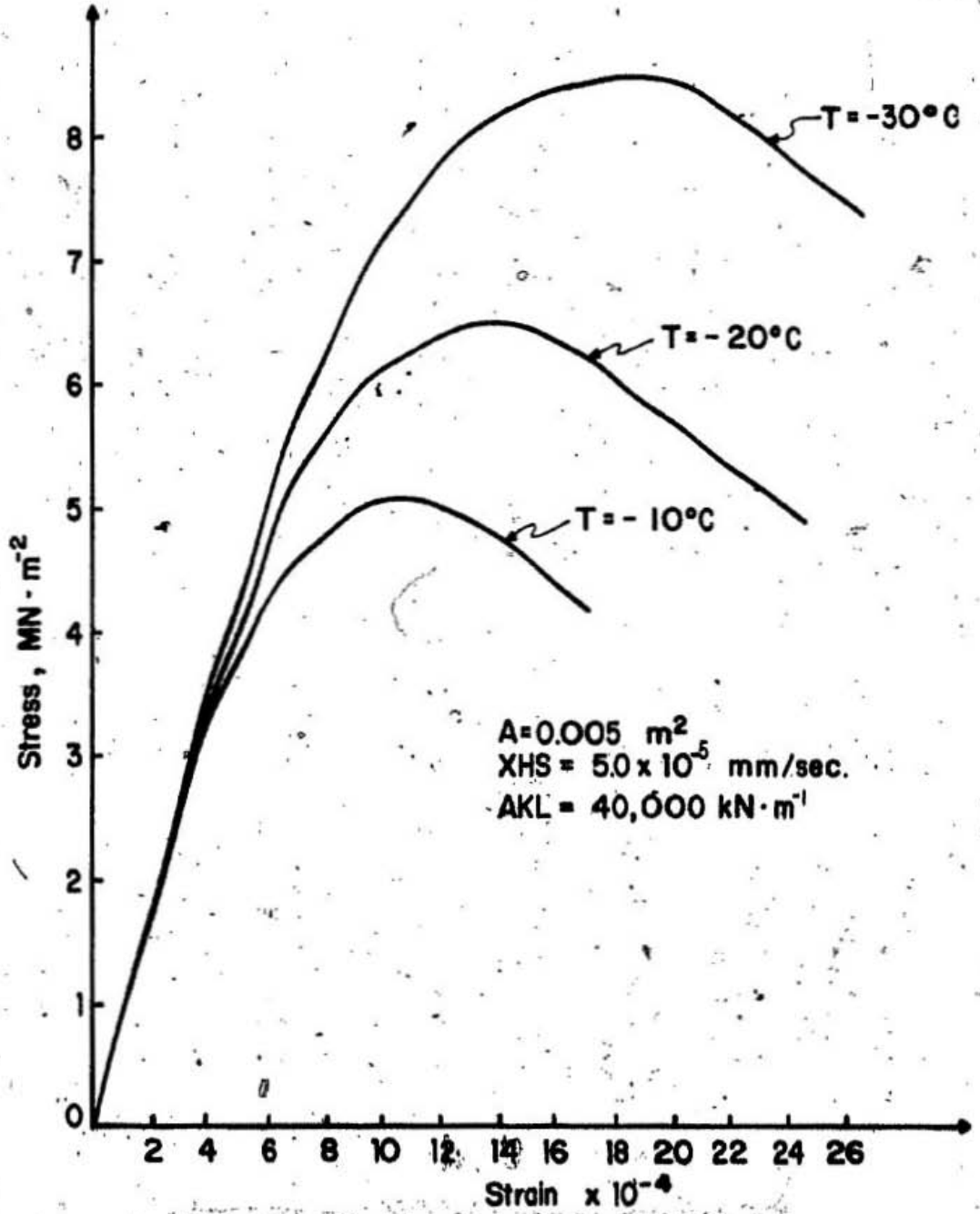

Fig. 21 Stress-Strain diagram for different test temperatures (T).

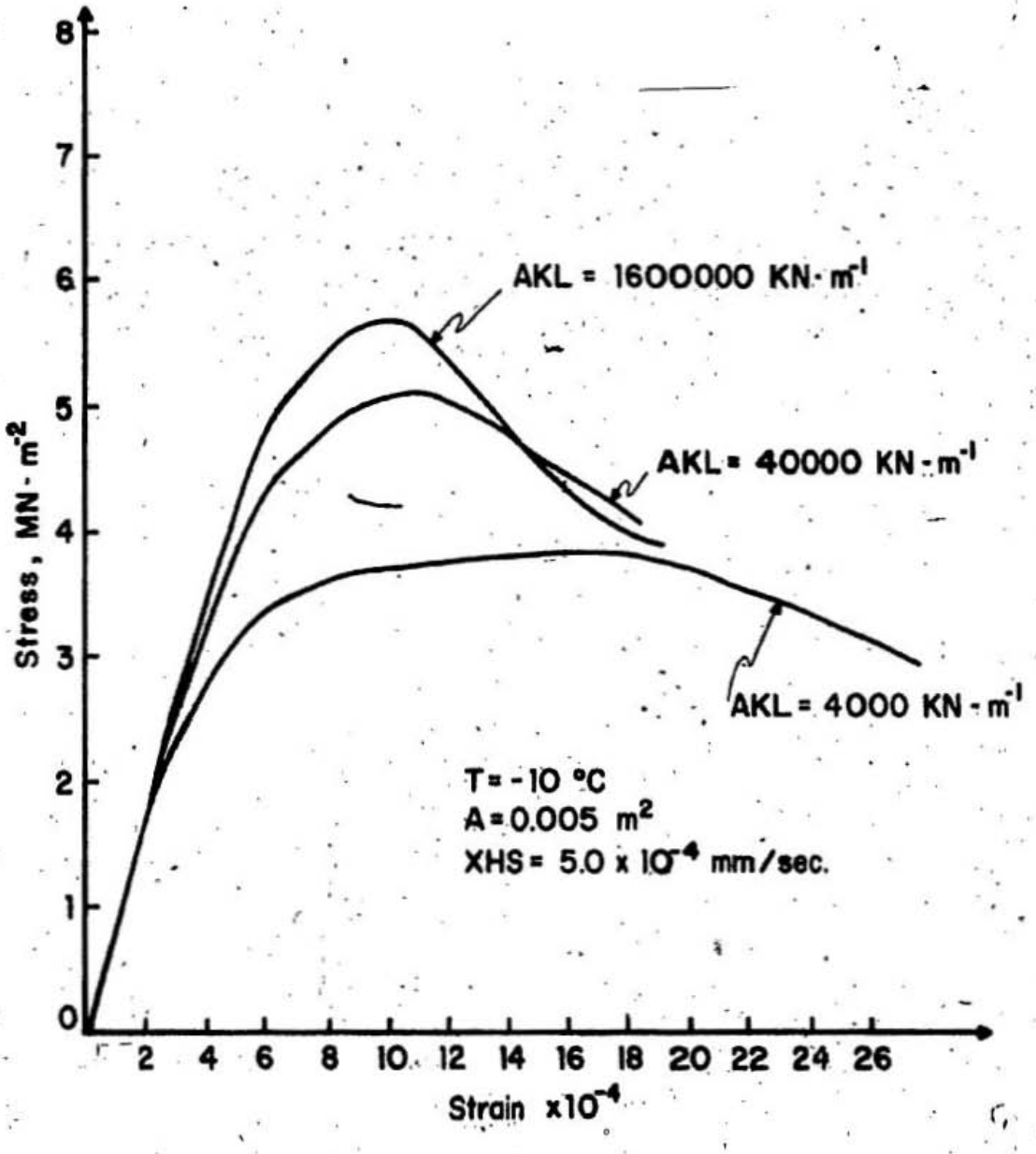

Fig. 22 Stress - Strain diagram for different test machine stiffness (AKL)

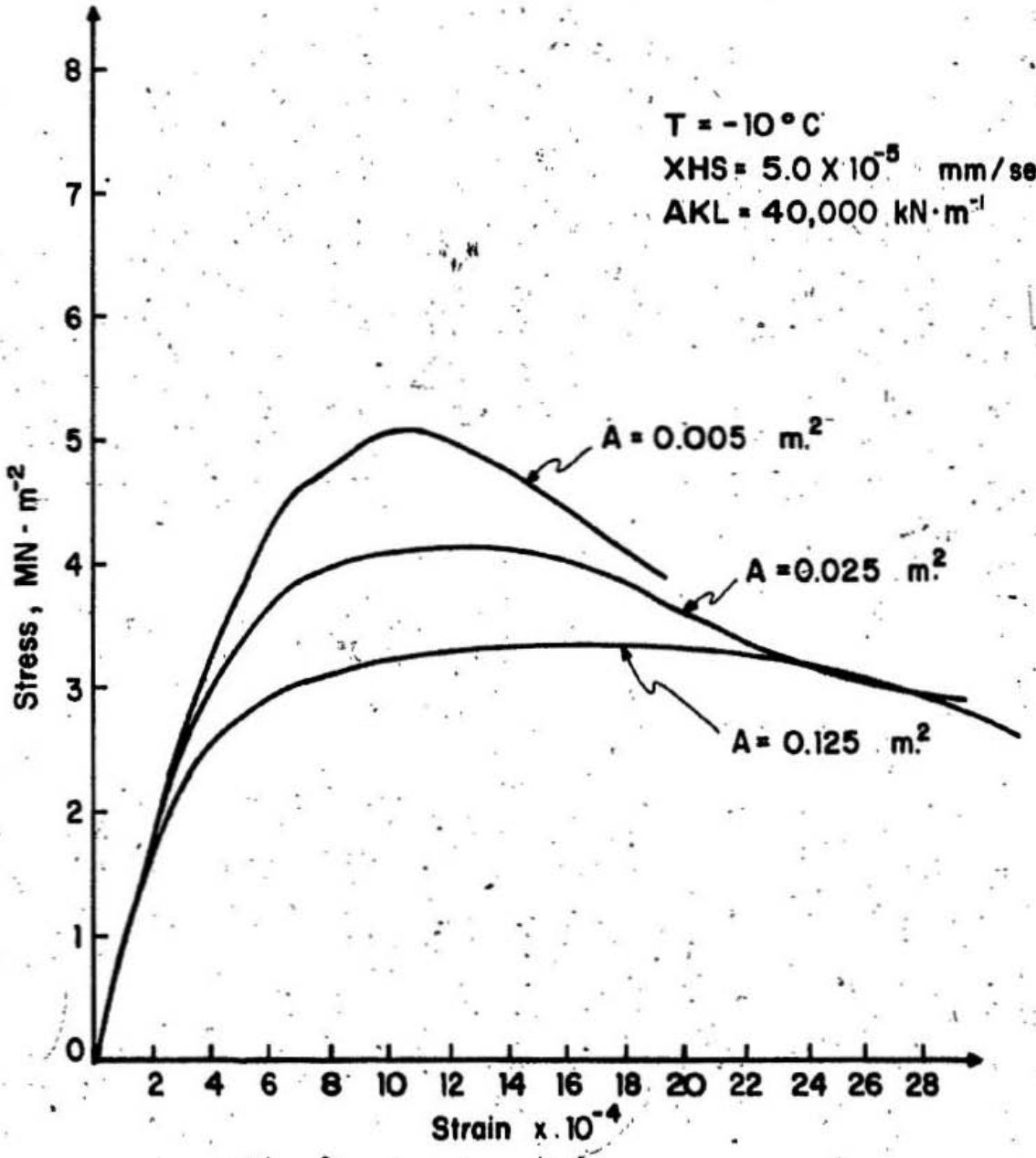

Fig. 23 Stress - Strain diagram for different sample cross-section area.

5. PLANE STRAIN FRACTURE TOUGHNESS (K_{1c}) OF FRESH WATER ICE

5.1 Scope

This chapter describes a small-scale experimental program which has been developed in order to determine the fracture toughness of artificially grown fresh water ice. The effect of rate of loading and test temperature, on the fracture toughness in terms of the critical value of the stress intensity factor (K_{1c}), has been investigated. The results show that values of K_{1c} decrease as rate of loading and test temperature increase.

5.2 Introduction

Cracks and flaws in any material act as stress concentrators which lead to a noticeable decrease in the apparent strength of the material. The classical tests of material strength properties of unnotched specimare not able to give much insight into the effect of these cracks on the overall strength of the material.

Fracture mechanics concepts provide powerful techniques to investigate crack initiation and growth problems and their effects on the total strength of a material. On a microstructural level, cracks start propagating when the normal tensile load exceeds the atomic bonding force. On a macrostructural level, crack growth starts when the stress state at the crack tip exceeds a critical level. This critical stress state is usually described in terms of a critical value of a stress intensity factor.

Griffith (1921, 1924) formulated a fracture criterion based on the

hypothesis of strain energy release rate. He proposed that cracks start propagating when the strain energy release rate reaches or exceeds a critical value which equals the energy required to form a new surface. Experiments have shown that Griffith's Criterion is very good for brittle materials. However, these same experiments have shown that there is a need for a modified criterion for ductile materials. Orowan (1950) and Irwin (1948, 1960) have suggested, for ductile and viscous materials, that the work available for crack propagation, should be equated to the sum of the surface energy and the work associated with plastic and viscous flow, i.e.

$$\frac{dF}{dc} = \frac{dw - du}{dc} = G \geq (2\gamma + p) \tag{91}$$

where

$dF = dw - du$

dw = work done by external forces

du = change in strain energy

G = Strain energy release rate

dc = increment of crack extension (original length of crack $= 2c$)

γ = surface energy

p = work associated with the plastic and viscous flow.

The strain energy release rate of a cracked body can be always related to the stress intensity factor (Irwin, 1957) as follows:

$$G = \frac{K_{1c}^2}{E} \quad \text{for plane stress}$$
$$= \frac{K_{1c}^2 (1 - \nu^2)}{E} \quad \text{for plane strain} \tag{92}$$

Only three previous preliminary estimates of the fracture toughness of fresh water ice are available and one estimate of the fracture toughness of sea water ice is available in literature.

Gold (1963) formed thermal cracks and then measured the depth to which these cracks propagated, and the time necessary for propagation after the blocks were brought together. He used a diffusion analysis to predict thermally induced stresses and hence deduced a value for the fracture toughness of fresh water ice.

Liu and Loop (1972) have used a compact tensile specimen to determine fracture toughness, and a wedge opening specimen to study crack arrest in fresh water ice. They studied the effect of rate of loading and test temperature on the fracture toughness. Their results show that K_{Ic} increases as test temperature and rate of loading decreases. More results are needed in order to investigate this trend and to help to understand this property for a wider range of temperature and strain rates.

In a recent study, Goodman (1977) describes the use of three and four point bending specimens and the median crack formation concept to estimate fracture toughness of fresh water ice.

Vaudrey (1977) reported some values for the fracture toughness of sea water ice. Four-point bending specimens were used to study the effect of brine volume on fracture toughness. Urabe et al (1980) have recently conducted an in-situ experimental program to measure the fracture toughness of sea ice. The reader is also referred to the work by Goodman (1980), Liu and Miller (1979), and Miller (1980).

The present chapter is concerned with a program of small-scale experiments which is developed in order to determine the fracture toughness of fresh water ice in terms of the critical value of the stress intensity

factor in the opening mode of failure (K_c). The three-point bending compact specimen has been used, which has been proposed in ASTM E-399 (1977), in order to determine the plane strain fracture toughness (K_{Ic}).

5.3 Experimental Procedure

Fresh water ice was grown in a commercially available cold room. This ice was practically free of air bubbles due to the use of boiled tap water. The ice was always grown at -23.00°C in boxes measuring 60.96 cm x 60.96 cm x 60.96 cm. Ice blocks of 15-18 cm thickness were formed in 4 to 5 days. A separate group of ice blocks was prepared in much the same manner except that the top surface of the water was seeded with natural snow or crushed ice using a 1.18 mm x 1.18mm screen. Ice blocks prepared in this fashion has a smaller average grain size (8 mm as compared to 12 mm).

Specimens (22.86 cm x 5.08 cm x 2.54 cm) were cut from the blocks by means of a bandsaw. The samples were cut so that the direction of growth was perpendicular to the 22.86 cm x 2.54 cm face. Fig. 24 shows the configuration of the specimens relative to the freezing boxes. A layer approximately 6.0 cm thick was always removed from the top of the block in order to make sure that the specimens do not include part of the initial layer made up of grains having randomly oriented C-axes.

Grain size was determined from thin sections cut from the ice blocks. These sections were frozen on a glass plate and their thickness reduced to about 1 mm using a microtome machine. These final thin sections were then examined and photographed under polarized light. Fig. 25 shows a vertical and horizontal cross section through one of the ice blocks.

A bandsaw was used to cut a notch into the specimens. This notch was subsequently sharpened by use of a very thin blade. This sharpening process was used instead of using fatigue precracking as mentioned in ASTM E-399 (1977). The specimens were left at the test temperature for 24 hours in order to insure that thermal steady state was reached.

The specimens were loaded by an Instron testing machine whose control console was located outside the cold room. This console was equipped with a plotter which supplied a record of the loading history. The machine was capable of providing cross head speeds between 0.01 to 500 mm/min. A typical bend test fixture, which is mentioned in ASTM E-399 (1977) was used and is shown in Fig. 26.

5.4 Results and Discussion

In order to have valid linear plane-strain values for K_{Ic}, three conditions should be satisfied:

1. The crack length and specimen thickness should be $\geq 2.5 (K_{Ic}/\sigma_y)^2$, where σ_y is the yield strength of fresh water ice. This condition could not be checked accurately because of the fact that σ_y for fresh water ice is not well known. However, 2.54 cm should be adequate for both the crack length and specimen thickness (Liu and Loop, 1972).
2. The load-deflection curve should satisfy the criterion mentioned in ASTM E-399 (1977). A typical load deflection curve is shown in Fig. 27.
3. The fracture appearance of each specimen should indicate a plane-strain mode of failure. A typical fracture appearance of one of the specimens is shown in Fig. 28.

The value of K_{1c} for columnar fresh water ice was determined at temperatures -40, -32.00, -21.00 and -4.00°C. At each temperature cross head speeds of 50, 5, 0.5, and 0.1 mm/min. were used. The values of K_{1c} were calculated using the following formula (ASTM, 1977).

$$K_{1c} = \frac{P_Q \cdot S}{B\, W^{3/2}} \cdot Y \qquad N/mm^{3/2} \tag{93}$$

where

$$Y = 2.9\, R^{1/2} - 4.6\, R^{3/2} + 21.8\, R^{5/2} - 37.6\, R^{7/2} + 38.7\, R^{9/2} \tag{94}$$

$R = a/w \qquad 0.45 < \frac{a}{w} < 0.55$

a = crack length, mm

w = depth of specimen, mm

B = thickness of specimen, mm

S = span length, mm

P_Q = load of failure, N

Values of K_{1c} are tabulated in Table 2 and plotted in Fig. 29 for four test temperatures and four rates of loading. The data shows that these values first increase, as temperature decreases, and then decrease.

The data also shows that values of K_{1c} increase (higher values of load of failure) as the rate of loading decreases. This reflects the viscoelastic property of ice under low rates of loading. The average test duration is tabulated in Table 4 from which rate of change of the stress intensity factor can be calculated.

Groups of specimens having average grain sizes of 12 mm and 8 mm were used to investigate the effect of grain size on the fracture tough-

ness of this material. Table 3 and Fig. 30 show values of fracture toughness versus rate of loading for the two groups of specimens.

5.5 References

ASTM, (1977)j "Standard Test Method for Plane-strain Fracture Toughness of Metallic Materials", Annual Book of ASTM Standards, E-399-74, pp. 505-524.

Gold, L.W., (1963), "Crack Formulation in Ice Plates by Thermal Shocks", Can. J. of Physics, V41, pp. 1712-1728.

Goodman, D.J., (1977), "Creep and Fracture of Ice and Surface Strain Measurements on Glaciers and Sea Ice", Ph.D. dissertation, Univ. of Cambridge, England.

Goodman, D.J., (1980), "Critical Stress Intensity Factor (K_{1c}) Measurements at High Loading Rates For Polycrystalline Ice", Physics and Mechanics of Ice, IUTAM Symp., ed. p. Tryde, pp. 129-146.

Griffith, A.A., (1921), "The Phenomena of Rupture and Flow in Solid", Phil. Trans. Roy. Soc. London, Ser. A221, pp. 163-198.

Griffith, A.A., (1924), "The Theory of Rupture", Proc. of the 1st. International Congress for Applied Mechanics", Delft. pp. 55-63.

Irwin, G.R., (1948), "Fracture of Metal", ASM, Cleveland.

Irwin, G.R., (1957), "Analysis of Stresses and Strains Near the End of a Crack Transversing a Plate", J. App. Mech., V24, N3, pp. 361-364.

Irwin, G.R., (1960), "Fracture Mechanics, in Structure Mechanics", Pergamon Press, London.

Liu, H.W. and Loop, Sp.W., (1972), (Draft Report), "Fracture Toughness of Fresh-Water Ice", CRREL, Hannover, New Hampshire, U.S.A.

Liu, H.W., and Miller, K.J., (1979), "Fracture Toughness of Fresh Water Ice", J. Glaciology, V22, pp. 133-143.

Miller, K.J., (1980), "The Application of Fracture Mechanics to Ice Problems", Physics and Mechanics of Ice, IUTAM Symp., ed. P. Tryde, pp. 263-277.

Orowan, E., (1950), "Fatigue and Fracture of Metals", Proceedings Massachusetts Institute of Technology Symposium, p. 139.

Vaudrey, K.D., (1977), "Ice Engineering - Study of Related Properties of Floating Sea-ice Sheets and Summary of Elastic and Viscoelastic Analysis", Tech. Rept. R860, Civil Engineering Laboratory, Naval Construction Battalion Center, Port Hueneme, California, U.S.

Urabe, N., Iwasaki, T. and Yoshitake, A., (1980), "Fracture Toughness of Sea Ice", Cold Regions Science and Technology, V3, N1, pp. 29-37.

TABLE 2: FRACTURE TOUGHNESS OF COLUMNAR FRESH WATER ICE, GRAIN SIZE = 8 mm.

Test Temp. °C	Cross-head Speed mm/min.	K_{Ic} (max) kN/m$^{3/2}$	K_{Ic} (min) kN/m$^{3/2}$	K_{Ic} (aver.) kN/m$^{3/2}$	Stand. dev. kN/m$^{3/2}$
-4.0 *	0.1	181	87	115	29
	0.5	99	51	69	17
	5.0	82	42	55	14
	50.0	45	29	36	4
-21.0 **	0.1	159	115	139	18
	0.5	139	84	101	23
	5.0	94	77	85	7
	50.0	69	57	63	5
-32.0 *	0.1	248	117	158	40
	0.5	198	125	149	27
	5.0	132	96	117	10
	50.0	90	50	72	12
-40.00*	0.1	192	99	142	30
	0.5	165	107	142	19
	5.0	127	103	114	7
	50.0	94	63	73	11

TABLE 3: FRACTURE TOUGHNESS OF COLUMNAR FRESH WATER ICE, GRAIN SIZE = 12 mm.

Test Temp. °C	Cross-head Speed mm/min.	K_{Ic} (max) kN/m$^{3/2}$	K_{Ic} (min) kN/m$^{3/2}$	K_{Ic} (aver.) kN/m$^{3/2}$	Stand. dev. kN/m$^{3/2}$
-4.0 ***	0.1	384	109	242	85
	0.5	360	164	222	71
	5.0	164	116	142	17
	50.0	101	51	77	16
-21.0 ***	0.1	578	255	416	86
	0.5	315	132	190	54
	5.0	158	99	129	17
	50.0	105	52	73	13

* Ten Replicate Tests

** Five Replicate Tests

*** Twenty Replicate Tests

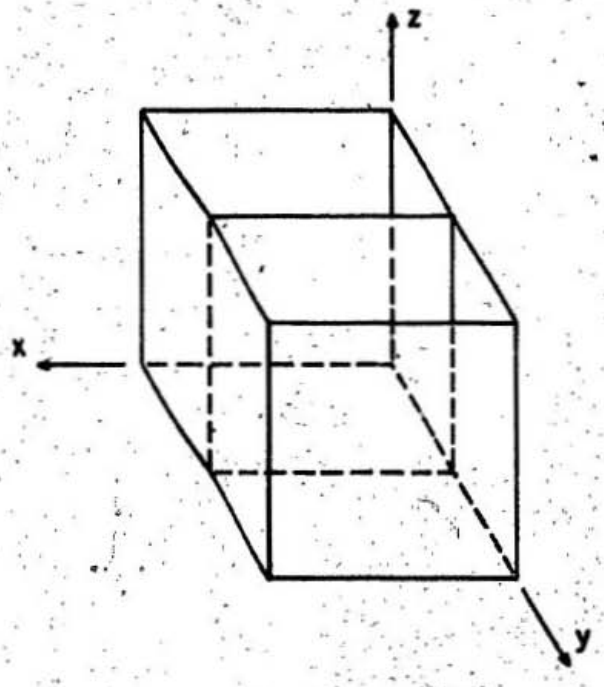

Dim. 60.96 x 60.96 x 60.96 cm

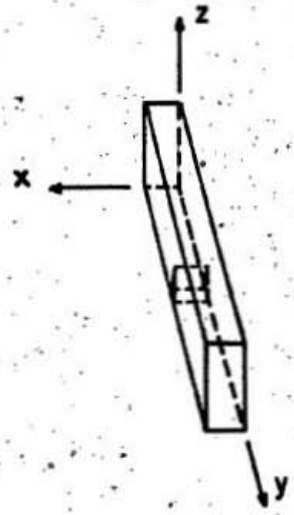

Dim. 22.86 x 5.08 x 2.54 cm

Fig. 24 Specimen geometry

BOTTOM

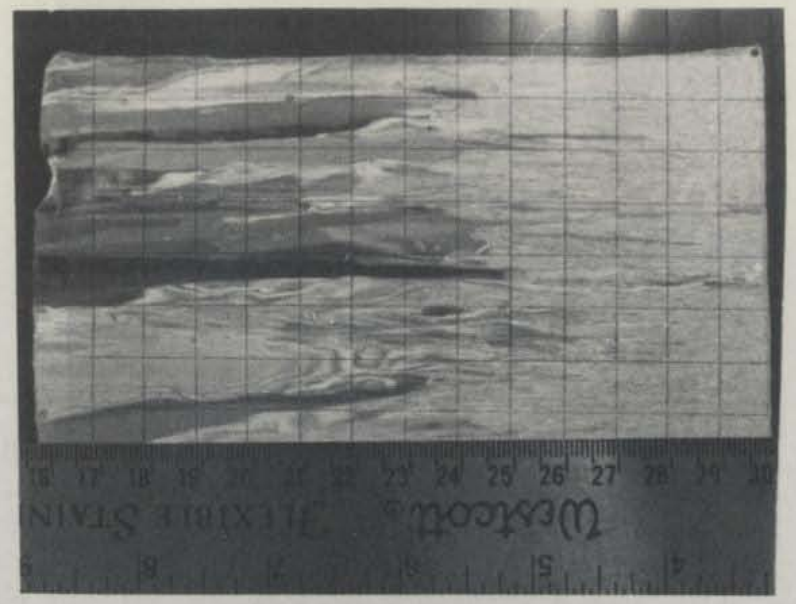

TOP

a - Vertical

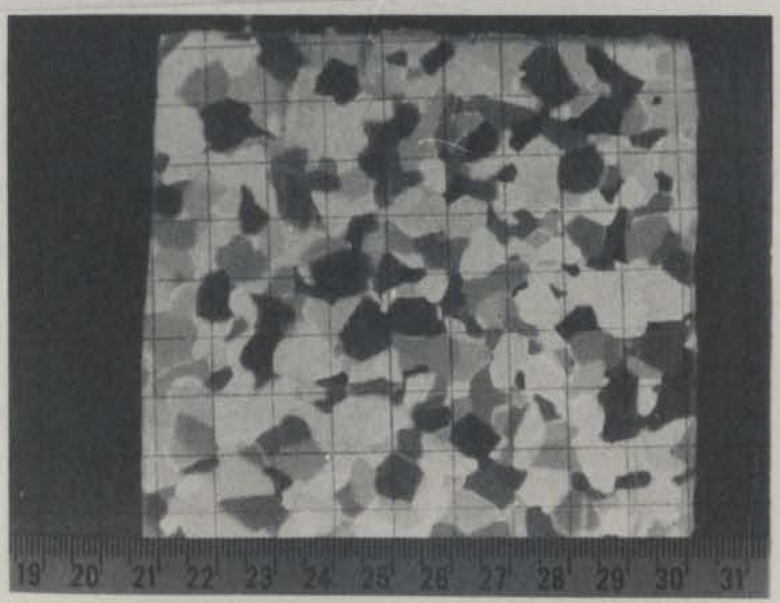

b - Horizontal

Fig. 25 Thin cross sections.

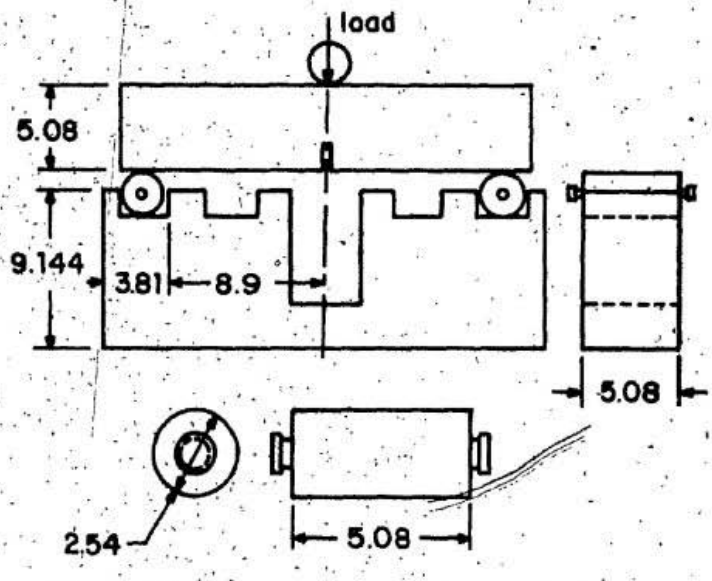

All dimensions in cm.

Fig. 26 Bend test fixture.

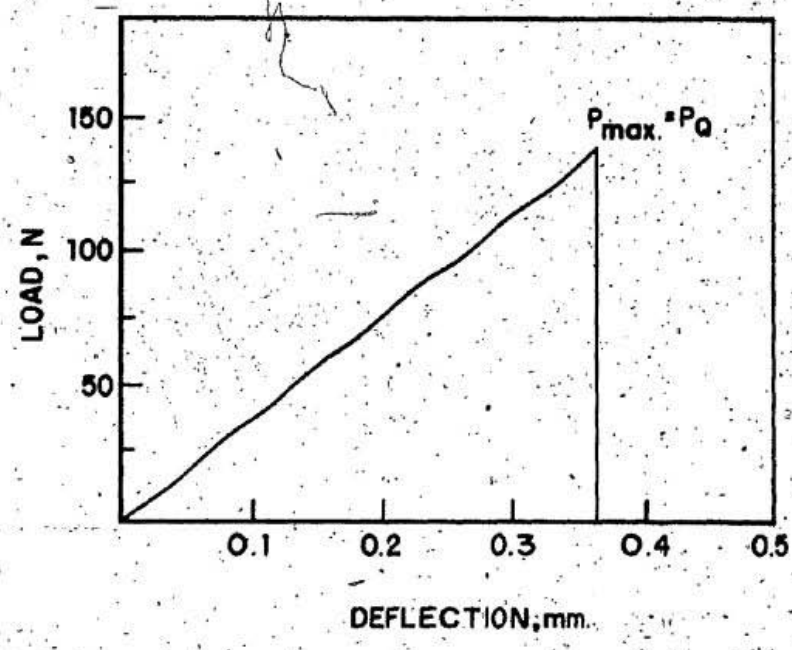

Fig. 27 Typical load deflection curve.

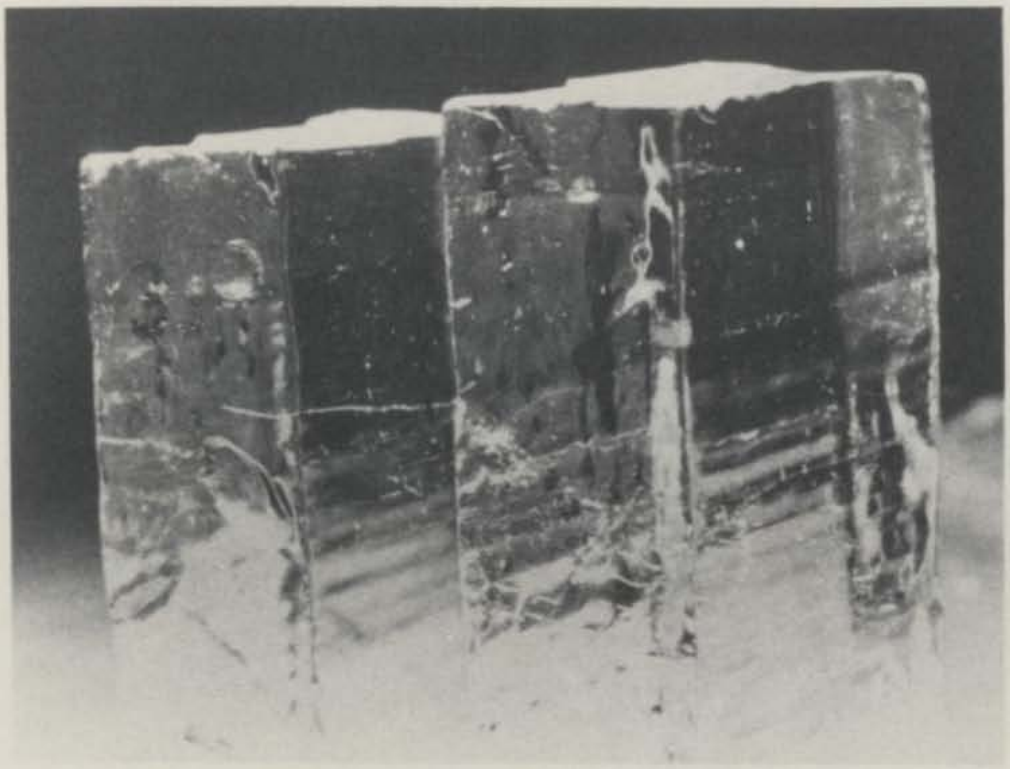

Fig. 28 Typical Fracture Surface.

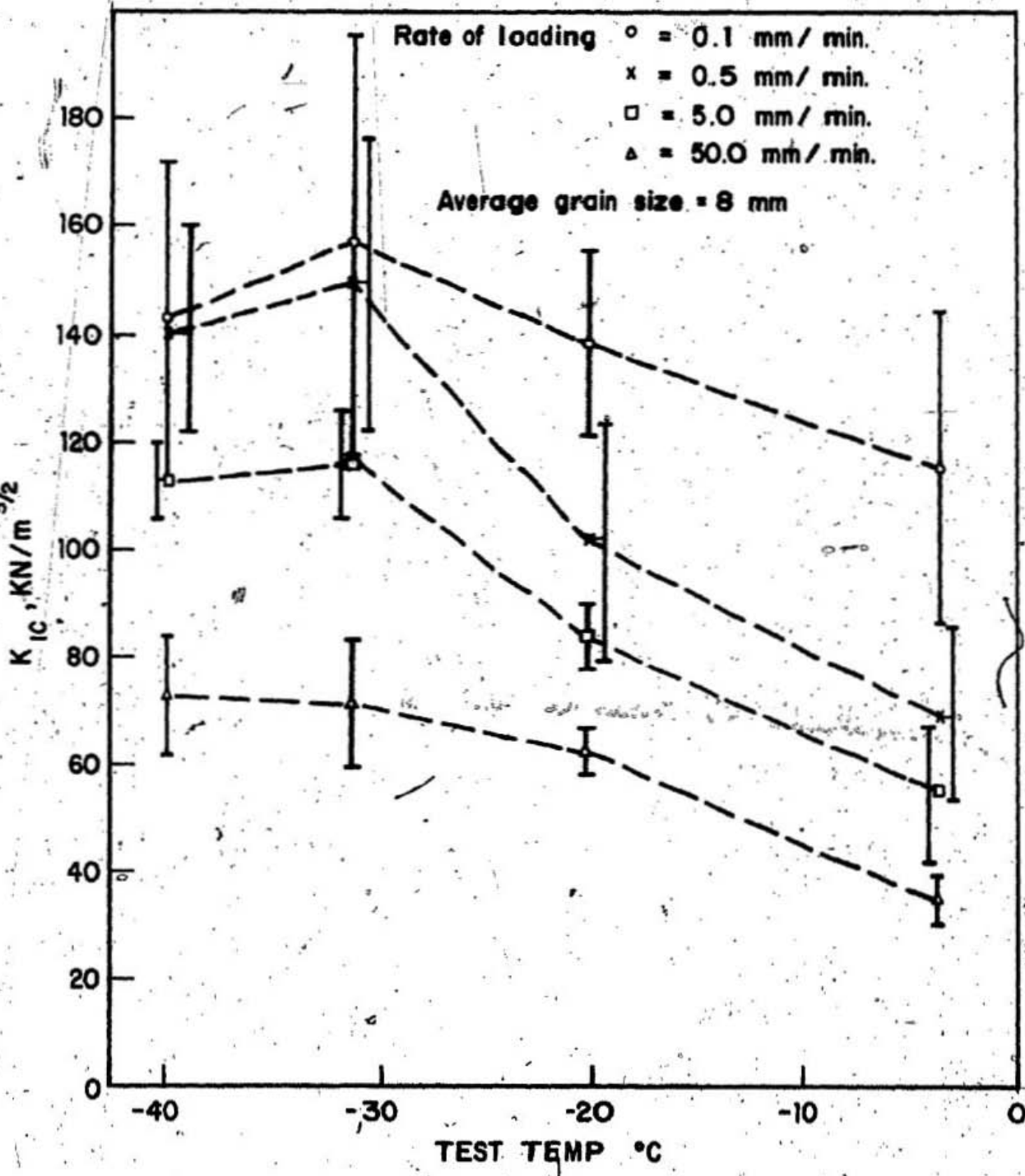

Fig. 29 Effect of temperature and rate of loading on fracture toughness of columnar fresh water ice.

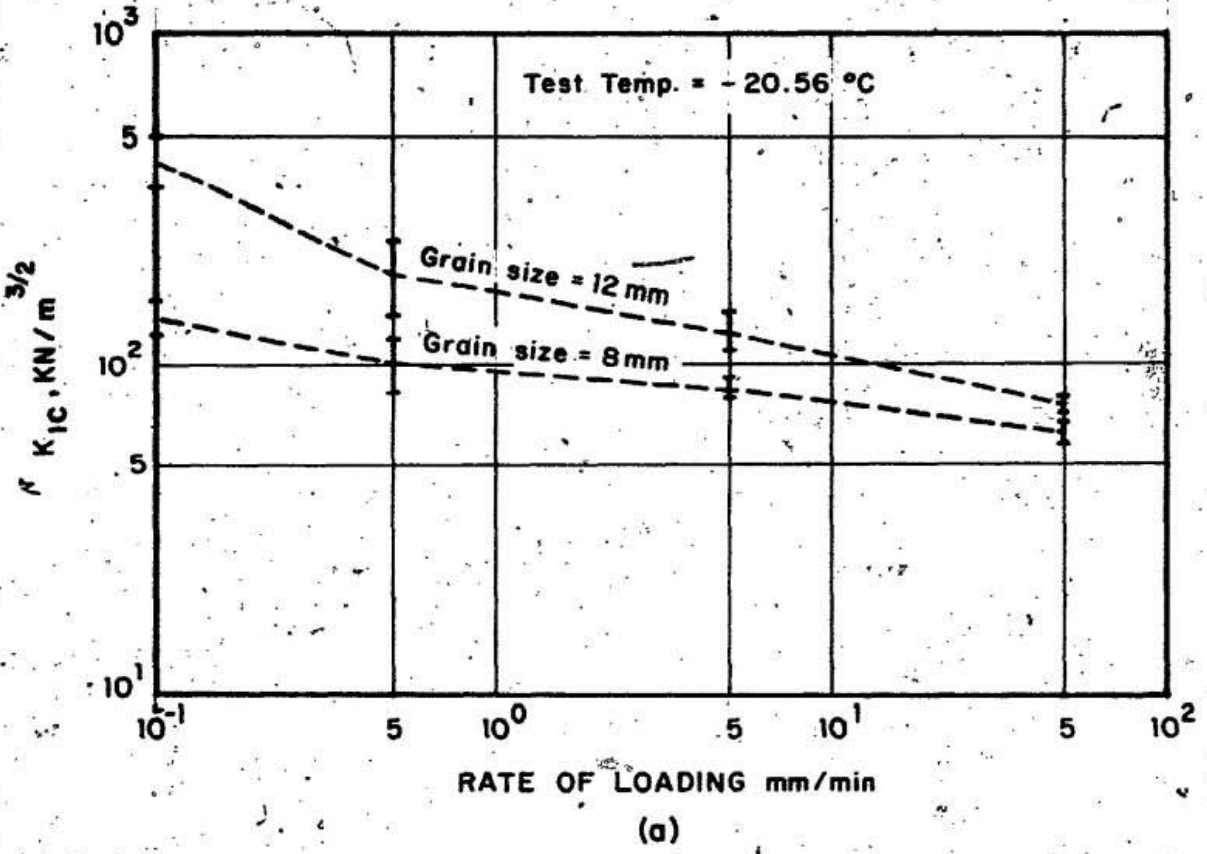

Fig. 30 Effect of rate of loading on fracture toughness of columnar fresh water ice

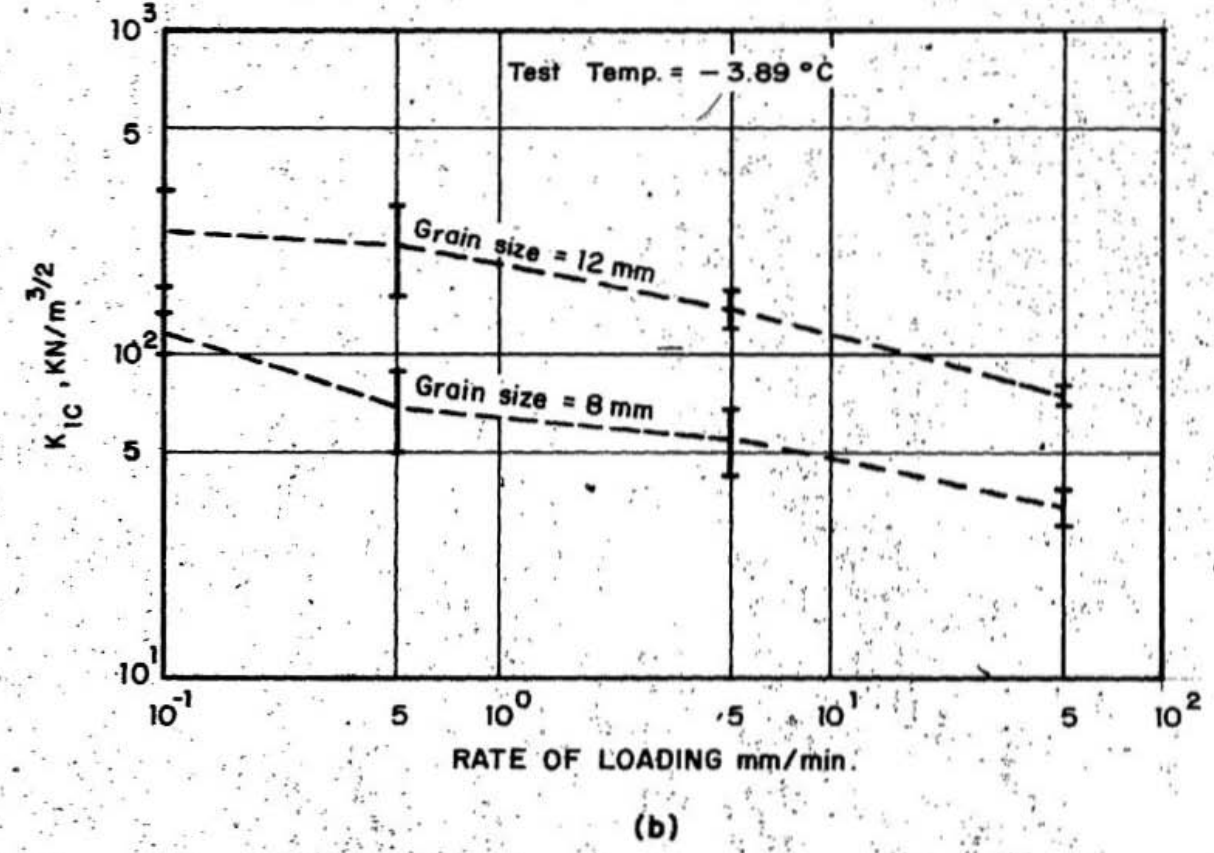

(b)

Fig. 30 Effect of grain size on fracture toughness of columnar fresh water ice.

6. NON-LINEAR FRACTURE TOUGHNESS OF FRESH-WATER ICE

6.1 Scope

In this chapter, the results of a small-scale experimental program, which has been developed to investigate the non-linear fracture toughness of fresh-water ice, are reported. During the program, the effect of loading rate, test temperature, specimen thickness, and span length have been investigated.

6.2 Introduction

The fracture of virtually all materials is preceeded by some plastic yielding in the immediate vicinity of a crack front. The size and the effect of this plastic zone on the fracture process depends primarily on the nature of the material, the stress conditions, and temperature at the crack tip. It is current practice to assume that the principles of linear fracture mechanics are applicable when the crack front plastic yield zone is small enough so it can be viewed as a small perturbation to the local crack front elastic stress field. Several concepts have been developed in order to deal with the fracture problems when the non-linear material behaviour is sufficient to negate the use of linear fracture mechanics principles. Some of these concepts are: Irwin plastic zone correction; J - Integral; R - Curve Analysis and Crack Opening Displacement.

In the present work, the crack opening displacement will be used as a parameter to evaluate the amount of ductility and/or viscoelasticity

developed in each ice test specimen. This concept is explained in a report on Crack Opening Displacement (COD) Testing, British Standards Institution (1972).

6.3 Experiment

Fresh-water ice was artificially grown in the laboratory and then the specimens were cut and prepared in the same way as explained in Hamza and Muggeridge (1979). (Chapter 5).

Several methods were tried, without success (due to the brittleness and the viscoelastic nature of ice) to measure the crack tip opening displacement. Finally, a special strain gauge extensometer developed by Instron which has a very low spring constant, was used successfully. Due to the difficulty of attaching the gauge directly to the specimen, a simple square frame was frozen onto the specimen to prevent any possibility of sliding and the gauge was attached to the frame (See Fig. 31). For each test specimen, the following data have been recorded: Specimen thickness; specimen width, loading span length; test temperature; duration of the test; load/displacement record; crack length, distance of the clip gauge away from test specimen surface; and critical crack opening displacement.

6.4 Results and Discussion

In order to determine the degree of non-linearity each specimen has exhibited, the crack tip opening displacement and the load histories were combined in one curve. In general, the load/displacement curve may be one of three types as shown in Fig. 32.

(i) In the case of a smooth continuous record in which the applied force rises with increasing displacement up to the onset of unstable fracture, and no prior crack extension has been detected (Fig. 32-i), the critical displacement (V_c) should be taken as the total value corresponding to maximum applied force (P_c) including both elastic plastic components. If failure occurs close to the linear range, the Secant Offset Procedure should be applied to test whether a valid K_{Ic} measurement can be made.

(ii) In some cases, the applied force/displacement curve shows a region of increasing displacement with falling or constant applied force followed by a further region of rising applied force before complete fracture (Fig. 32-ii). When this is associated with crack extension, the critical displacement shall be taken as the total value (V_c) corresponding to the applied force (P_c) at the first instability or curve discontinuity.

(iii) Where the applied force/displacement curve goes through a maximum point and increasing displacement is observed with falling applied force, it can be assumed that stable crack growth is occurring (Fig. 32-iii). The critical displacement required is that value at the point at which an amount of crack growth commenced. If such a method is not available the COD for crack initiation cannot be measured; for material comparison purposes, a crack opening displacement (δ_m) calculated from the clip gauge displacement (V_m) at the first attainment of a maximum load can be used.

During the present experimental work, the load/displacement was always of the type (i).

Two methods have been proposed in a report, British standards institution (1972) to calculate the critical crack opening displacement (δ_c). The two methods assume deformation to occur by a hinge mechanism about a centre of rotation at a depth of r(w-a) below the crack tip (See Fig. 33). The first method is based on a theoretical approach and uses the following equations:

$$\delta_c = \frac{0.45\ (w - a)}{0.45W + 0.55a + z}\ [V_c - \frac{\gamma\sigma_y\ w(1 - \nu^2)}{E}] \qquad (95)$$

$$\text{for } V_c \geq \frac{2\delta\sigma_y\ w(1 - \nu^2)}{E}$$

or

$$\delta_c = \frac{0.45\ (w - a)}{0.45w + 0.55a + z}\ [\frac{V_c^{\,2}\ E}{4\delta\sigma_y\ w(1 - \nu^2)}] \qquad (96)$$

$$\text{for } V_c < \frac{2\delta\sigma_y\ w\ (1 - \nu^2)}{E}$$

where:

γ is a non-dimensionalized limiting value of elastic clip gauge displacement

σ_y is the material yield strength

E is the elastic modulus

ν is Poisson's ratio

The second method is derived from experimental calibration and assuming the deformation to occur at a depth of 1/3 (w - a).

$$\delta_c = \frac{v_c\,(w - a)}{w + 2a + z} \qquad (97)$$

In all the test specimens made of S2 ice, the load/displacement curve was of the type (i) in Fig. 32, which has indicated that the fracture failure was due to unstable crack propagation.

In Figs. 34-36, the values of the critical crack opening displacement (v_c) are plotted for three cross-head speeds and three test temperature. The data shows that the value of v_c increases as cross-head speed and test temperature decreases. It can be noticed, also, that at low test temperatures (e.g. -31-67°C) the ice tends to respond in a brittle manner and has almost constant critical crack opening displacement. The values for v_c are plotted in Fig. 37 for different test specimen thickness and span length. The data shows that v_c increases as the test specimen thickness increases and span length increases. This is due to the fact that the effective applied stress rate decreases as the specimen thickness and span length increase. It was, also, observed that as the specimen thickness increases, the apparent ductility and/or viscoelasticity exhibited by the specimen increases.

6.5 Conclusions

The present work is unique in the ice mechanics literature, as it investigates the possibility of applying non-linear fracture techniques to ice. The following conclusions may be made:

i. The available non-linear fracture mechanics techniques have been used to measure the ductile and/or viscoelastic fracture toughness of ice.

The experimental data obtained during the present work show some scatter. This can be explained and predicted using the numerical model developed in Chapter (4) together with probabilistic techniques to describe the expected scatter and randomness in the microstructure of ice under consideration. The author believes that a small scatter in the viscoelastic material constants of ice will cause much more scatter in the observed final viscoelastic response of ice. This is due to the nonlinear nature of the constitutive equations representing ice under viscoelastic (nonlinear) conditions.

ii. The test specimen dimensions have an important effect on the amount of ductility and/or viscoelasticity exhibited by ice.

iii. At very low temperature, ice will tend to respond in a brittle manner which indicates that K_{1c} can be used to describe the fracture toughness.

iv. As the loading rate decreases, the induced internal stresses in ice will have had a chance to relax which will lead to larger values of δ_c.

6.6 References

British Standards Institution, 1972, "Methods for Crack Opening Displacement (COD) Testing", Draft for Development, DD19.

Hamza, H. and Muggeridge, D.B., 1979, "Plane Strain Fracture Toughness (K_{1c}) of Fresh Water Ice", POAC 79, The Norwegian Institute of Technology, Trondheim, Norway.

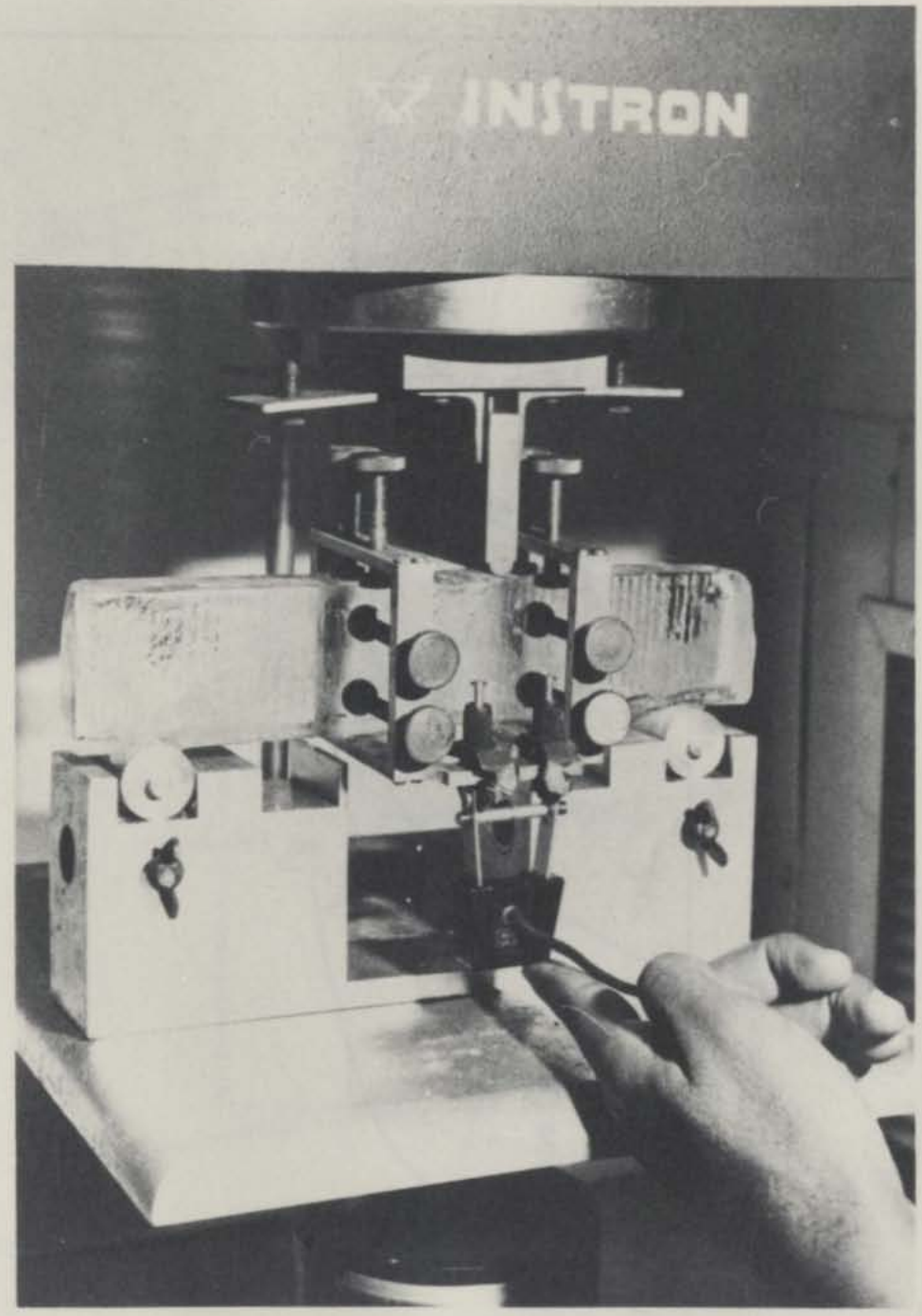

Fig. 31 The COD extensometer attached to the square frame.

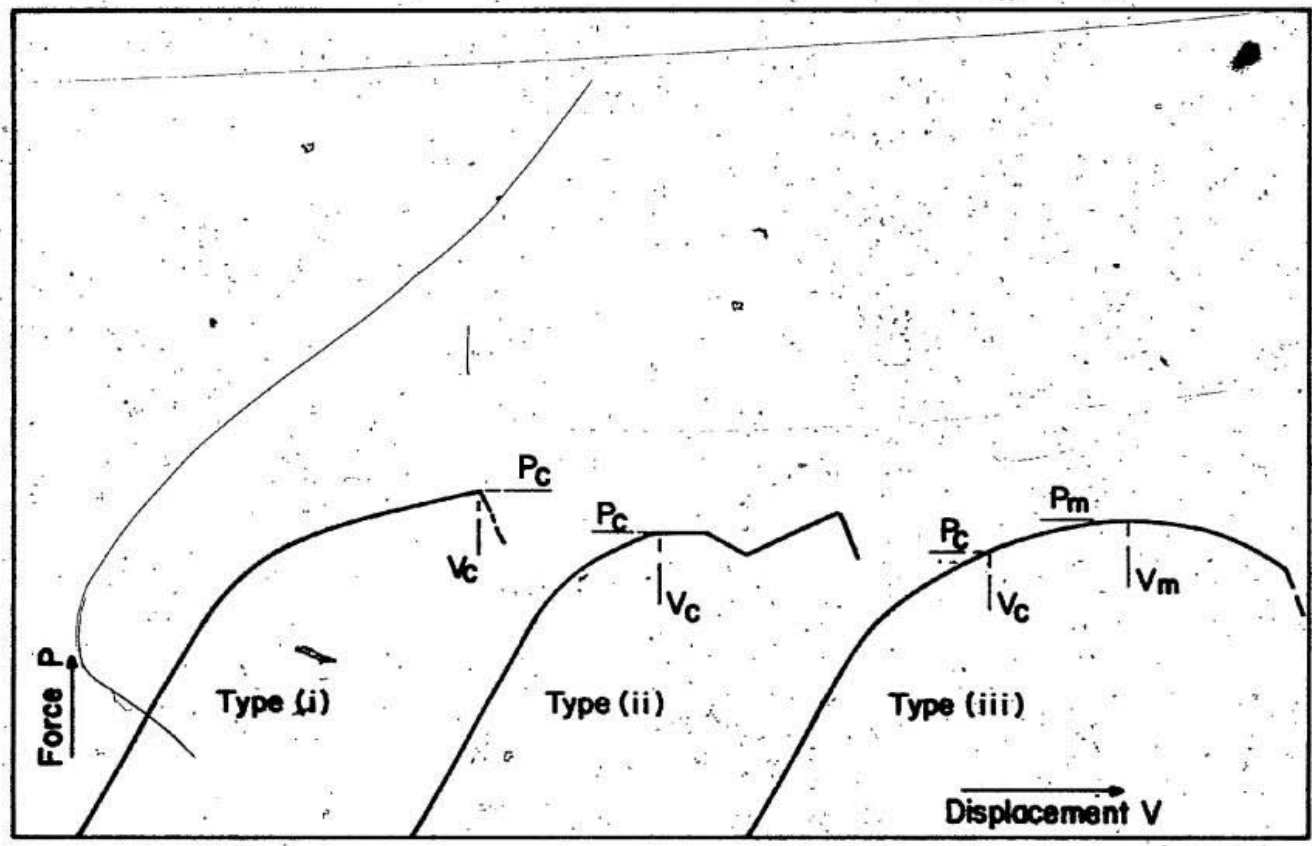

Fig. 32 Force / Displacement records for calculation of COD.

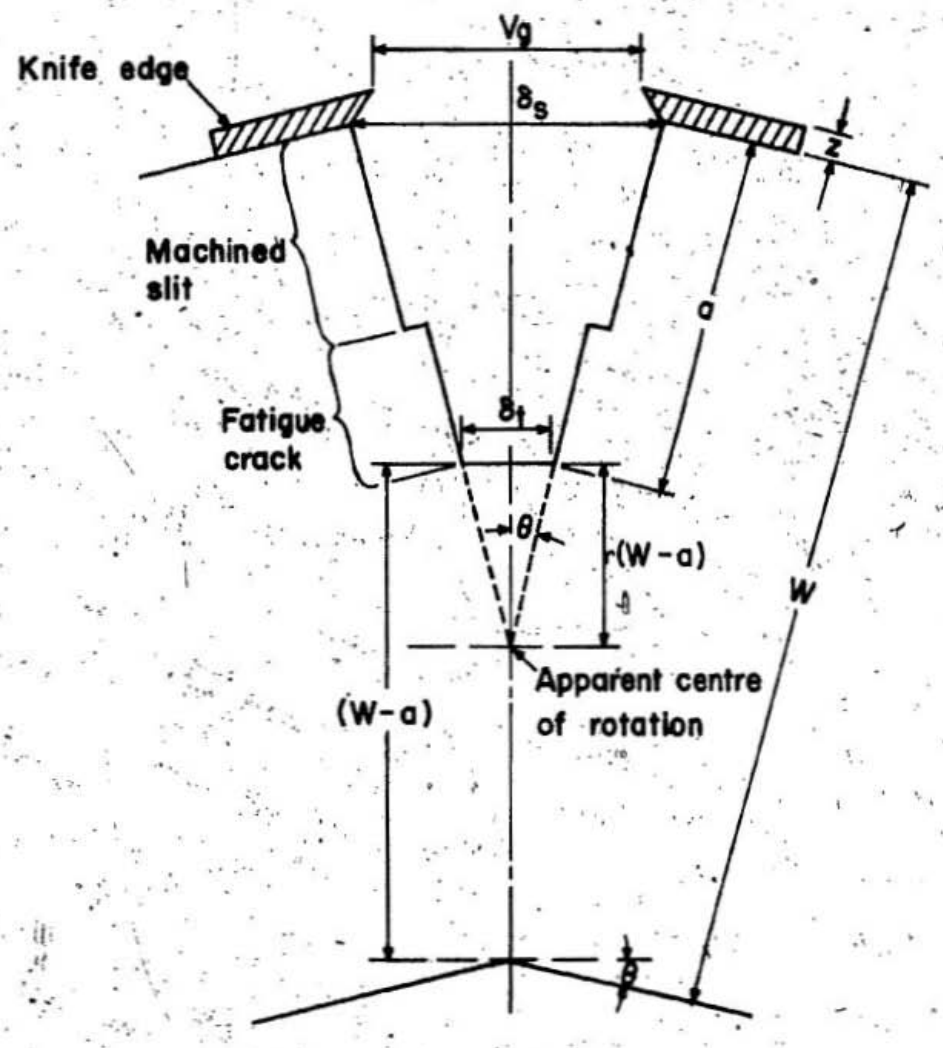

Fig. 33 Representation of the notch profile during bending.

*$V_c = V_g$ and $\delta_c = \delta_t$ at the load of failure

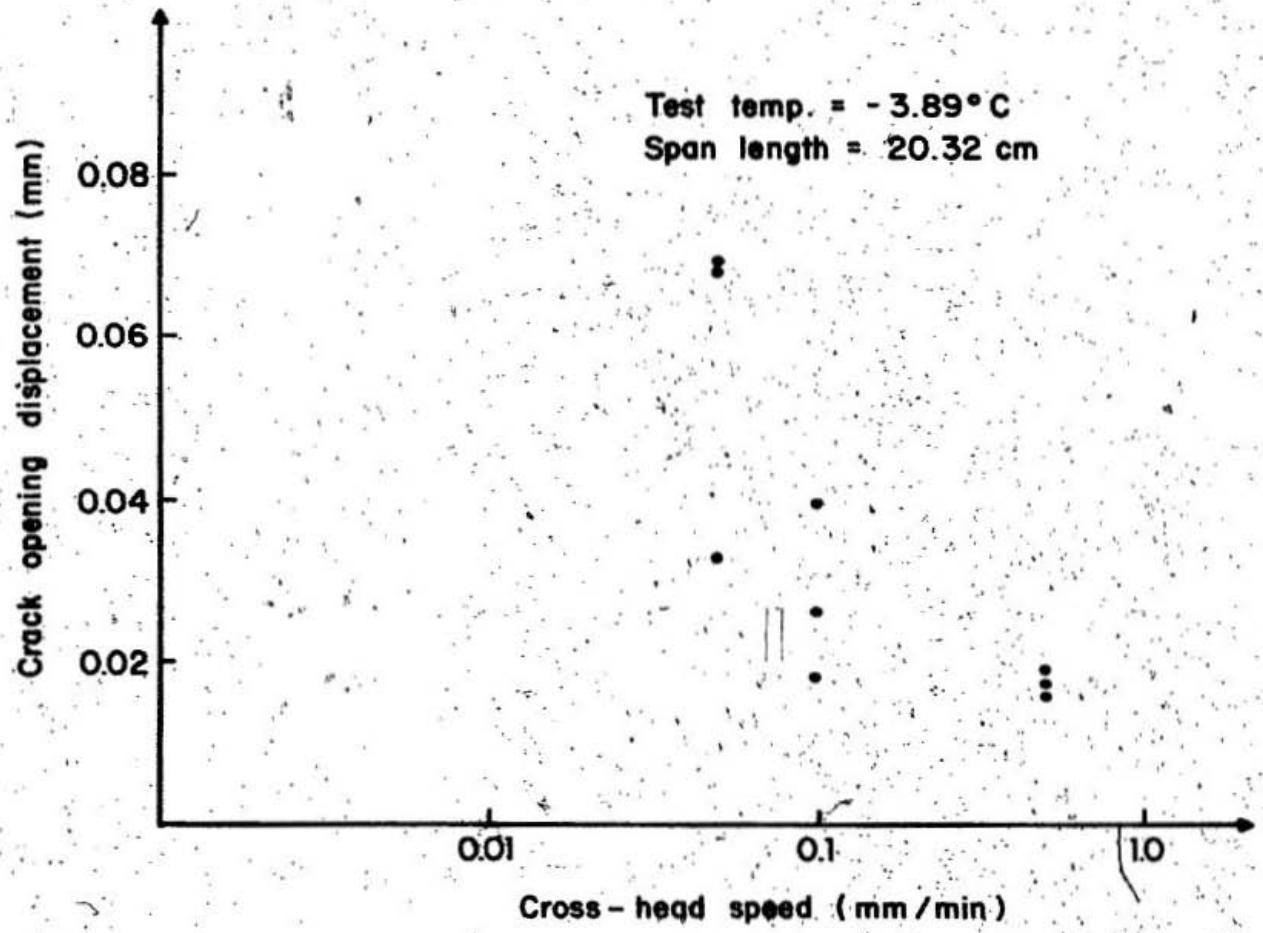

Fig. 34. Critical crack opening displacement for different cross-head speeds, T = -3.89°C.

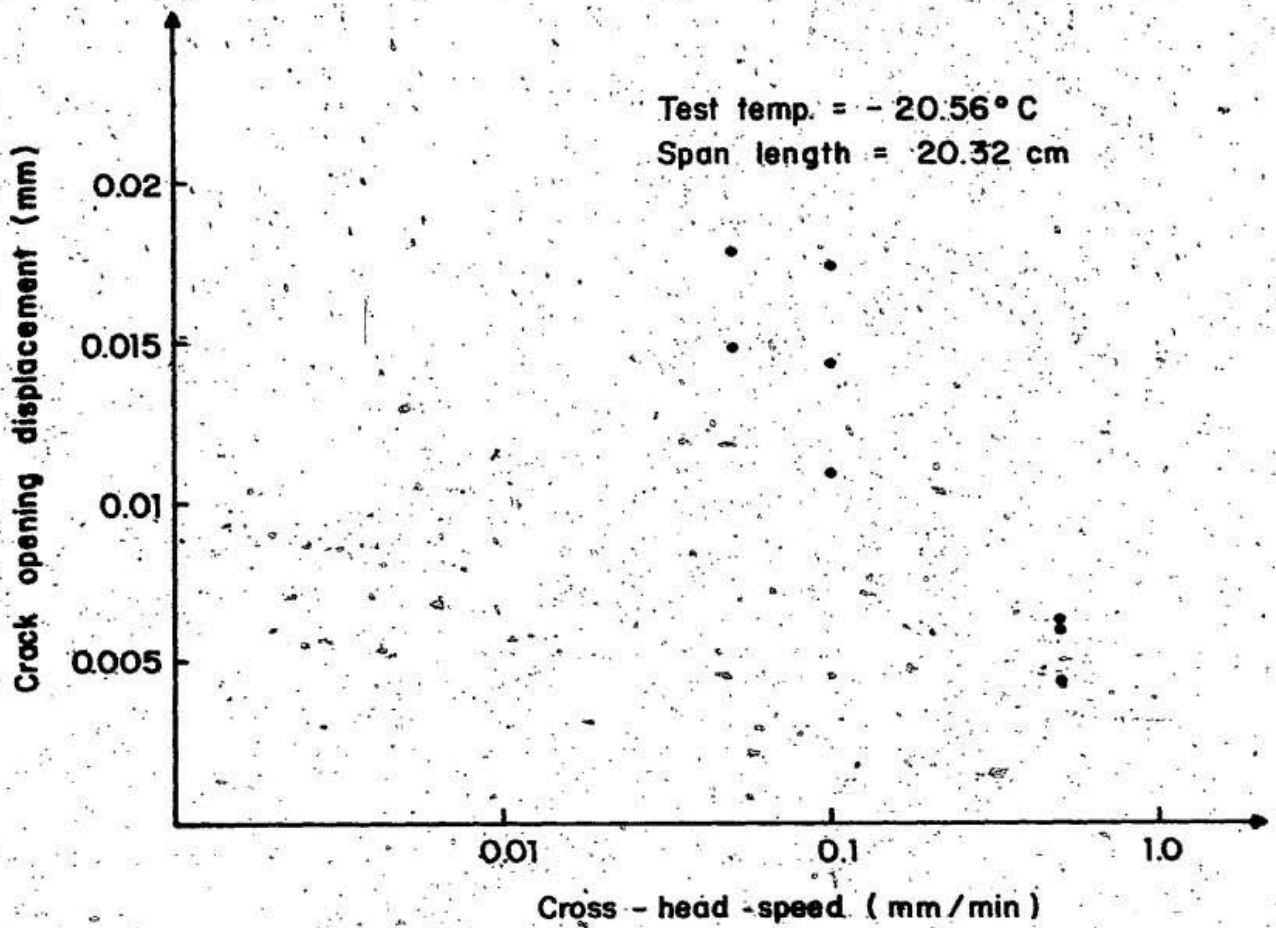

Fig. 35 Critical crack opening displacement for different cross - head speeds , T = - 20.56° C.

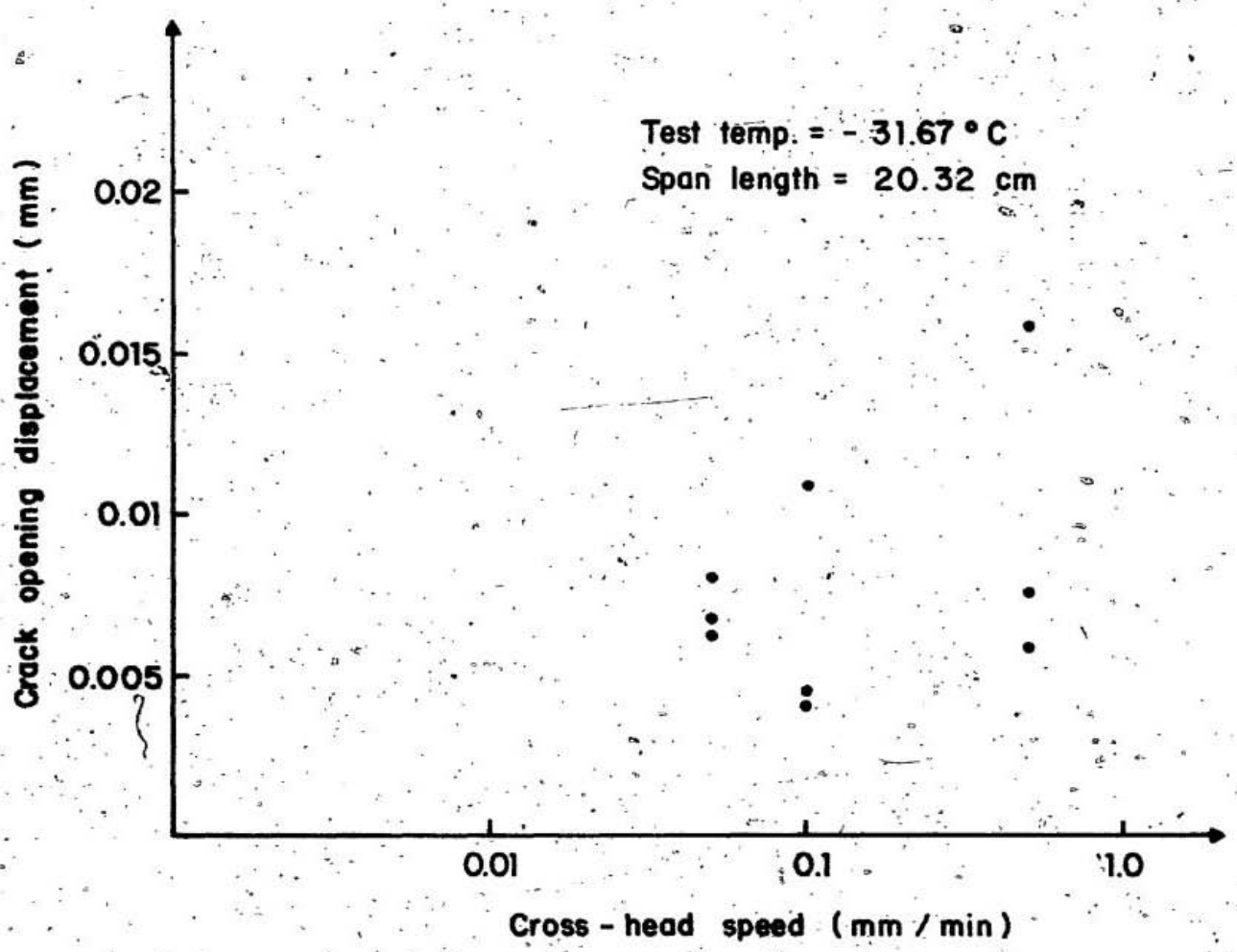

Fig. 36 Critical crack opening displacement for different cross - head speeds, T = - 31.67 ° C.

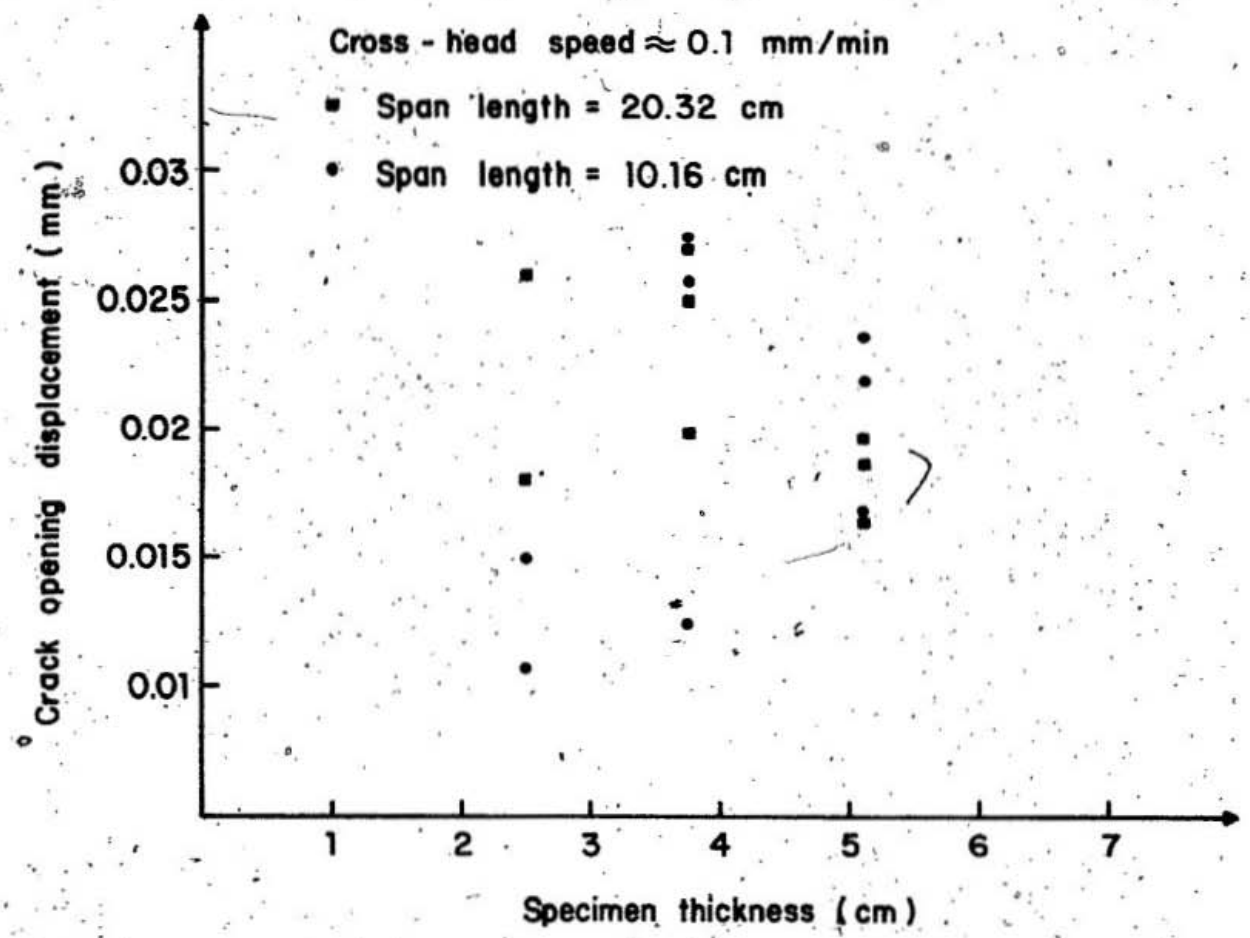

Fig. 37 Effect of specimen dimensions on the critical crack opening displacement, T = - 3.89°C.

7. PRIMARY INVESTIGATION INTO A COMPLETE FAILURE CRITERION FOR ICE

7.1 Scope

In this chapter the critical stored energy is proposed as an adequate failure criterion for ice. The small scale experimental results produced by the author and others available in the literature support this proposed criterion. The criterion indicates that the critical stored energy which ice can absorb decreases as the rate of loading increases and the temperature decreases. More experimental data is needed to support and validate the proposed criterion.

7.2 Introduction

Several yield theories are reported in the literature:

(i) Distortion Energy Theory, Von Mises Yield Condition

The "distortion energy theory" assumes that yielding begins when the distortion energy equals the distortion energy at yield in simple tension.

The yield condition is:

$$\frac{1}{2}[(\sigma_1 - \sigma_2)^2 + (\sigma_2 - \sigma_3)^2 + (\sigma_3 - \sigma_1)^2] = \sigma_y^2 \quad (K) \qquad (98)$$

where σ_1, σ_2, and σ_3 are the principal stresses and σ_y is the yield stress in simple tension.

In the case of ice, Jones (1978) has observed an initial increase in strength as the hydrostatic pressure increases. However after a maximum strength is reached, further increase in the hydrostatic pressure has caused a monotonic decrease in the ice strength.

(ii) Maximum Shear Stress Theory, Tresca Criterion

The maximum shear stress theory assumes that yielding occurs when the maximum shear stress reaches the value of the maximum shear stress occurring under simple tension.

The maximum shear stress is given by half of the difference between the maximum and minimum principal stresses.

In simple tension the maximum shear at yield is $\frac{1}{2}\sigma_y$. Yielding will occur if one of the following conditions is reached.

$$\begin{aligned} &|\sigma_1 - \sigma_2| = \sigma_y \\ \text{or} \quad &|\sigma_2 - \sigma_3| = \sigma_y \\ \text{or} \quad &|\sigma_3 - \sigma_1| = \sigma_y \end{aligned} \tag{99}$$

This is the Tresca condition, which is in agreement with the assumption that hydrostatic pressure does not influence yielding.

(iii) Maximum Stress Theory, Johansen Criterion

This theory assumes that the yielding occurs when one of the principal stresses becomes equal in absolute value to the yield stress in simple tension, σ_y.

This criterion establishes that yielding will occur when any one of the following three conditions is reached:

$$\begin{aligned} \sigma_1 &= \pm \sigma_y \\ \sigma_2 &= \pm \sigma_y \\ \sigma_3 &= \pm \sigma_y \end{aligned} \tag{100}$$

(iv) Yield Criteria for Plate Bending

In the previous section the yield criteria were written in a general three dimensional form.

For plate bending analysis the yield condition is more conveniently written in terms of bending moments. Assuming that the entire thickness of the plate is either fully elastic or fully plastic and that the plate is only loaded normally to the middle plane, the yield conditions may be written as follows:

Von Mises:

$$F = M_{xx}^2 - M_{xx} M_{yy} + M_{yy}^2 + 2M_{xy}^2 - M_p^2 = 0 \qquad (101)$$

Tresca:

$$\left.\begin{aligned} F &= \frac{M_{xx}+M_{yy}}{2} + \left\{\frac{1}{4}(M_{xx}-M_{yy})^2 + M_{xy}^2\right\}^{1/2} \pm M_p = 0 \\ F &= \frac{M_{xx}+M_{yy}}{2} - \left\{\frac{1}{4}(M_{xx}-M_{yy})^2 + M_{xy}^2\right\}^{1/2} \pm M_p = 0 \end{aligned}\right\} \text{For } M_x M_y \geq M_{xy}^2 \qquad (102)$$

or $2\left(\frac{1}{4}(M_{xx}-M_{yy})^2 + M_{xy}^2\right)^{1/2} \pm M_p = 0$ for $M_x M_y < M_{xy}^2$

Johansen:

$$F = \frac{M_{xx}+M_{yy}}{2} + \left\{\frac{1}{4}(M_{xx}-M_{yy})^2 + M_{xy}^2\right\}^{1/2} \pm M_p = 0$$

or $$F = \frac{M_{xx}+M_{yy}}{2} - \left\{\frac{1}{4}(M_{xx}-M_{yy})^2 + M_{yy}^2\right\}^{1/2} \pm M_p = 0 \qquad (103)$$

where M_p represents the fully plastic moment ($M_p = \sigma_y^2 \left(\frac{t}{2}\right)^2$).

The Von Mises, the Tresca and Johansen Yield Criteria are represented in Figures 38, 39 and 40 respectively.

Hawkes and Mellor (1972) have investigated the uniaxial tensile and compressive strength of a fine grained polycrystalline ice. They have reported the relation between the work done on the specimen to cause failure and the applied strain rate (See Fig. 41). In a more recent work, Beltaos (1977) has proposed that the critical value of strain energy be used as a failure criterion for floating ice covers. The criterion appeared to agree with the field experiment in predicting the onset of failure and the final failure of fresh-water and sea-water ice covers.

7.3 Results and Discussion

The experimental results produced by the author (Chapter 5) and other data available in the literature provide primary experimental support for the following hypothesis (See Fig. 42):

i. Failure can be explained from the fracture mechanics point of view as the generation of a minimum amount of new surfaces during the cracking process, which will require a certain amount of energy proportional to the specific surface energy of ice.

ii. As the rate of loading decreases, the total specific surface energy for ice will increase due to the increase in the energy dissipated due to viscoelastic deformation. An increase in the outside temperature will reduce the total specific surface energy for ice. This is due to the fact that at very low rates of loading the amount of energy dissipated due to the viscoelastic deformation will be much larger than the thermodynamic specific surface energy by one or two orders of magnitude.

iii. The author thinks that any anisotropy could have some effect on the critical energy of failure because of the fact that the failure surface could be developed in any direction where the required specific surface energy is minimum.

iv. The critical energy of failure may depend on the mode of failure, i.e. tension, compression, or bending.

v. The minimum value for the critical energy corresponds to the energy which causes the failure of ice under impact loading.

vi. As the applied rate of loading decreases, the critical energy becomes temperature independent and reaches a maximum constant value.

In Table 4 the duration of the test and the load of failure are tabulated for different test temperatures and cross-head speeds. From this table we notice:

i. The duration of test increases as the cross-head speed decreases and test temperature increases.

ii. The load of failure increases as the cross-head speed decreases and test temperature decreases.

iii. The load of failure reaches almost a constant value for all test temperatures for relatively small cross-head speed.

The above information will indicate that the amount of energy induced inside the samples to cause failure increases as test temperature and cross-head speed decrease. This critical energy will be temperature independent for relatively very low cross-head speeds. This conclusion agrees with the data published by Hawkes and Mellor (1972) (See Fig. 41).

7.4 Conclusion

The small-scale experimental results produced by the author and Hawkes and Mellor (1972) indicate that the critical energy criterion as demonstrated in Fig. 42, may be an adequate failure criterion to predict the failure of ice for a wide range of rates of loading..

7.5 References

Beltaos, S., 1977, "A Strain Energy Criterion for Failure of Floating Ice Sheets", Can. J. Civil Eng., V.5, N3, pp. 352-361.

Hawkes, I., and Mellor, M., 1972, "Deformation and Fracture of Ice Under Uniaxial Stress", J. of Glaciology, V11, N.61, pp. 103-131.

Jones, S., 1978, "Triaxial Testing of Polycrystalline Ice", Proc., Third International Conference on Permafrost, V1, pp. 670-674.

TABLE 4 Loads of Failure and Duration of Test for Columnar Fresh-Water Ice, Grain Size = 8 mm.*

Test Temp °C	Cross-Head Speed mm/min	Load of Failure N	Test Duration Sec
-4.0	0.1	62.1	113.7
	0.5	37.26	14.4
	5.0	29.7	1.59
	50.0	19.44	0.132
-21.0	0.1	75.06	93.1
	0.5	54.54	16.8
	5.0	45.9	1.35
	50.0	34.02	0.12
-32.0	0.1	85.32	91.5
	0.5	80.46	15.36
	5.0	63.18	1.32
	50.0	38.88	0.12
-40.0	0.1	76.68	73.33
	0.5	76.68	12.6
	5.0	61.56	1.12
	50.0	39.42	0.12

*The above test data is based on Table 2 on page 92

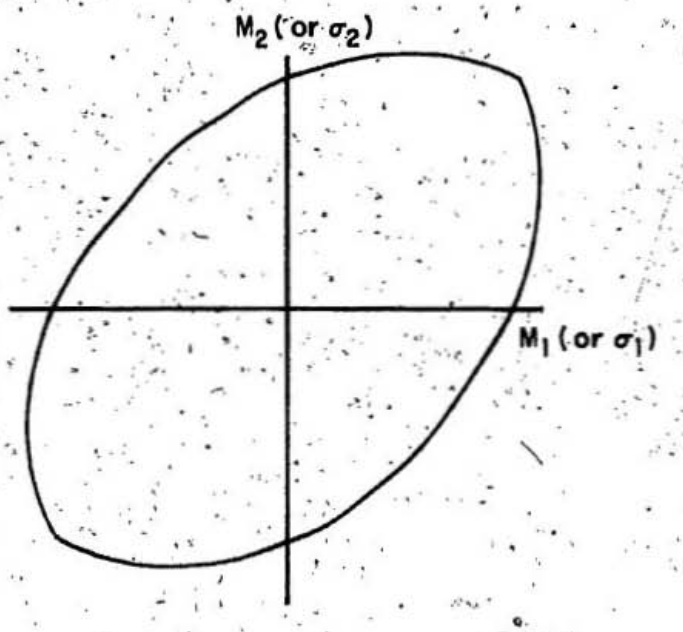

Fig. 38 Von Mises yield criterion.

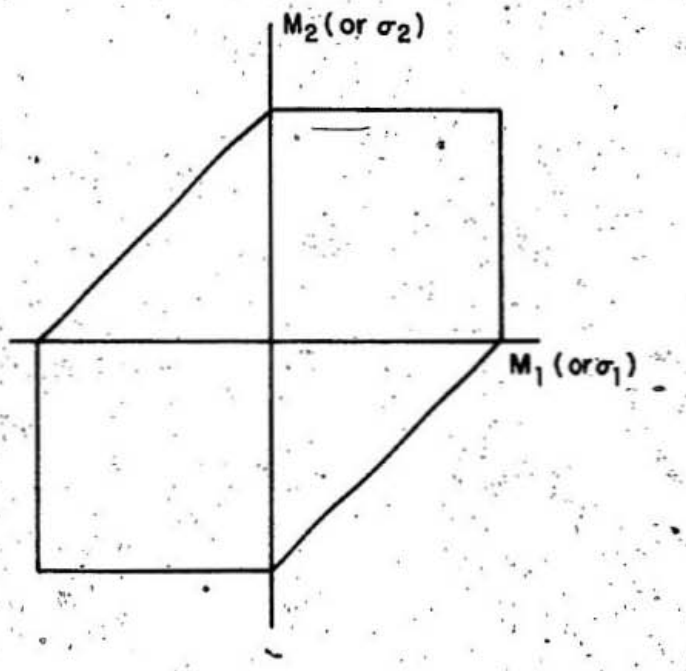

Fig. 39 Tresca yield criterion.

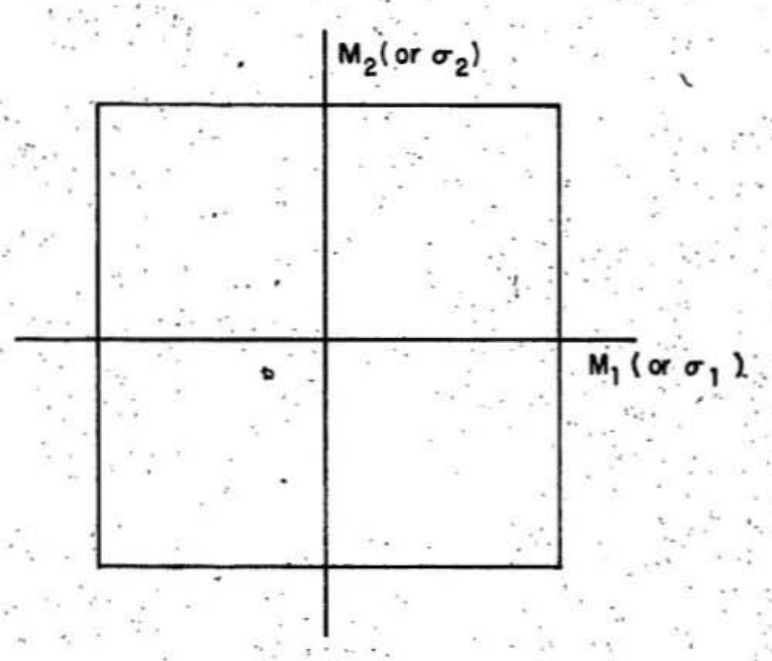

Fig. 40 Johansen yield criterion

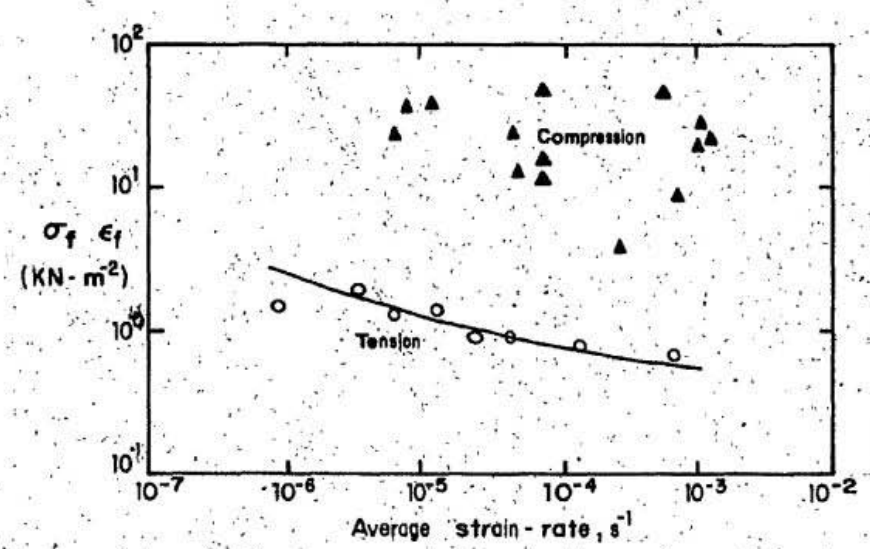

Fig. 41 Relation between the product $\sigma_f \epsilon_f$ and average strain - rate.
(From Hawkes and Mellor, 1972.)

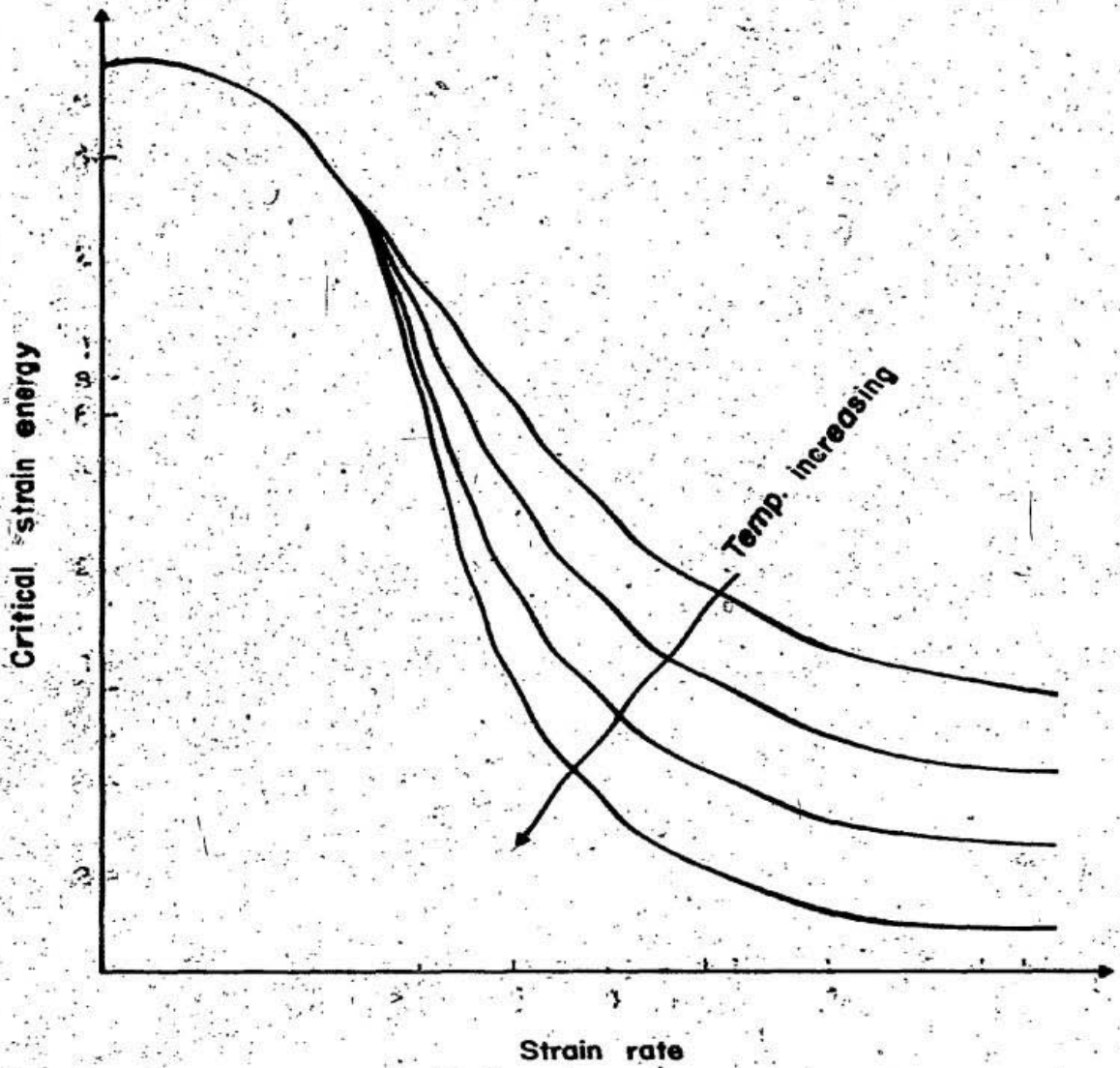

Fig. 42 The proposed critical strain energy criterion.

8. CLOSURE

The present research program has been initiated with a goal to develop computer models which can predict the time of safe operation for a field operation on a floating ice cover, predict the ductile and/or viscoelastic response and failure of ice during small-scale experiment, and calculate the generated forces during ice cover - offshore structure interaction. In order to achieve these goals, the following experimental and theoretical work has been done:

1. A small-scale experimental program has been initiated to study the linear and non-linear fracture toughness of ice. The main objectives of this program were to produce more data about the linear fracture toughness of ice which should hopefully help to answer any questions which have been questioned by the investigators, investigate the possibility of applying the non-linear fracture mechanics techniques to ice, produce primary data and select adequate criterion which controls the failure of ice under rates of loading and temperature.

During this program the effect of cross-head speed, test temperature, grain size, specimen thickness and span length on the linear and non-linear fracture toughness of ice, have been investigated. The data shows that ice has a higher fracture toughness for lower rates of loading and test temperatures. It was observed, also, that the test specimen dimensions have a very important effect on the apparant non-linear response of ice.

A careful analysis of the collected data together with the available literature, indicates that the absorbed energy could be an adequate

parameter which controls the failure of ice. The critical stored energy increases as the rate of loading decreases and temperature increases. The maximum value of this critical stored energy will correspond to the failure of ice under constant loading condition, i.e., for creeping ice. This maximum value will be temperature independent. When enough data is available to support this criterion, it can be used, using the appropriate computer model, to predict the failure of ice in small-scale experiments, determine the time of safe operation of a loaded floating ice cover, and predict the failure of an ice cover moving against offshore structures.

2. The finite element method together with thick plate theory has been used to develop a creep bending model and the appropriate software. The model can solve, using any creep law, the general creep problem of a floating ice cover under a general loading configuration and general boundary conditions. The model has shown good agreement with available creep models and with the data collected during a field load bearing capacity test on a fresh-water ice cover. The model utilizes the critical stored energy, as a failure criterion to predict the onset of failure, to predict the time of safe operation of any loaded floating ice cover.

3. A very recent small-scale experimental investigation by Sinha (1979) has shown that the apparent viscoelastic response of ice depends on the stiffness of the test machine together with the test specimen dimensions. This has indicated the need for a theoretical model which can explain this phenomena and hopefully when generalized will help in solving some ice related problems. The ice is treated as homogeneous, isotropic

and linearly viscoelastic material under uniaxial constant cross-head speed loading. The model is then generalized to multiaxial loading using the finite element method together with the initial strain approach. The numerical results obtained from the model for the uniaxial case, have shown the same viscoelastic response observed in previous experimental work. When there is enough experimental data to support the critical stored energy as a failure criterion, it can be implemented in the computer model which will enable to predict the viscoelastic response together with the final failure of ice under different loading conditions.

General Conclusions

The following are the general conclusions and findings of the present work:

1. A new creep model has been developed which represents a simple and accurate way to solve creep bending problems. The model utilizes a flow rule which has been used before to generalize the uniaxial creep constitutive equation. Good agreement has been obtained between the new model and available numerical creep model as well as field data.

2. A simple equation has been developed to predict the time of safe operation for any loaded ice cover. The formula utilizes the critical strain energy as a failure criterion. Good agreement was observed between the formula and available field data.

3. A numerical model has been developed which can predict the response of viscoelastic materials under different loading conditions. The model proves that the material will show an apparent yield stress when

the internal deformation rate reaches the strain rate applied by the testing machine.

4. A small scale experimental program has been initiated to investigate and measure the linear and non-linear fracture toughness of fresh water ice. It was observed that the fracture toughness depends on: Rate of loading, test temperature, grain size, and test specimen dimensions.

5. The strain rate dependent critical strain energy is proposed as an adequate failure criterion for ice and other viscoelastic materials. The criterion agrees with the available experimental data. The author believes that more research is needed to investigate and support this failure criterion.

Recommendations for Future Research

The author feels that more research is needed in the following areas:

a. Non-linear fracture toughness of fresh-water and sea-water ice: An adequate fracture toughness criterion should be established and the effect of sample dimensions, temperature, brine volume, loading rate, grain size, and grain orientation should be investigated.

b. The present creep bending model should be extended for a multi-layer ice cover. The model should allow for different creep constants for different layers which are made up of different types of ice. This will allow more accurate simultation of the ice covers in the field.

c. Three-dimensional software should be developed for the visco-elastic response of a floating ice cover or ice floes moving against another domain (which could be an offshore structure or an artificial drilling island). The model should be able to predict stress, deformation and interaction force histories for stiff (fixed) and flexible structures.

d. Experimental and theoretical studies should be made of crack initiation and propagation process in fresh-water and sea-water ice. The appropriate crack initiation and growth criterion should be investigated. The fracture criteria would be assessed on the basis of the following requirements:

1. The parameter must be a measure of the stress deformation state in the vicinity of the crack tip,
2. The critical value of the parameter must be independent of initial crack length and specimen geometry.
3. The parameter must be employable in instability analyses.

4. The parameter should be applicable to three-dimensional crack geometries, for example an elliptic surface flaw.
5. The parameter should be generalizable to mixed mode fractures, though the critical value will depend on the relative ratio of shear to flat fracture.
6. The parameter should remain constant during crack extension. This is an attractive but not an essential feature. In an R-curve approach, the resistance parameter will increase with crack extension.

From the computational viewpoint, the viable parameter should possess the following additional properties:

7. The parameter must be relatively insensitive to finite element modeling, to mesh size, process zone size, and load/displacement increment size.
8. The parameter should be computable within a reasonable computational cost.

From the experimental viewpoint the viable parameter should have an additional feature:

9. The parameter should be obtainable from global measurements remote from the crack, but if this is not possible it must be obtainable from local measurements near the crack tip.

APPENDIX (I)

Ice Growth Diary

ICE GROWTH DIARY

DATE	ICE	WEATHER & COMMENTS
Dec 24		No snow on ice
25	9 cm	Light snow cover
Jan 4	½ pond open water	
7	15-18 cm	Snow on most of ice. Evidence of snow freezing on top of ice sheet. In spots snow-ice layer 4 cm thick.
8		Wet snow & windy
9	18 cm	Pond mostly clear of snow
10		Snow fluries
11		Clear & cold, pond patchy to clear
12	23 cm	Clear & cold, pond mostly clear
15	23 cm	Patches of snow
18		Rain & milder
20		Rain & milder
21		Clear & cold
22		Cold
23	31 cm	Clear & cold - light snow cover
24		Snow & wet snow
25		Blowing snow. Put up fence posts
26		Fluries
27		Clear
28		Snow
29		Clear
Feb 4	37 cm	Clear & windy
5	37 cm	Clear & cold
18	37 cm	Water with frozen crust on top. Still 30 cm of water at load.

APPENDIX (II)

Ice Classification

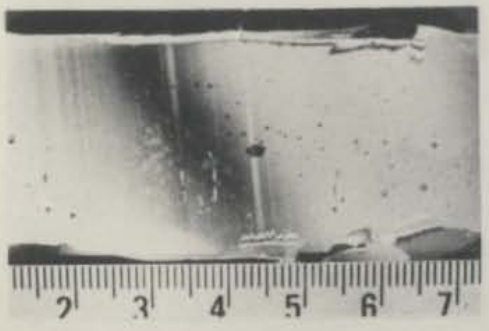

1-V

1-H

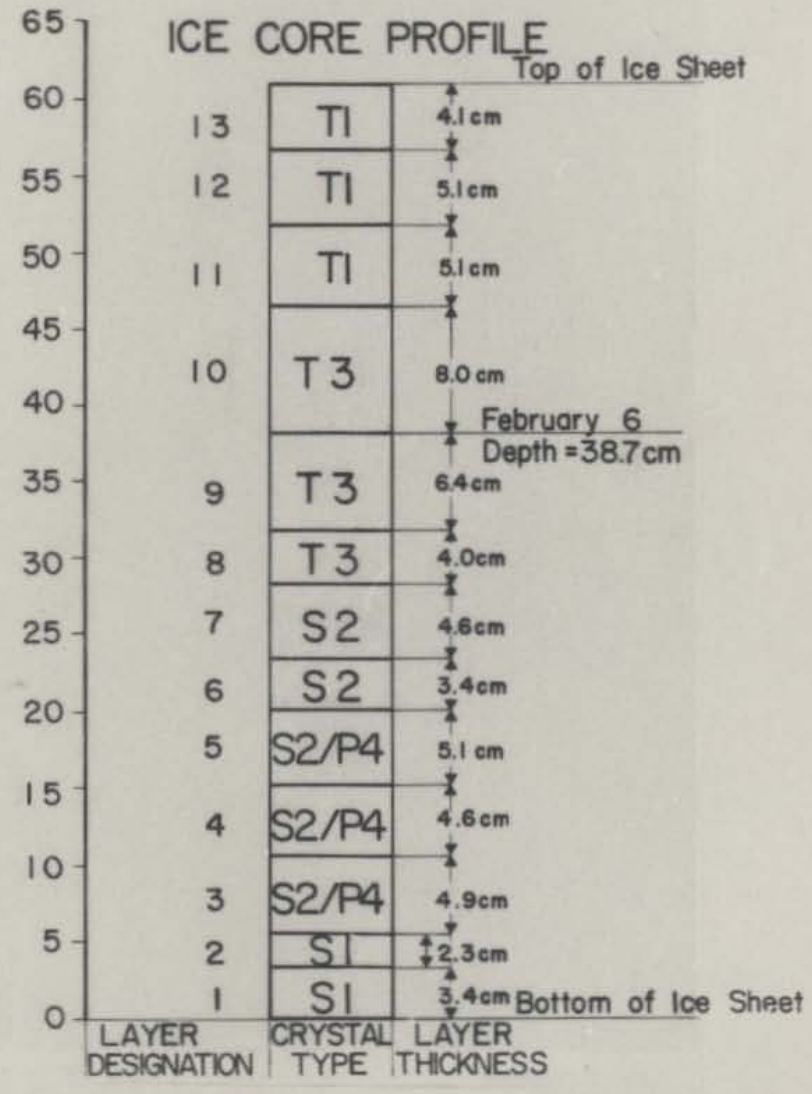

Figure II-a Ice Core Analysis

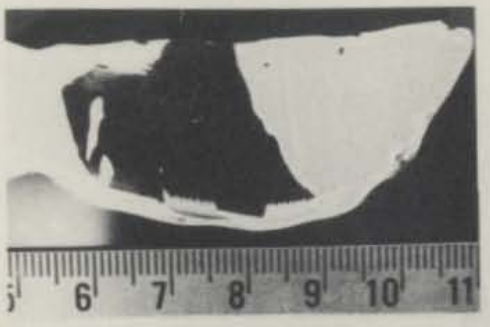

5-V

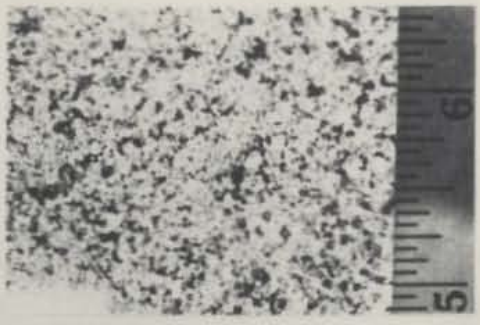

5-H

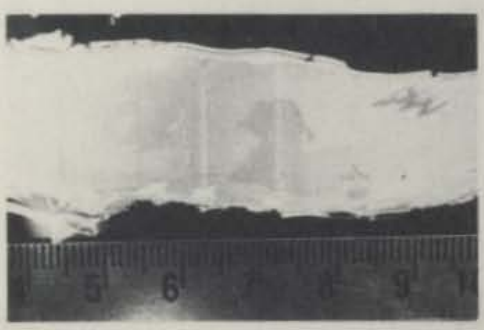

4-V

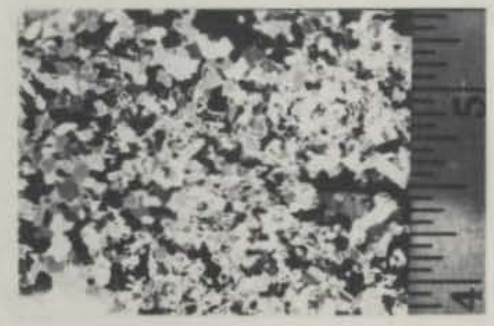

4-H

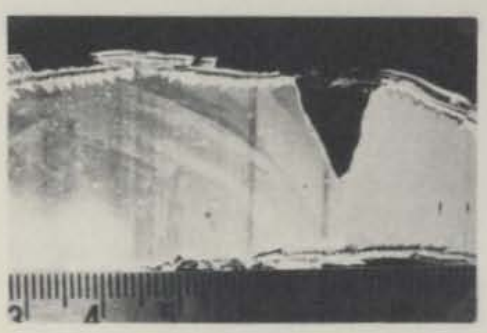

3-V

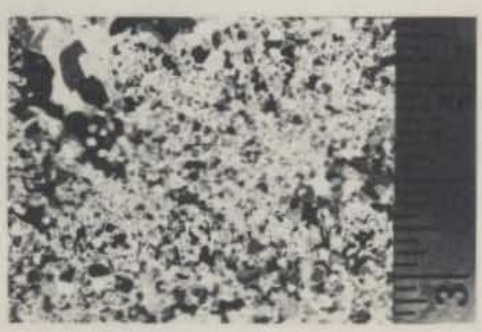

3-H

2-V

2-H

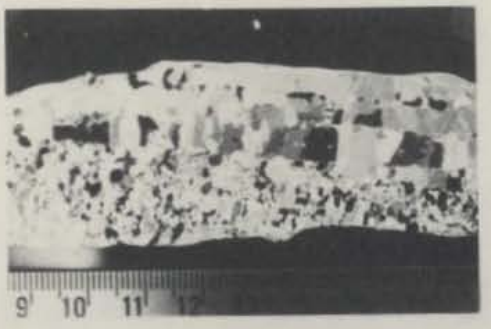

9-V

9-H

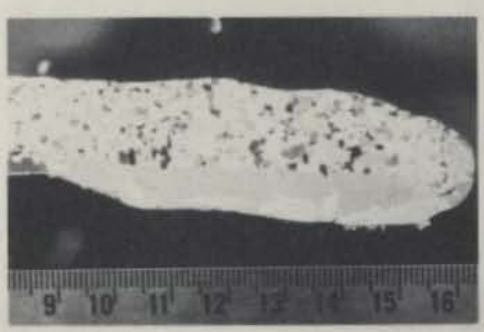

8-V

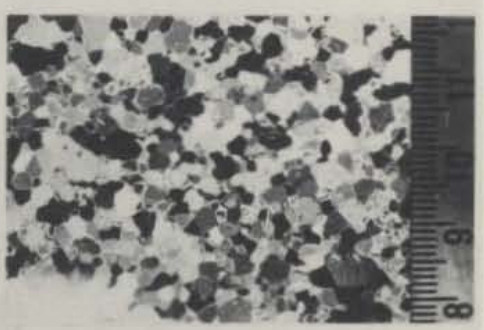

8-H

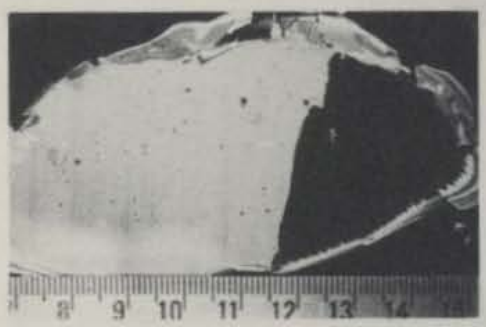

7-V

7-H

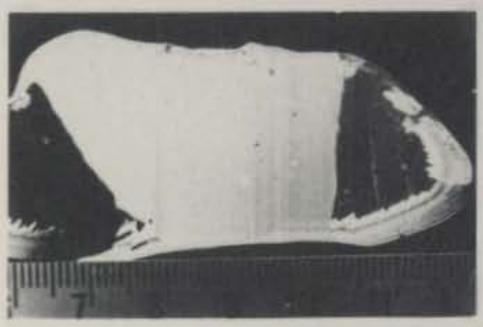

6-V

6-H

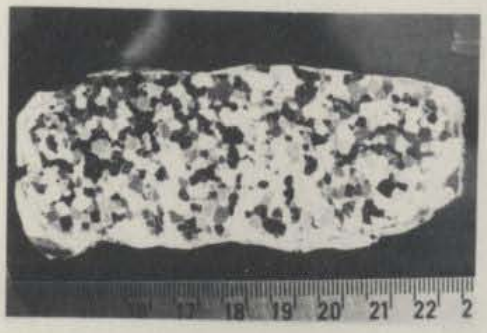

13-V

13-H

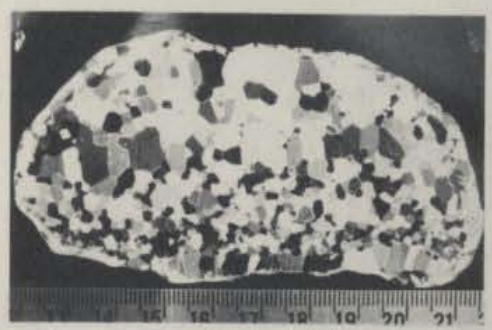

12-V

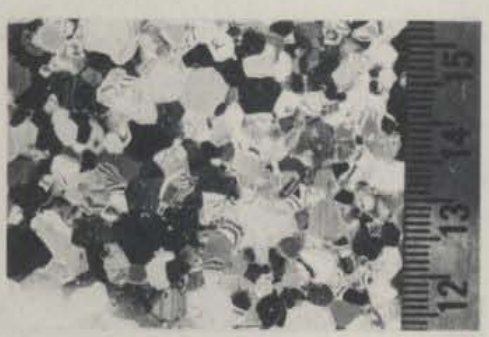

12-H

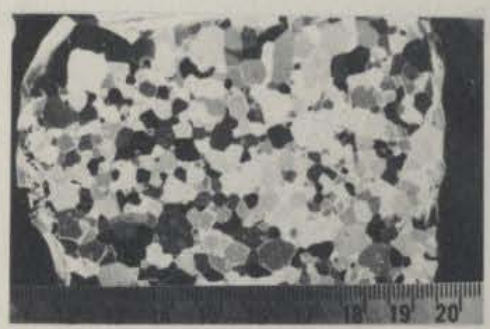

11-V

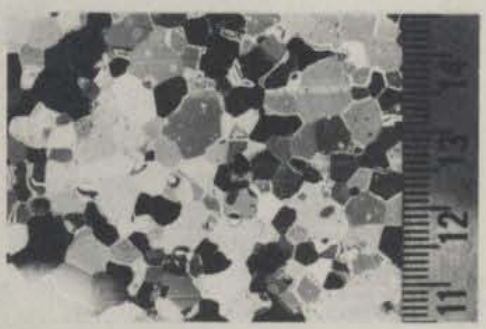

11-H

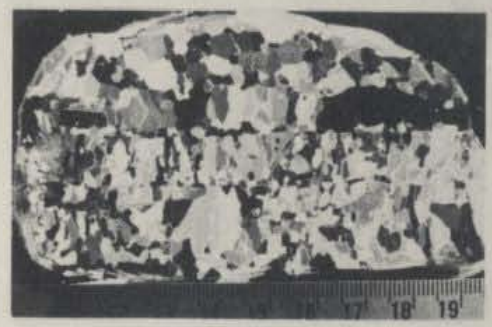

10-V

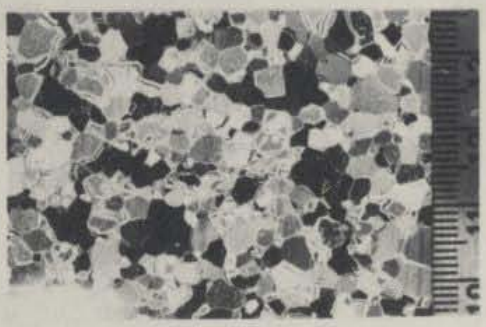

10-H

APPENDIX (III)

Elastic Plate Bending Finite Formulation

And Input Data Instructions for the Computer Program

*adapted from "Finite element programming"
by E. Hinton and D.R.J. Owen

III-a Elastic plate bending finite element formulation:

The finite element used in the present work specifies an independent variation of the lateral displacement (w) and two angles define the line originally normal to the middle surface (θ_x, θ_y).

The strain components in the cartesian coordinates are defined as follows:

$$\{\varepsilon\} = \{\varepsilon_s\} = \begin{Bmatrix} \frac{\partial u}{\partial x} \\ \\ \frac{\partial v}{\partial y} \\ \\ \frac{\partial u}{\partial y} + \frac{\partial v}{\partial x} \\ \\ \frac{\partial u}{\partial z} + \frac{\partial w}{\partial x} \\ \\ \frac{\partial v}{\partial z} + \frac{\partial w}{\partial y} \end{Bmatrix}$$

where u, v, w are the displacements in the three cartesian directions.

The corresponding stress components are defined as:

$$\{\sigma\} = [D]\ \{\varepsilon\}$$

where $[D] = \begin{bmatrix} [D_f] & 0 \\ 0 & [D_s] \end{bmatrix}$

where D_f and D_s are the flexural and shear elasticity matrix respectively.

The energy expression will have the following form:

$$\iiint \delta\, \varepsilon^T \sigma\, dx\, dy\, dz = \iiint \delta\, \varepsilon^T D\, \varepsilon\, dx\, dy\, dz$$

$$= \int\int \delta\, \bar{\varepsilon}^T \begin{bmatrix} -z\, I_3 & 0 \\ 0 & I_2 \end{bmatrix} D \begin{bmatrix} -z\, I_3 & 0 \\ 0 & I_2 \end{bmatrix} dz\ \bar{\varepsilon}\, dx\, dy$$

$$= \int\int \delta\, \bar{\delta}^T\, \bar{\sigma}\, dx\, dy$$

where $\bar{\sigma} = \bar{D}\,\bar{\varepsilon}$

$$\bar{D} = \begin{bmatrix} \int D_f z^2 \, dz & 0 \\ 0 & \int D_s \, dz \end{bmatrix}$$

The stiffness matrix will have the following form:

$$\int \int B^T \bar{D} B \, dx \, dy \, \delta = R$$

where R is the load vector

B is the strain matrix

The strain matrix associated with node r is B_r.

$$B_r = \begin{bmatrix} 0 & -\frac{\partial N_r}{\partial x} & 0 \\ 0 & 0 & -\frac{\partial N_r}{\partial y} \\ 0 & -\frac{\partial N_r}{\partial y} & -\frac{\partial N_r}{\partial x} \\ \frac{\partial N_r}{\partial x} & -N_r & 0 \\ \frac{\partial N_r}{\partial y} & 0 & -N_r \end{bmatrix} = \begin{bmatrix} B_f \\ B_s \end{bmatrix}_r$$

where N_r is the matrix of shape functions at node r

III-b Flow Chart for the computer program:

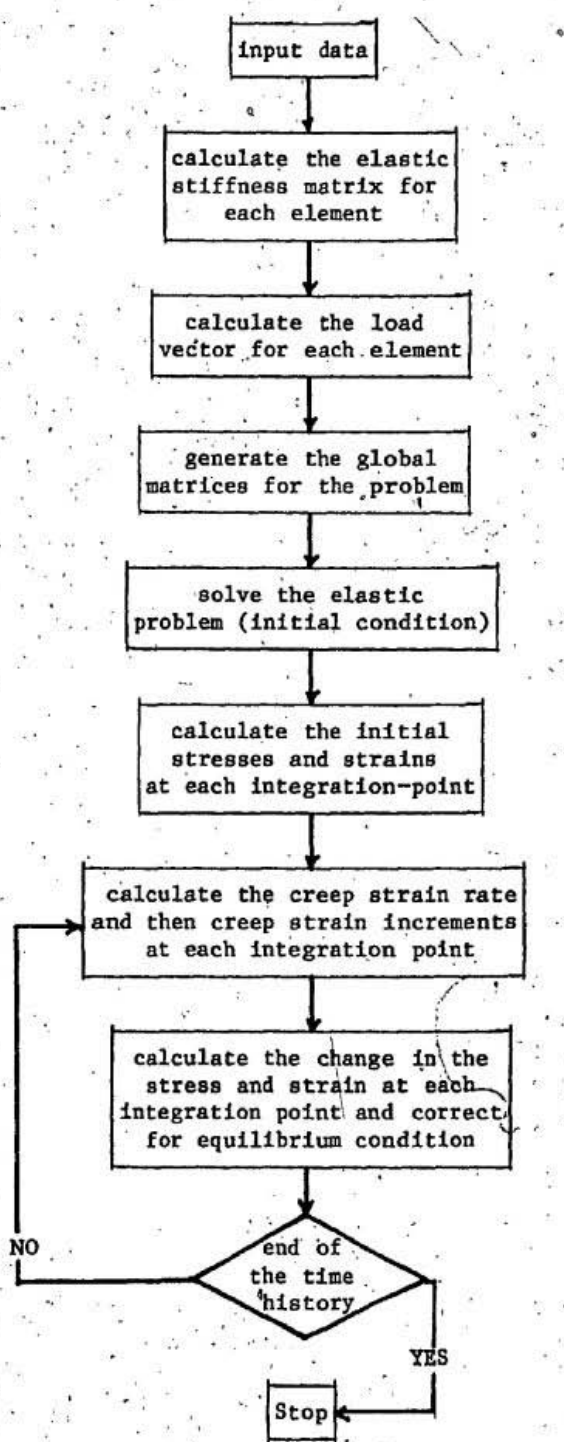

III-c User's Manual:

CARD SET 1 PROBLEM CARD (I5) -- One card

Cols. 1-5	NPROB	Total number of problems to be solved in one run

CARD SET 2 TITLE CARD (12A6) -- One card

Cols. 1-72	TITLE	Title of the problem -- limited to 72 alphanumeric characters

CARD SET 3 CONTROL CARD (1215) -- One card

Cols. 1-5	NPOIN	Total number of nodal points
6-10	NELEM	Total number of elements
11-15	NVFIX	Total number of restrained boundary points -- where one or more degrees of freedom are restrained
16-20	NCASE	Total number of load cases to be analysed
21-25	NTYPE	Blank
26-30	NNODE	Number of nodes per element (=8)
31-35	NDOFN	Number of degrees of freedom per node (=3)
37-40	NMATS	Total number of different materials
41-45	NPROP	Number of independent properties per material (=4)
46-50	NGAUS	Order of integration formula for numerical integration (generally use 2)
51-55	NDIME	Number of coordinate dimensions (=2)
56-60	NSTRE	Number of independent generalised stress components (=5)

61-65 AK Modulus of elastic foundation

66-70 N Power Exponent in the creep law

71-75 CI Creep constant in the creep law

CARD SET 4 ELEMENT CARDS (10I5) -- One card for each element.
Total of NELEM cards (see Card Set 3)

Cols. 1-5 NUMEL Element number

6-10 MATNO(NUMEL) Material property number

11-15 LNODS(NUMEL,1) 1st Nodal connection number

16-20 LNODS(NUMEL,2) 2nd Nodal connection number

.
.
.

46-50 LNODS(NUMEL,8) 8th Nodal connection number

Note: The nodal connection numbers must be listed in an anticlockwise sequence, starting from any corner node; the element being viewed from above the plane z = 0. (See Fig. 3.3).

CARD SET 5 NODE CARDS (It,2F10.5) -- Once card for each node whose coordinates are to be input.

Cols. 1-5 IPOIN Nodal point number

6-15 COORD(IPOIN,1) x-coordinate of node

16-25 COORD(IPOIN,2) y-coordinate of node

Notes 1) The coordinates of the highest numbered node must be input, regardless of whether it is a midside node or not.

2) The total number of cards in this set will generally differ from NPOIN (see Card Set 3) since for element sides which are

linear it is only necessary to specify data for corner nodes; intermediate nodal coordinates being automatically interpolated if on a straight line.

CARD SET 6 RESTRAINED NODE CARDS (1X,I4,2X,3I1,2F10.6) -- One card for each restrained node. Total of NVFIX cards (see Card Set 3).

Cols. 2-5 NOFIX(IVFIX) Restrained node number

8 IFPRE(IVFIX,1) Condition of restraint on nodal displacement, w

- 0 No displacement restraint
- 1 Nodal displacement restrained

9 IFPRE(IVFIX,2) Condition of restraint on nodal rotation, θ_x

- 0 No rotation restraint
- 1 Nodal rotation restrained

10 IFPRE(IVFIX,3) Condition of restraint on nodal rotation, θ_y

- 0 No rotation restraint
- 1 Nodal rotation restrained

11-20 PRESC(IVFIX,1) The prescribed value of nodal displacement, w

21-30 PRESC(IVFIX,2) The prescribed value of nodal rotation, θ_x

31-40 PRESC(IVFIX,3) The prescribed value of nodal rotation, θ_y

CARD SET 7 MATERIAL CARDS (I5,4F10.5) -- One card for each different material. Total of NMATS cards (see Card Set 3)

Cols. 1-5 NUMAT Material identification number

6-15 PROPS(NUMAT,1) Elastic modulus, E

16-25 PROPS(NUMAT,2) Poisson's ratio, v

26-35 PROPS(NUMAT,3) Material thickness, t

36-45 PROPS(NUMAT,4) Intensity of any uniformly distributed load

CARD SET 8 LOAD CASE TITLE CARD (12A6) -- One card

Cols. 1-72 TITLE Title of the load case -- limited to 72 alphanumeric characters

CARD SET 9 LOAD CONTROL CARD (I5) -- One card

Cols. 1-5 IPLOD Applied point load control parameter

- 0 No applied nodal loads to be input
- 1 Applied nodal loads to be input

CARD SET 10 APPLIED LOAD CARDS (It,3F10.3) -- One card for each loaded nodal point

Cols. 1-5 LODPT Node number

6-15 POINT(1) Load component in the z direction

16-25 POINT(2) Nodal couple in the xz plane

26-35 POINT(3) Nodal couple in the yz plane

Notes 1) The last card should be that for the highest numbered node whether it is loaded or not

2) If IPLOD = 0 in Card Set 9, omit this set.